The copyright of this thesis vests in the author. No quotation from it or information derived from it is to be published without full acknowledgement of the source. The thesis is to be used for private study or non-commercial research purposes only.

Published by the University of Cape Town (UCT) in terms of the non-exclusive license granted to UCT by the author.

University of Cape Town

THE USE OF HYDROTALCITE DERIVED CATALYST PRECURSORS IN THE FISCHER-TROPSCH SYNTHESIS

Thesis submitted for the Taught Masters in Catalysis degree in the Department of Chemical Engineering at the University of Cape Town.

University of Cape Town

by

THILOSHINI NAIDOO

B.Sc. Hons(Chemistry) (University of Kwa-Zulu Natal)

Supervisor: Prof. Eric van Steen, UCT

Co-Supervisor: Dr Tracy Bromfield, Sasol

Cape Town

2007

ACKNOWLEDGEMENTS

I would like to thank my supervisor Dr Eric van Steen and co-supervisor Dr Tracy Bromfield for their guidance throughout the project.

I would also like to thank Dr Johannes Retief and Beatrice Breedt for their invaluable assistance with conducting the XRD experiments and with the analysis of the experimental data. Thank you also to Melene Hauman and Kobus Wagener for their assistance with the TGA experiments.

For funding the project I would like to thank the Catalysis Department at Sasol Technology and the head of the department Philip Gibson for giving me the opportunity to do the taught masters course. A special thank you to my lecturers at UCT for the lessons learned as well as for your patience and dedication in helping and teaching.

Thank you to all my loved ones for their support, and especially to my husband for his constant encouragement and understanding.

University of Cape Town

ABSTRACT

The current fused iron catalyst used in the high temperature Fischer-Tropsch process is not very responsive to chemical promotion. Thus the optimisation of the selectivity of this catalyst is restricted. In the development of a catalyst the aim is to obtain the best combination of activity, selectivity and stability with the optimum number of effective active sites of the catalyst exposed to the reaction medium [Gibson, 1999]. Catalysts that have a large catalytically active surface area exposed to the reaction can be obtained by having very small catalyst particles well dispersed on a support material [Augustine, 1996]. Supporting the iron metal used in the HTFT process onto a basic support should eliminate the problem associated with supported iron catalysts namely, the effect of "alkali dilution" caused by the migration of the alkali onto the support material [Dry, 1981].

Hydrotalcites have been shown to provide a high surface area basic support [Schaper, 1989]. Supporting the iron metal used in Fischer-Tropsch synthesis onto the basic hydrotalcite eliminates the problems associated with supported alkali promoted iron catalyst and results in a catalyst system that can be controlled and optimised to produce catalysts with specific compositions and characteristics. Alternatively, the iron can be incorporated into the hydrotalcite structure to form an Mg-Fe hydrotalcite. This allows for interaction between the elements which may result in possible synergistic effects.

The use of a Mg-Fe hydrotalcite in the Fischer-Tropsch synthesis was investigated in this study. Mg-Fe hydrotalcites were prepared with a molar ratio of Mg to Fe of 2:1. The catalyst was thereafter heat treated and activated prior to synthesis. The hydrotalcite derived catalyst showed an overall CO conversion of ca. 75% and conversion to FT products of ca. 40%. The performance was comparable to that of a standard fused catalyst which is typically used in the High Temperature Fischer-Tropsch process.

University of Cape Town

The selectivity results of the hydrotalcite derived catalyst also compared well with the fused catalyst but differed in that the former produced a lighter more paraffinic hydrocarbon spectrum. Thus the hydrotalcite derived catalyst had the advantages of a supported catalyst, as only a small amount of iron was required to achieve similar conversions as a bulk catalyst. In addition, the magnesium appears to have a satisfactory basicity with respect to its selectivity compared to the fused catalyst. The hydrotalcite derived catalyst offered an additional benefit in that the acid production during synthesis was lower compared to the fused catalyst.

The responsiveness of the hydrotalcite derived catalyst towards chemical promotion was also investigated. It has been shown that both the activity and the selectivity of the Mg-Fe hydrotalcite catalyst in the Fischer-Tropsch synthesis is dependent on the Mg/Fe ratio [Shen, 1996]. An increase in the ratio would result in an increase in the basicity and a decrease in the reducibility of the catalyst.

Potassium was added to the calcined hydrotalcite in an attempt to increase the basicity without adversely affecting the reducibility of the iron. The results from this catalyst however were in contradiction to what was expected from a potassium promoted iron catalyst used in the Fischer-Tropsch process.

The hydrotalcite derived catalysts did not undergo complete reduction under the conditions used and copper was added in an attempt to increase the amount of active metallic iron present and to thereby improve the catalytic activity. This was successful as the copper promoted catalyst had improved conversions and showed a marked decrease in the amount of methane formed compared to the unpromoted catalyst. The catalyst also produced a much higher quantity of ethanol and similar amounts of the other alcohols compared to the fused catalyst.

University of Cape Town

Further work should be done to optimize the preparation conditions of the catalyst as well as the activation and synthesis conditions. The work is directly related to the investigations that need to be carried out to further characterise the catalyst, bulk and surface phases and the determination of the possible changes in these phases under synthesis conditions. This will provide insight into the limitations or flexibility of the catalyst systems.

University of Cape Town

TABLE OF CONTENTS

University of Cape Town

University of Cape Town

University of Cape Town

LIST OF TABLES

University of Cape Town

CHAPTER 4: EXPERIMENTAL RESULTS

LIST OF FIGURES

CHAPTER 1: INTRODUCTION

CHAPTER 2: HYDROTALCITES - A LITERATURE REVIEW

CHAPTER 3: EXPERIMENTAL APPARATUS AND PROCEDURES

University of Cape Town

CHAPTER 4: EXPERIMENTAL RESULTS

University of Cape Town

CHAPTER 5: DISCUSSION

University of Cape Town

Chapter 1

INTRODUCTION

1.1. Background

At present the world's fuel and chemical production is mainly derived from petroleum crude oil. However the known reserves of methane and coal exceed that of crude oil by factors of about 1.5 and 25 respectively [Dry, 2002]. Methane and coal can be converted into synthesis gas (also known as syngas), which can be subsequently converted to fuels and chemicals via the Fischer Tropsch (FT) process. Hence, methane and coal can be used as an alternative to the use of crude oil.

The Fischer-Tropsch process can be described as a heterogeneous surface catalyzed polymerization reaction [Anderson, 1984]. The reaction entails the hydrogenation of carbon monoxide over certain metal catalysts to form a range of hydrocarbons as represented by the following general equation:

$$CO + H_2 \rightarrow (CH_2)_n + H_2O \qquad (1.1)$$

The product spectrum of the FT process is complex and contains a mixture of linear and branched hydrocarbons and oxygenated products. Linear paraffins and α-olefins are the predominant products of the process, and alcohols, ketones, aldehydes and acids make up the minor product fraction [Dry, 1981]

University of Cape Town

The process is generally operated at two distinct temperature ranges namely, 300-350°C and 200-240°C, referred to as the high temperature Fischer-Tropsch (HTFT) and low temperature Fischer-Tropsch (LTFT) processes respectively. The HTFT process produces predominately shorter chain olefinic and branched products whereas the LTFT process produces longer chain linear paraffinic products (see Table 1.1).

Table 1.1: Typical product distribution (mass %) for low temperature (LTFT) and high temperature (HTFT) Fischer-Tropsch process [Geertsema, 1995]

Product	**HTFT**	**LTFT**
CH_4	7	4
C_{2-4} Olefins	24	4
C_{2-4} Paraffins	6	4
Gasoline (C_{6-10})	40	18
Distillate (C_{11-23})	12	19
Oils and Waxes (C_{24+})	9	51

University of Cape Town

In both the high temperature (HTFT) and the low temperature (LTFT) process a wide range of products is obtained. Thus, these processes are non-selective towards a specific product. There is a huge cost involved in the separation and work-up of the different products downstream from the FT synthesis and thus there is an incentive for a more selective process which would result in a "cleaner" product spectrum.

In the high temperature (HTFT) Fischer-Tropsch process a number of highly valuable chemical products are formed, such as ethylene and propylene (see Table 1.1). Optimization of the selectivity of this process towards such products could improve the overall economics of the process. The selectivity of the process can thus be enhanced by selecting a suitably promoted metal catalyst.

1.2. Product formation in the Fischer-Tropsch synthesis

The Fischer-Tropsch process is a non-selective process yielding a wide range of products. However, there always appears to be an interrelation between the products, which originates from the stepwise growth process that takes place on the catalyst surface [Dry, 2002] (see Figure 1.1).

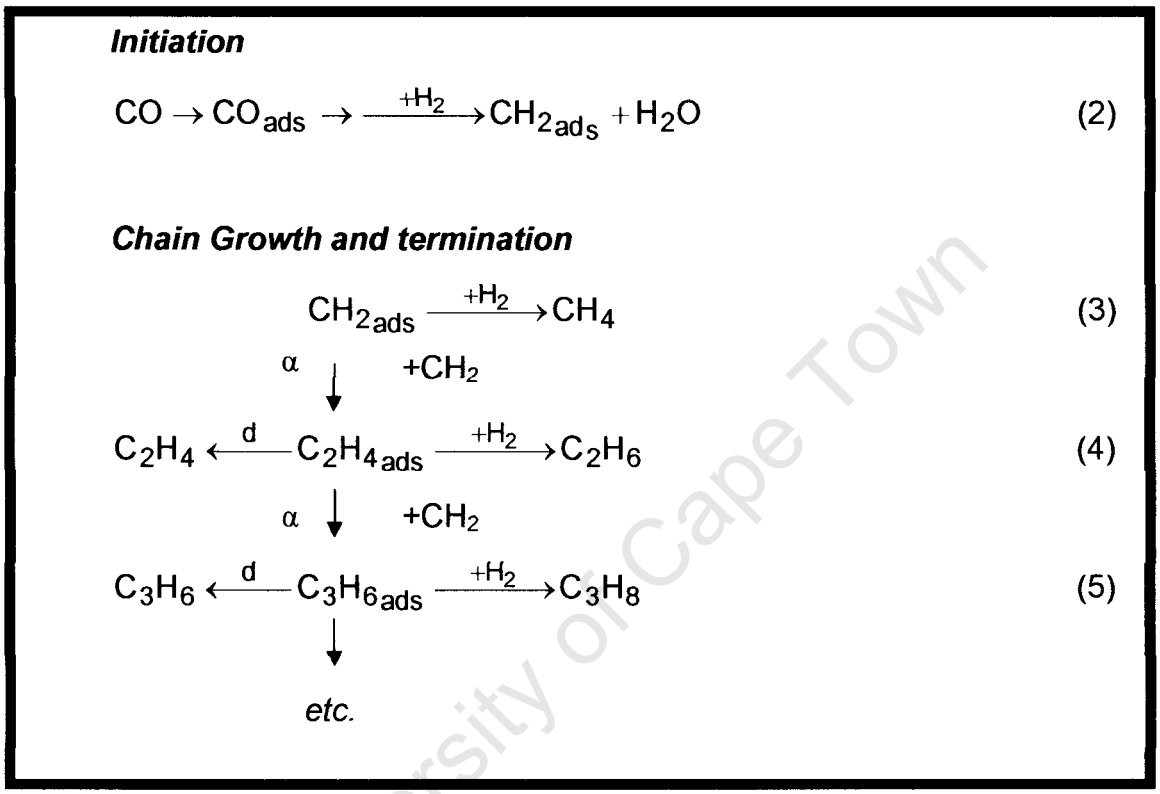

Figure 1.1: Schematic view of the stepwise growth process in the Fischer-Tropsch synthesis (no specific mechanism implied) [Dry, 2002]

University of Cape Town

The initiation step starts with the adsorption of CO on the catalyst surface. Hydrogenation of adsorbed CO may lead to the formation of the chain starter and the monomer (in Figure 1.1 visualized as a CH_2-unit). At each stage of growth, the adsorbed hydrocarbon species can desorb as an alkene or can be hydrogenated and desorbs as an alkane, or it can add another CH_2 monomer and continue the chain growth process. The probability that the chain may continue growing is given by the chain growth factor α. Thus the probability of desorption is given by 1-α. The product spectrum of the Fischer-Tropsch synthesis can be described by the Anderson-Schulz-Flory distribution which is a

mathematical description of the above growth process assuming that the chain growth probability α is independent of carbon number.

$$\frac{W_n}{n} = \frac{(1-\alpha)^2 \cdot \alpha^n}{\alpha} \qquad (1.1)$$

with W_n = weight fraction of products with n carbon atoms in organic products

n = carbon number

α = chain growth probability factor (assumed to be independent of n)

The chain growth probability therefore determined the product distribution [Dry, 1981]. Figure 1.2 shows the expected distribution of the organic product spectrum as a function of chain growth probability α. Only methane and wax (C_{20+}) can be obtained with high selectivity at a chain growth probability of 0 and

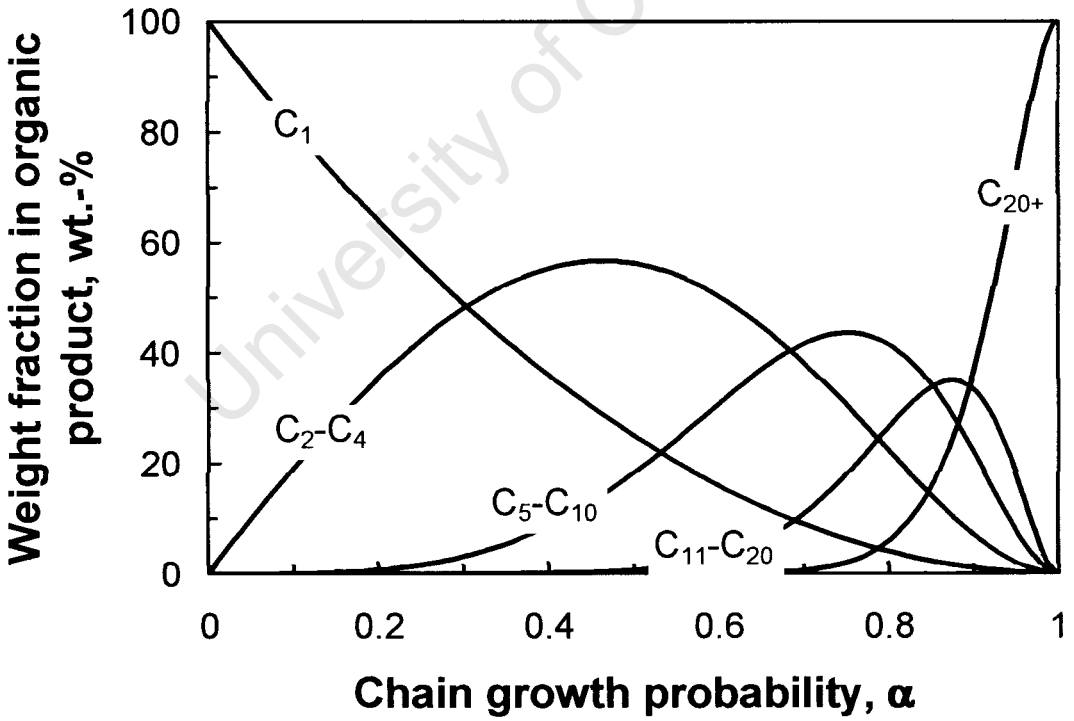

Figure 1.2: Product distribution as a function of the chain growth probability α according to the ideal Anderson-Schulz-Flory distribution

University of Cape Town

1 respectively. All other products in certain carbon number fractions are obtained with a limited selectivity (e.g. the maximum selectivity for C_2-C_4 is 57 wt.-% at a chain growth probability of 0.46, the maximum selectivity for hydrocarbons in the gasoline range (C_5-C_{10}) is 43.5 wt.-% at a chain growth probability of 0.76, and the maximum selectivity for diesel (C_{11}-C_{20}) is 34.9 wt.-% at a chain growth probability of 0.88).

The real product distribution of the Fischer-Tropsch synthesis shows some marked differences from the ideal Anderson-Schulz-Flory distribution [Claeys and van Steen, 2004]. The selectivity for methane is typically higher than predicted by the Anderson-Schulz-Flory distribution, which has been explained by the existence of non-specific sites on the Fischer-Tropsch catalyst [Schulz et al., 2002], or on mechanistic grounds [Claeys and van Steen, 2004]. The selectivity for C_2 is typically lower than expected based on the Anderson-Schulz-Flory distribution, which has been ascribed to the high reactivity of ethene leading to incorporation of ethene in the chain growth process [Schulz and Claeys, 1999a]. Furthermore, the chain growth probability increases with increasing carbon number for long chain hydrocarbons. This has been attributed to the re-incorporation of long chain olefins in the chain growth process [Schulz and Claeys, 1999b].

University of Cape Town

1.2.1. Effect of process variables on selectivity in the Fischer-Tropsch synthesis

Table 1.2 summarizes the effect of the process variables on the selectivity of the Fischer-Tropsch synthesis [Roper, 1983]. Increasing the space velocity (decreasing the residence time) increases the olefin and alcohol selectivity. These products are therefore believed to be one of the primary products of the Fischer-Tropsch synthesis.

A higher H_2/CO ratio results in a more hydrogenating environment inside the reactor and consequently this leads to the formation of more hydrogenated

products. Since hydrogen can terminate chain growth, it also results in a decrease in the chain length [Dictor and Bell, 1986].

Table 1.2: Effect of process parameters on the selectivity in the Fischer-Tropsch synthesis [Roper, 1983]

	SV	H_2/CO	T	P	Conversion
Methane Selectivity	-	+	+	-	+
Chain Length	*	-	-	+	*
Branching	*	*	+	-	*
Olefin Selectivity	+	-	*	*	-
Oxygenates Selectivity	+	-	-	+	-
Carbon Deposition	*	-	+	*	+

T= Temperature, P=Pressure, SV=Space Velocity

+ : Increase with increasing parameter

- : Decrease with decreasing parameter

* : Complex relationship

An increase in reaction temperature yields a decrease in the chain length, an increase in the methane selectivity and an increase in the degree of branching. This is related to the relative activation energy for the chain growth, chain branching and chain desorption step.

The reactor pressure in addition to temperature also plays a significant role in the selectivity of the Fischer-Tropsch synthesis. The effect of pressure is a compounded effect, since it reflects the change in the partial pressures of the kinetically relevant compounds, such as hydrogen and carbon monoxide. An increase in the conversion also reflects the change in the partial pressures of the kinetically important variables, such as hydrogen and carbon monoxide.

University of Cape Town

1.3. Catalysts for the Fischer-Tropsch synthesis

The Fischer-Tropsch synthesis is typically catalyzed by group VIII metals, of which only iron, cobalt, nickel and ruthenium have the required FT activity for commercial application [Dry, 2004].

Considering the costs of the metals (see Table 1.3), ruthenium is by far the most expensive metal. Aside from the cost, the amount of Ru that is available is not sufficient for large scale application. Nickel produces far too much methane under practical operating conditions and is therefore not used commercially. This leaves only iron and cobalt as viable catalytic metals for commercial scale FT synthesis [Dry, 2002]

Table 1.3: Relative price of metals with suitable activity in the Fischer-Tropsch synthesis for commercial application [Dry, 2002]

Metal	Relative Price
Fe	1
Ni	250
Co	1000
Ru	50000

University of Cape Town

Cobalt-based catalysts are only used in the low temperature Fischer-Tropsch process (LTFT) and more specifically in the low temperature Fischer-Tropsch process utilizing synthesis gas originating from natural gas [Dry, 2004]. They are not suitable for high temperature application, since methane selectivity increases dramatically with temperature.

Iron-based catalysts can be used in both the high temperature and low temperature processes [Dry, 1988]. Iron also catalyses the water-gas shift reaction, and thereby permits the use of synthesis gas with a low H_2/CO ratio, such as that obtained from the gasification of coal [Xu, 1998]. This however also

results in the production of CO_2 during the Fischer-Tropsch synthesis, which needs to be removed downstream from the process.

The metals used as catalysts for the Fischer-Tropsch synthesis are generally promoted to enhance the activity and selectivity of the catalyst. There are two main groups of promoter, namely, structural and chemical promoters. Structural promoters increase and stabilize the available active metal surface area, i.e. they give structural stability and porosity to the catalyst matrix. Chemical promoters influence the "chemistry" of the catalytic process and generally affect the product selectivity.

Cobalt is generally dispersed on high area stable supports such as, Al_2O_3, SiO_2 or TiO_2 in order to maximize the available surface area of the metal, since it is an expensive metal The catalyst is also usually promoted with a small amount of noble metal, e.g. Pt, Ru or Re which enhances the reduction process and keeps the catalyst surface "clean" during FT synthesis [Dry, 2002].

Iron-based Fischer-Tropsch catalysts are usually bulk-type of catalysts with a binder, such as silica in the low temperature Fischer-Tropsch (LTFT) catalyst, and structural promoters such as Al_2O_3 or MgO in the high temperature Fischer-Tropsch catalyst [Dry, 2002]. Iron catalysts are generally promoted with alkali, usually K_2O, since the addition of small amounts of alkali to the catalyst has a significant influence on both the activity and selectivity of the catalyst [Anderson, 1984] (see Table 1.4)

Alkali promoters typically improve the adsorption capabilities of carbon monoxide relative to hydrogen on the iron metal surface. Consequently the product spectrum is shifted towards longer chain molecules and the amount of methane produced is reduced. Furthermore, the product becomes more olefinic. It also results in an increase in the activity of the catalyst [Anderson, 1984]. However as the alkali is increased, the activity of the catalyst passes a maximum where it either levels off or starts to decline.

University of Cape Town

This is due to the increased coverage of the catalyst surface with strongly bound CO that does not desorb easily as products and eventually results in the formation of coke on the catalyst. The basicity of the iron Fischer-Tropsch catalyst is thus extremely important.

Table 1.4: Influence of alkali on activity and selectivity of the fused magnetite catalyst tested in a fixed bed reactor at 328°C [Dry, 1981]

K_2O Level	Relative Activity	CH_4, %	C_3H_6/C_3H_8
0	1	41	0.2
1.8	1.43	20	3.0
2.1	1.43	15	5.7
2.7	1.46	13	7.4
3.4	1.49	12	11
4.0	1.48	10	12

The iron-based catalyst for the high temperature Fischer-Tropsch (HTFT) process is usually prepared by a fusion process. This entails melting iron oxides, chemical (K_2O and Na_2O) and structural promoters (Al_2O_3, MgO, CaO) in an electric furnace. The chemistry involved in the fusion process is complicated and difficult to control.

Under the high temperatures required for fusion of the magnetite, some of the structural promoters and impurities in the raw materials, particularly silica, combine with a significant portion of the chemical promoters in solid-state reactions [Anderson, 1984]. This renders the chemical promoters in the catalyst less effective. Thus, the fused catalyst is relatively unresponsive to chemical promotion and optimization of the selectivity of this catalyst is restricted. The high fusion temperature also results in the volatilization of some of the promoters such as the K_2O.

After fusion of the iron with the promoters, the melt is cast into pans to cool and solidify before crushing and milling. During the solidification process,

University of Cape Town

segregation of the promoters takes place. A promoter concentration gradient thus exists from the segment of the material solidifying first to that solidifying last. This gives rise to higher levels of promoter in the latter section. This is undesirable since ideally all particles should have a similar quantity of promoters after crushing and milling, so that each particle would have similar catalytic properties.

A further disadvantage of fusion is the lack of control on the final composition of the catalyst. Fluctuations in the level of impurities in the raw materials that are used to prepare the catalyst influence the effectiveness of the promoter in the catalyst due to the solid-state reactions that take place during fusion. This results in the subsequent variation in the performance of the catalyst. This catalyst is however very cheap, robust and is capable of withstanding the turbulent environment of a fluidized bed reactor, which is used in the high temperature Fischer-Tropsch (HTFT) process.

A more reproducible iron-based catalyst might be obtained by creating a supported iron catalysts, on which small iron crystallites are dispersed. This will yield a catalyst with a large catalytically active surface area, which are far more efficient than the bulk metal catalysts [Augustine, 1996]. The support material provides thermal stability for the small catalyst particles by inhibiting/minimizing sintering of the crystallites, and it also provides mechanical strength for the catalyst.

The problem that is experienced with supported iron Fischer-Tropsch catalysts is the migration of the alkali promoter, onto the support material [Anderson, 1984]. This results in a "dilution" of the effect of the alkali in the catalyst, which results in poor selectivity, most notably, higher methane and a decrease in olefin production. Supporting the iron metal on a basic support should in principle provide an ideal solution to this problem. This might be achieved by deriving a catalyst from hydrotalcites [Shen et al., 1996].

University of Cape Town

Hydrotalcites have been shown to have similar basicity and improved stability towards heat and steam when compared to pure magnesium hydroxide [Schaper, 1989]. They could provide a high surface area basic support onto which iron can be impregnated. Alternatively the iron can be incorporated, in minor amounts, with magnesium into the hydrotalcite structure to form a high surface area Mg-Fe hydrotalcite. This allows for interaction between the elements which may result in possible synergistic effects.

1.4. Hypothesis and Thesis Aims

The current fused iron catalyst used in the high temperature Fischer-Tropsch synthesis is not very reproducible. A supported iron catalyst might be a suitable substitute for the current utilized catalyst. Iron-based Fischer-Tropsch catalysts require a basic promoter to minimize methane formation and maximize the olefin formation. Traditional support materials are not suited due to migration of the basic promoter. Hydrotalcites are basic and it is therefore hypothesized that *a Mg-Fe hydrotalcite derived catalyst will provide a high surface area basic catalyst suitable for Fischer-Tropsch synthesis.*

The aims and scope of the thesis entails:

- Preparation of a Mg-Fe hydrotalcite derived catalyst
- Characterisation of the catalyst
- Determination of the Fischer-Tropsch activity and selectivity of the catalyst
- Assessment of the responsiveness of the catalyst to chemical promotion

University of Cape Town

Chapter 2

HYDROTALCITES – A LITERATURE REVIEW

University of Cape Town

2.1. Hydrotalcite structure

Hydrotalcite or magnesium-aluminium hydroxycarbonate is a naturally occurring anionic clay. The name *hydrotalcites* will be taken as the reference name for the many other isomorphous and polytypic compounds. The structure of these compounds is similar to the structure of brucite, $Mg(OH)_2$, where the octahedral edges of the Mg^{2+}, which are co-ordinated to OH^- ,are shared to form infinite sheets (Figure 2.1). These sheets are stacked on top of each other and are held together by hydrogen bonding [Cavani, 1991].

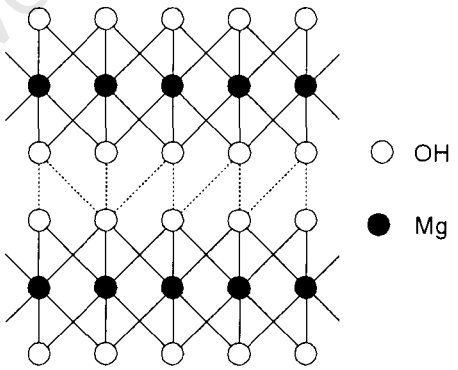

Figure 2.1: Brucite ($Mg(OH)_2$) structure (dotted lines represent H-bridging between the sheets) [Spamer, 2000]

The Mg^{2+}-ions in the brucite sheets can be replaced with trivalent ions with similar ionic radius. This leads to a net positive charge of the sheets. The charge is compensated for by anions, positioned between the sheets in the inter-layer region along with the water of crystallization [Cavani, 1991]. The basic structure of hydrotalcite is shown in Figure 2.2 and can be represented by the general formula: $[M_{1-x}^{2+}M_x^{3+}(OH)_2]^{x+}[A^{n-}_{x/n}].mH_2O$, where $x = M^{3+}/ M^{2+} + M^{3+}$ [Cavani, 1991].

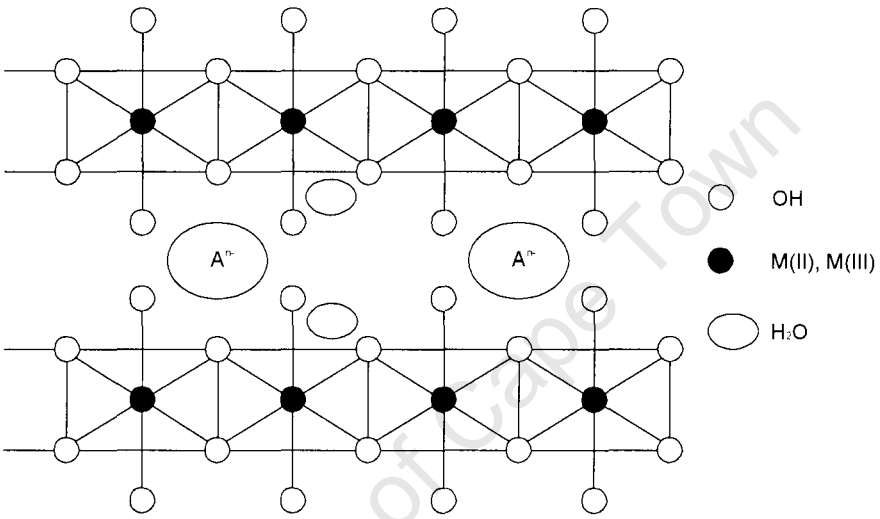

Figure 2.2: Hydrotalcite structure [Spamer, 2000]

University of Cape Town

In the hydrotalcite structure the nature and ratio of metal ions, type and charge of balancing anion, and amount of interlayer water can be varied. In naturally occurring hydrotalcite, the fraction of trivalent ions in the structure, x, is usually 0.25, and carbonate ions are present to balance the charge [Cavani, 1991]. Pure synthetic hydrotalcites are generally produced with M^{2+}/ M^{3+} ratios of between 4:1 and 2:1 (or x between 0.2 and 0.33) [Vaccari, 1999]. In the case of Mg-Al hydrotalcites, it has been observed that this prevents the formation of adjacent Al^{3+} ions [Vaccari, 1999]]. At values of x larger than 0.33, the number of octahedral Al^{3+}-ions increases, which leads to the formation of $Al(OH)_3$. With a low Al^{3+}-content, the density of octahedral Mg^{2+} is high, which results in the formation of $Mg(OH)_2$.

Table 2.1: Cations with ionic radii suitable for hydrotalcite preparation [Cavani, 1991]

M^{2+}	Mg	Cu	Ni	Co	Zn	Fe
	0.65	0.69	0.72	0.74	0.74	0.76
M^{3+}	Ga	Ni	Co	Fe	Mn	Cr
	0.62	0.62	0.63	0.64	0.66	0.69

Hydrotalcites have however been synthesized outside the above mentioned range of M^{2+}/ M^{3+} ratios of between 4:1 and 2:1 [Schaper, 1989, Shen, 1996]. Shaper *et al.* have synthesized Mg-Al hydrotalcites with Mg/Al ratios of between 5:1 and 10:1 without the formation of considerable amounts of separate magnesium compounds. This was achieved by carefully controlling the co-precipitation conditions such as mixing, pH and temperature. Outside these Mg/Al ranges however, large quantities of $Mg(OH)_2$ were observed [Schaper, 1989]

The anions and water molecules in the interlayer region form bonds with the skeletal hydroxide ions. For the Mg-Al hydrotalcite containing the carbonate anion, hydrogen bonds are formed between the oxygen atoms of the carbonate and water molecules and the hydrogen atoms of the hydroxide ions (see Figure 2.3). The thickness of the interlayer region is dependent on the size and charge of the anion, amount of the M^{3+}, and the bond strength between the anions and hydroxide ions. Increasing the interlayer thickness by increasing the size of the anions is referred to as pillaring. Some of the anions that may be used include $[Fe(CN)_6]^{4-}$, $PMo_{12}O_{40}$, $PW_{12}O_{40}$ and organic acids such as adipic, oxalic and succinic acid [Cavani, 1991].

University of Cape Town

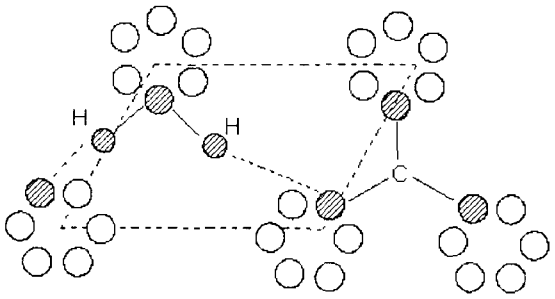

Figure 2.3: Bonding in the interlayer region of a hydrotalcite [Cavani, 1991]

2.2. Hydrotalcite synthesis

The synthesis of hydrotalcites usually includes the following steps: precipitation, ageing, washing, drying and calcination (see Figure 2.4). The metals are precipitated out using a base. The precipitate is typically aged to transform amorphous material into crystalline material and to grow small crystals. In the washing step alkali metals and nitrate ions are removed. The excess solvent is removed during the drying and calcination step.

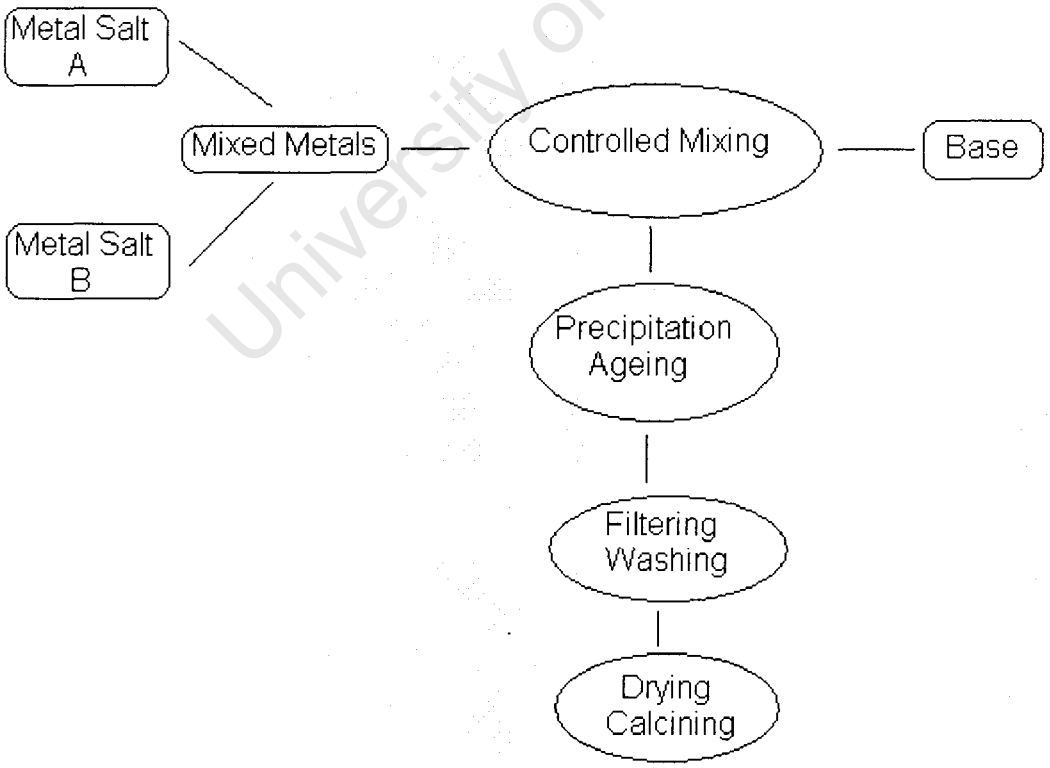

Figure 2.4: Flow diagram of the synthesis of hydrotalcites

University of Cape Town

Co-precipitation is typically the first step in the preparation of hydrotalcites. Almost all the metal hydroxides forming hydrotalcites will precipitate at a pH of between 8 and 10 [Cavani, 1991]. The precipitation methods used are the increasing pH method, the constant pH method at high super-saturation, and the constant pH method at low super-saturation.

The increasing pH method involves addition of an alkali solution to a solution containing the metal ions until the desired pH is reached. This method often results in the sequential precipitation of ions and in such cases it is not possible to directly precipitate a pure hydrotalcite [Cavani, 1991]. In the preparation of the Mg-Al hydrotalcite, $Al(OH)_3$, which precipitates at a lower pH than the Mg-Al hydrotalcite, is also formed (see Figure 2.4).

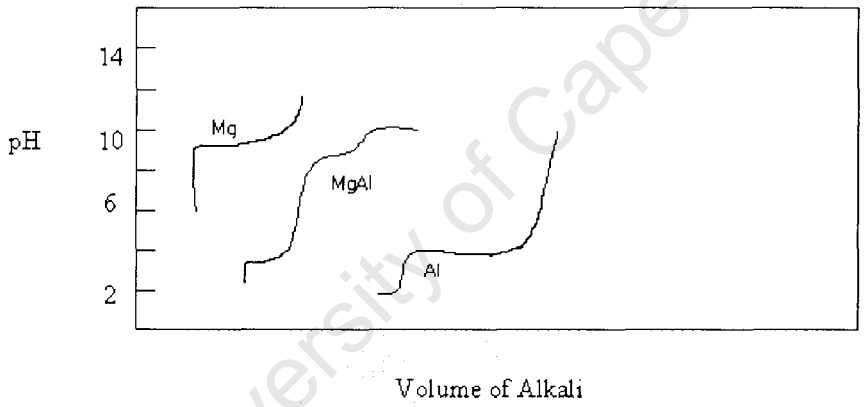

Figure 2.4: pH of the solution as a function of the volume of alkali added in the precipitation of $Mg(OH)_2$ (Mg), $Al(OH)_3$ (Al) and hydrotalcite (MgAl) [Cavani, 1991]

Preparation using the constant pH method at high super-saturation is carried out by rapidly adding a solution containing the metal ions to an alkali solution. This method generally gives rise to a large number of particles, which are usually small in size because the rate of nucleation is higher than the rate of crystal growth [Cavani, 1991].

University of Cape Town

Precipitation at constant pH under conditions of low super-saturation is achieved by having low concentrations of the reagents and low flow rates of the two streams when the solution of metal ions is added to the alkali solution. This precipitation method produces a precipitate, which is more crystalline, compared to the one obtained at high super-saturation conditions [Cavani, 1991].

The precipitation method generally used for preparing these compounds is precipitation at low super-saturation and constant pH. The conditions most commonly utilized are a pH ranging from 7 to 10 (depending on the metals being precipitated), a precipitation temperature between 60 and 80°C, and a low concentration of reagents and low flow rate of the reagent streams. Washing is carried out with warm water and is usually followed by ageing under precipitation conditions. The precipitate is finally dried at temperatures that do not exceed 120°C [Cavani, 1991].

Changes in the preparation conditions affect the properties of the compounds produced. The effect of the preparation variables on the hydrotalcite synthesis are summarized in Table 2.2.

Table 2.2: Influence of synthesis conditions in hydrotalcite synthesis on final product

Synthesis Conditions	**Catalyst Properties Influenced**
Precipitation pH	Purity of Hydrotalcite
Precipitation Temperature Reagent Concentration Flow Rate of Reagents Ageing	Crystallite Size

University of Cape Town

Preparation using an increasing or varying pH may result in the formation of other phases in addition to the hydrotalcite. Therefore, under such conditions, it is not possible to precipitate pure hydrotalcite compounds [Cavani, 1991].
The precipitation temperature affects the crystallite size. An increase in the precipitation temperature results in an increase in the rate of nucleation, and thus smaller crystallites are obtained. A similar effect is observed by increasing the reagent concentration and the rate at which they are added together. These effects can be minimised or eliminated by ageing [Cavani, 1991].

2.2.1. Calcination

The calcination may affect structural changes in the compounds, which is exemplified in Figure 2.6 for a Mg-Al hydrotalcite with carbonate anions. Heating to temperatures above 200°C results in the loss of water molecules, but the skeletal hydroxide and the interlayer carbonate are retained [Vaccari, 1999]. Skeletal hydroxide groups and carbonate ions are removed from the structure (in the form of water and carbon dioxide respectively) upon further heating from 275-450°C. This happens without extensive change in crystal morphology and is accompanied by an increase in the surface area and pore volume of the solid [Vaccari, 1999]. Calcination at this temperature results in the formation of a mixed oxide catalyst.

Rehydration with a carbonate-containing aqueous solution will regenerate the hydrotalcite, if the calcination temperature did not exceed 600°C. This is the so-called "memory effect". Heat treatment above 600°C results in irreversible changes to the crystal structure [Cavani, 1991].

The evolution of carbon dioxide is almost complete at 500°C for hydrotalcites with a lower Al ion content. It has been concluded that the carbonate ions are located in the positively charged area around the Al ions, and the amount of carbonates in the calcined material increases with increasing Al-content [NIRE Report, 2002]. Mg-Al hydrotalcites with a high Al content retain ca. 20-30% of the carbonate ions upon calcination at temperatures up to 500°C.

University of Cape Town

The evolution of these carbonates takes place at higher temperatures at which the Al ions have been found to migrate into the tetrahedral positions to form spinel structures with the Mg ions.

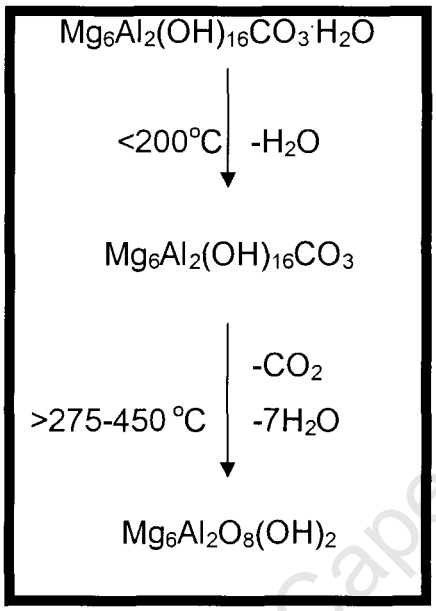

Figure 2.6: Changes occurring during heat treatment of a Mg-Al hydrotalcite with carbonate anions

The influence of calcination temperature on the bulk and surface properties of a Mg/Al mixed oxide derived from a hydrotalcite precursor was investigated by Shen *et al.* (1998) (see Table 2.4). The samples that were analysed were calcined at 400, 600 and 800°C. The surface area of the Mg-Al samples decreased from 194 to 115m^2/g on increasing the calcination temperature. This was compared to the decrease in surface area of MgO with increasing calcination temperature from 256 to 38m^2/g (Table 2.3) indicating the Mg-Al binary oxide was more stable under heat treatment, which is in agreement with the work done by Shaper *et al.*(1989).

University of Cape Town

Calcination at different temperatures also resulted in changes in the acid/base properties of the compounds [Shen, 1998]. This was attributed to the phase transitions that occurred during the calcination. Calcination at temperatures above 400°C resulted in the transition of the Al^{3+} from the octahedral position (Al_O) to the tetrahedral position (Al_T) with the corresponding formation of a spinel-like phase. This resulted in a decrease in the basicity of the compounds.

Table 2.3: Influence of calcination temperature on the physical properties of hydrotalcite and MgO samples [Shen, 1998]

Mg-Al Hydrotalcite			
$T_{calcination}$, °C	S_{BET}, m^2/g	V_{pore}, cm^3/g	d_{pore}, nm
400	194	0.43	8.9
600	132	0.41	13
800	115	0.45	15
MgO			
$T_{calcination}$, °C	S_{BET}, m^2/g	V_{pore}, cm^3/g	d_{pore}, Å
400	256	0.42	6.6
600	200	0.35	7.0
800	38	0.16	16.5

At temperatures above 600 °C a further transition occurred from the Al_T-O-Mg to Al_T-O-Al_O. It was postulated [Shen, 1998] that the migration of the Al_T away from the Mg^{2+} might leave more O^{2-} anions surrounding Mg^{2+}, which would account for the observed increase in basicity. This latter transition was reversed to some extent in the sample calcined at 800°C and thus the basicity of the samples was found to decrease in the following order: MgO>600°C> 800°C>400°C. The acidity of the samples decreased in the following order: Al_2O_3>400°C>600°C~800°C. This was attributed to the decrease in the Al_O/Al_T ratio which occurred upon increasing the calcination temperature [Shen, 1998].

University of Cape Town

2.3. Acid/Base properties of hydrotalcites

The nature, density and strength of the surface acid/base sites were found to depend on the Mg/Al ratio [Di Cosimo, 1998]. The investigations by *Cosimo et al.* (1998), using CO_2 as a probe molecule for adsorption/desorption studies on hydrotalcites calcined at 500°C with varying Mg/Al ratio, showed that the compounds contained surface sites of varying basicity. A decrease in the Mg/Al ratio resulted in: a decrease in the basicity of the compounds as the low and medium basic sites were found to increase; as well as a decrease in the density of the surface basic sites because of Al surface enrichment.

Catalytic conversion of ethanol over these compounds showed that the selectivity of the products formed was dependent on the composition of the hydrotalcite precursor and hence the acid/base nature of the surface. Alcohols can undergo conversion to aldehydes (see Figure 2.7) and they can also be dehydrated to olefins over acid/base catalysts (see Figure 2.8). The former reaction requires a catalyst with a stronger basicity and maxium rates for this reaction was observed at higher Mg/Al ratios [Di Cosimo, 1998].

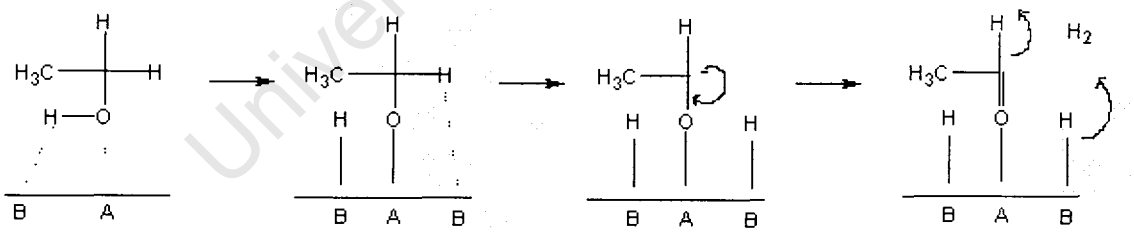

Figure 2.7: Proposed mechanism for the conversion of ethanol yielding acetaldehyde over a hydrotalcite [Di Cosimo, 1998].

University of Cape Town

Both the formation of acetaldehyde and the formation of ethene, as illustrated in Figures 2.7-2.8, involves in the first step the adsorption of the ethanol molecule and cleavage of the O-H bond, on an acid-base pair site giving rise to a surface ethoxy group. Formation of the aldehyde requires abstraction of the H on the ethoxy group by a strong basic site. The olefin is formed by abstraction of an acidic α hydrogen from the neighbouring carbon atom. Thus the formation of the aldehyde is favoured by catalysts containing strong basic sites and olefin formation is preferred on catalysts with lower basicity.

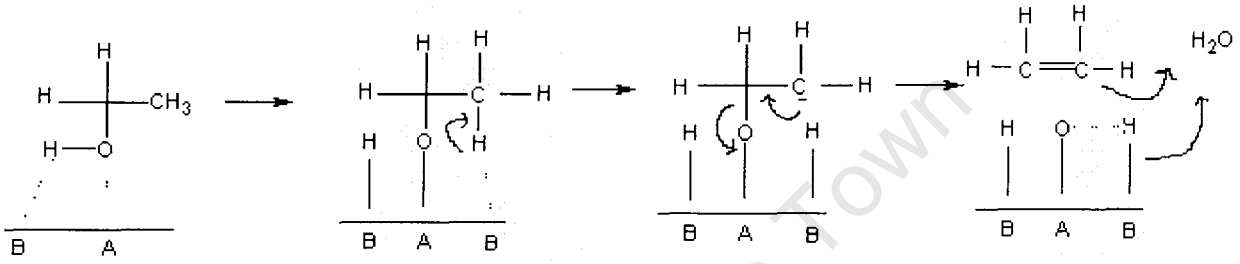

Figure 2.8: Proposed mechanism for the conversion of ethanol yielding ethene over a hydrotalcite [Di Cosimo, 1998].

Table 5: Catalytic Results for Ethanol Conversions on MgO, Al_2O_3 and Hydrotalcites with Varying Mg/Al Ratios [Di Cosimo, 1998].

	Ethanol	**Formation Rate/μmol/h m^2**	
Sample	**Conv/μmol/h m^2**	**Acetaldehyde**	**Ethylene**
MgO	0.89	0.28	0.04
Mg/Al = 8	8.35	4.64	0.06
Mg/Al = 4	4.24	2.55	0.07
Mg/Al = 3	4.55	1.10	0.08
Mg/Al = 1	9.17	0.29	0.57
Mg/Al = 0.5	9.84	0.26	0.60
Al_2O_3	48.15	0.08	28.57

University of Cape Town

2.4. Reduction behaviour of iron-containing hydrotalcites

Reduction is a typical pre-treatment prior to utilisation of the catalyst in the actual Fischer-Tropsch synthesis. Hence, an understanding on the actual reduction behaviour of the hydrotalcites is of importance. Shen et al. [1996] investigated the reduction of Fe-Mg hydrotalcites with different Mg/Fe ratios in addition to a pure iron catalyst. Reduction of the Mg-Fe samples was found to proceed in two steps from Fe^{3+} to α-Fe through Fe^{2+}. Pure iron samples were completely reduced to α-Fe at 400°C however less than 60% of the Fe species in the calcined Mg-Fe hydrotalcite samples were reduced to α-Fe at 500°C (see Table 2.5). This is possibly due to the migration of the Fe^{3+} from the octahedral position to the tetrahedral position with the subsequent formation of a stable spinel-like compound that may be more difficult to reduce.

Table 2.5: Distribution of iron species of calcined Mg-Fe hydrotalcites reduced at 400 and 500°C [Shen, 1996]

Sample	**400°C**			**500°C**		
	Fe^{3+}	Fe^{2+}	Fe^{0}	Fe^{3+}	Fe^{2+}	Fe^{0}
1Mg/Fe	0	62	38	0	40	60
3Mg/Fe	0	100	0	0	76	24
6Mg/Fe	36	64	0	0	75	25

University of Cape Town

2.5. Hydrotalcites as catalysts for the Fischer-Tropsch synthesis

Shen et al. [1996] investigated the Fischer-Tropsch activity of Fe-Mg hydrotalcites. Pure iron as well as Mg-Fe hydrotalcites with different Mg/Fe ratios were tested. The samples were pre-reduced in H_2 at 500°C for 4 hours. The reaction was carried out at 320°C and atmospheric pressure with a H_2/CO ratio of 2. The obtained results are summarized in Table 2.6.

With increasing magnesia content, the methane production decreased while the production of higher hydrocarbons (C_2-C_5) and the olefin/paraffin ratio in the hydrocarbon products increased. This was attributed to the increase in the basicity of the catalyst with increasing Mg/Fe ratio. Increased magnesia content however also resulted in a decrease in the activity of the catalyst. This decrease was attributed to the decrease in the degree of reduction of the iron species to elemental iron, which appeared to be retarded by the presence of the Mg [Shen, 1996].

University of Cape Town

Table 2.6: Activity of an iron catalyst and hydrotalcites with different Mg:Fe ratios in the Fischer Tropsch synthesis at 320°C and atmospheric pressure with a H_2/CO ratio of 2 (catalyst reduced in H_2 at 500°C for 4 hours) [Shen, 1996]

Catalyst		Iron	1 Mg/Fe	3 Mg/Fe	6 Mg/Fe
CO Conv/%		96.7	82.2	24.3	17.8
CO_2 Selectivity/%		9.5	40.9	37.7	41.4
Hydrocarbon Distribution	C_1	58.4	48.8	34.0	37.7
	C_2	18.7	20.4	17.2	18.1
	C_3	14.9	21.2	31.8	28.6
	C_4	4.6	5.1	11.9	10.4
	C_5	3.4	4.6	5.1	5.2
Olefin/Paraffin Ratio	$C_2^=/C_2$	0.009	0.07	0.44	0.98
	$C_3^=/C_3$	0.006	0.32	0.65	5.55
	$C_4^=/C_4$	0.25	0.11	0.55	0.42

University of Cape Town

2.5.1. Further development of hydrotalcites as catalysts for the Fischer-Tropsch synthesis

The increase in reducibility and decrease in basicity of the Mg-Fe hydrotalcite is a function of the Mg/Fe ratio and will thereby lead to an optimum in the Fischer-Tropsch activity and selectivity. The calcination temperature will however also affect the activity. This relationship is however more complex. The addition of alkali, such as K_2O may help to increase the basicity of the catalyst without the addition of further magnesium thus avoiding the negative impact of the magnesium on the reducibility of the iron. Copper may also be added to the catalyst as it has been shown to enhance the reducibility of the iron [Bukur, 1990a]. This may improve the activity of the catalyst or it may allow for a higher amount of magnesium to be used if needed.

In the development of a hydrotalcite catalyst for use in the Fischer Tropsch process, these aspects along with the preparation and operating conditions need to be investigated and optimized.

University of Cape Town

Chapter 3

EXPERIMENTAL PROCEDURES

University of Cape Town

3.1 Catalyst Preparation

The preparation procedure includes the following steps: precipitation, using the technique mentioned in the previous chapter; ageing, to transform amorphous material into crystalline material and to grow small crystals; washing, to remove the alkali metals and nitrate ions; drying; and calcination.

Precipitation at constant pH under conditions of low super-saturation is the preferred method for the preparation of the hydrotalcites as it affords a more crystalline precipitate, compared to the one obtained at high super-saturation conditions [Cavani, 1991]. Low super-saturation, constant pH conditions are achieved by having low concentrations of the reagents and low flow rates of the two streams when the solution of metal ions is added to the alkali solution.

The hydrotalcite with ratio Mg/Fe = 2/1 was prepared (from chemically pure reagents) starting from a solution containing 1 mol/dm^3 of $Mg(NO_3)_2 \cdot 6H_2O$ and 0.05 mol/dm^3 of $Fe(NO_3)_3 \cdot 9H_2O$ (supplied by Merck). The solution was prepared using deionised water. A second solution was made with 3.5 mol/dm^3 NaOH and 1 mol/dm^3 Na_2CO_3 (supplied by Merck) in deionised water.

A 100 ml of each of the two solutions were then added into 200ml of deionised water in a round bottom flask at room temperature. This addition was carried out drop-wise and under vigorous stirring so as to maintain the pH between 8 and 10. The precipitate was then aged at 65 °C for 18 hours. Thereafter the aged slurry was filtered and washed until the filtrate was at a pH of approximately 7. The filtered precipitate was then dried at 100 °C for 18 hours. Hydrotalcites with different Mg/Fe ratios were prepared (see Table 3.1) in the same manner, adjusting the molar ratio of Mg^{2+}/ Fe^{3+} (2:1; 3:1 and 6:1) keeping the total number of moles of Mg^{2+} plus Fe^{3+} constant at 1.5 mol/dm^3.

Work done on Mg-Al hydrotalcites by *Shen et al.*(1998) have shown that the basicity of the hydrotalcites calcined at 600°C was the highest, compared to those calcined at 400 and 800°C. Rehydration of the hydrotalcite may take place if the calcinations temperature does not exceed 600°C (memory effect) [Cavani, 1991]. In-situ calcinations studies that were done in the present work show that at temperatures around 625°C, the mixed metal oxides forms. Taking all the above mentioned considerations into account, the calcination of the prepared hydrotalcites in this study were carried out at 625°C, in a static oven under air. The calcinations were done in a stepwise manner which entailed; heating the sample in 100°C increments at a heating rate of approximately 3.5°C/min and keeping the sample at a constant temperature for 30 minutes after each increment.

Two calcined hydrotalcite samples were chemically promoted via impregnation, viz. one with 0.2g of K_2O and the other with 6g Cu per 100g iron. The required amount of promoter precursor (KNO_3 or $Cu(NO_3)_2$) (supplied by Merck) was dissolved in a mixture of methanol and water (3 parts methanol to 1 part water). The impregnation solution was mixed with the calcined hydrotalcite. The solvent was removed in a rotary evaporator at 80°c, 200mbar and 60rpm. A homogeneous distribution, of the promoter material onto the surface of the calcined hydrotalcite, was obtained by controlling the drying rate and rotation

University of Cape Town

speed. After evaporation the impregnated catalyst was calcined again up to 300 °C in a static oven, under air and in the stepwise manner as described above to remove any residual nitrates.

3.2. Catalyst Characterisation

3.2.1. Chemical Composition

All elements present in the samples with the exception of iron were analysed with Inductively Coupled Plasma Atomic Emission Spectroscopy (ICP-AES). The samples were dissolved under reflux in a known quantity of hydrochloric acid and diluted to a set volume. They were thereafter analysed with the ICP-AES. Standards containing the same amount of iron as the samples were prepared.

The ICP-AES used was a Varian model sequential instrument with a glass concentric design nebuliser, a PTFE spray chamber and a glass torch. The RF source was a 40MHz source and the instrument was set at a forward power of 1.3kW.

The iron content of the samples was determined by titration. The samples were dissolved in hydrochloric acid. The Fe^{3+} in the acid solution was then reduced to Fe^{2+} with $SnCl_2$. The residual Sn^{2+} was reduced to Sn^0 with $HgCl_2$. The Fe^{2+} in the sample was then titrated with a 0.05M $K_2Cr_2O_7$ solution and sodium di-phenyl amine sulphonate as an indicator to the endpoint.

University of Cape Town

3.2.2 Catalyst Morphology

3.2.2.1 Crystallographic Phase Analysis

X-ray diffraction (XRD) analysis was performed on the prepared hydrotalcites to verify the presence of the hydrotalcite structure. The XRD scans were done with either the Phillips or the Siemens Unit. The calcined hydrotalcites were also

submitted for XRD, after grinding and sieving to a particle size of between 38-150μm.

Table 3.1: Experimental conditions for recording X-ray diffraction patterns

	Philips	**Siemens**
High voltage	40 kV	40 kV
Tube current	25 or 40 mA	25 or 40 mA
Divergence slit	1 °	1 °
Anti-scatter slit	2 °	1 °
Detector	X'Celerator	Scintillation
Scan from	5 °2θ	5 ° 2 θ
Scan to	105 °2θ	105 °2θ
Soller slits	0.04 rad	0.04 rad
Scanning	Continuous	Step
Duration of scan	2 hours	45 minutes
Atmosphere	Air	Air
Temperature	Ambient	Ambient
Source	Cobalt	Cobalt
Wavelength	1.78897 Å	1.78897 Å

In-situ calcination and reduction studies were carried out with the Philips unit. The conditions of the instrument were as shown above in table 3.1 with the following exceptions:

Calcination Studies

Detector: HT camera

Duration of scan: 15 minutes

Atmosphere: Nitrogen

Temperature: 5°C/min (heating rate)

University of Cape Town

Reduction Studies

Tube current	50mA
Duration of scan:	15 minutes
Atmosphere:	Hydrogen
Temperature:	5°C/min (heating rate)

3.2.2.2 Surface Area Analysis

The catalyst surface area was determined using the physiosorption of nitrogen on a Micromeritics Gemini instrument. The samples were degassed under a nitrogen blanket for an hour at 90°C. The oven temperature was then increased to 250°C for 4 hours to clean up the catalyst surface. The saturation pressure was set to 760mm Hg and the measurement was done at 77K.

The strength of the physical adsorption of gases by solids increases with a decrease in temperature and an increase in pressure. The equation used for the relationship between the amount of gas adsorbed and the total surface area of the solid is commonly known as the BET equation.

$$\frac{P}{[V_a \cdot (P_0 - P)]} = \frac{1}{V_m \cdot C} + \frac{(C-1)}{V_m \cdot C} \cdot \frac{P}{P_0} \qquad (3.1)$$

With:
- P_0: saturation pressure of nitrogen
- P: Pressure at measurement point
- V_a: Quantity of nitrogen gas adsorbed at pressure P
- V_m: Quantity of nitrogen gas adsorbed when entire surface is covered with monolayer
- C: Constant

From a plot of $P/(V_a \cdot (P_0-P))$ versus P/P_0 the volume of the monolayer, and thus the surface area can be calculated (assuming that the area of a N_2 molecule is 16.2Å).

University of Cape Town

3.2.3 Thermal Gravimetric Analysis (TGA)

Thermal gravimetric analysis (TGA) was carried out on an unpromoted hydrotalcite with Mg/Fe=2/1 to determine its thermal behavior. The TGA was carried out in a SDT 2960 Simultaneous DSC-TGA instrument. The DSC-TGA instrument was coupled to a Pfeiffer Thermostar Quadrole Mass Spectrometer.

Approximately 10mg of sample was loaded into the TGA instrument. The sample was heated in air at 10°C/min up to 1000°C. The experiment was repeated at a heating rate of 1°C/min with the aim of achieving better resolution of the peaks and to determine if there were any other transitions taking place that may have been missed at the higher heating rate. A further experiment was done where the sample was heated in nitrogen at 1°C/min to determine if thermal decomposition of the hydrotalcite would be influenced by an inert atmosphere.

3.2.4 Temperature Programmed Reduction (TPR)

A Micromeritics Autochem 2910 instrument was used to perform the TPR on an unpromoted hydrotalcite derived catalyst in order to determine the temperature at which the catalyst reduces. Approximately 0.05g of sample was weighed out into a quartz U-tube. A helium flow 50ml/min was passed over the sample at 120°C to dry the sample. The temperature programmed reduction was performed with 10% H_2 in argon at a flow rate of 50ml_n/min. The sample was heated at a rate of 10°C/min up to 900°C. The concentration of hydrogen in the effluent was measured using a Thermal Conductivity Detector (TCD). The effluent passed through a Dewar containing dry-ice and acetone prior to entering the TCD to condense any water in the carrier gas line to the detector as the presence of water in the gas would influence the TCD signal.

University of Cape Town

3.3 FISCHER-TROPSCH SYNTHESIS

The catalysts were tested with an experimental set-up (see Figure 3.1) consisting of a feed gas unit, a reactor, hot and cold traps to collect the products, and on-line GCs (TCD and FID) for the analysis of the feed and tail gas products.

University of Cape Town

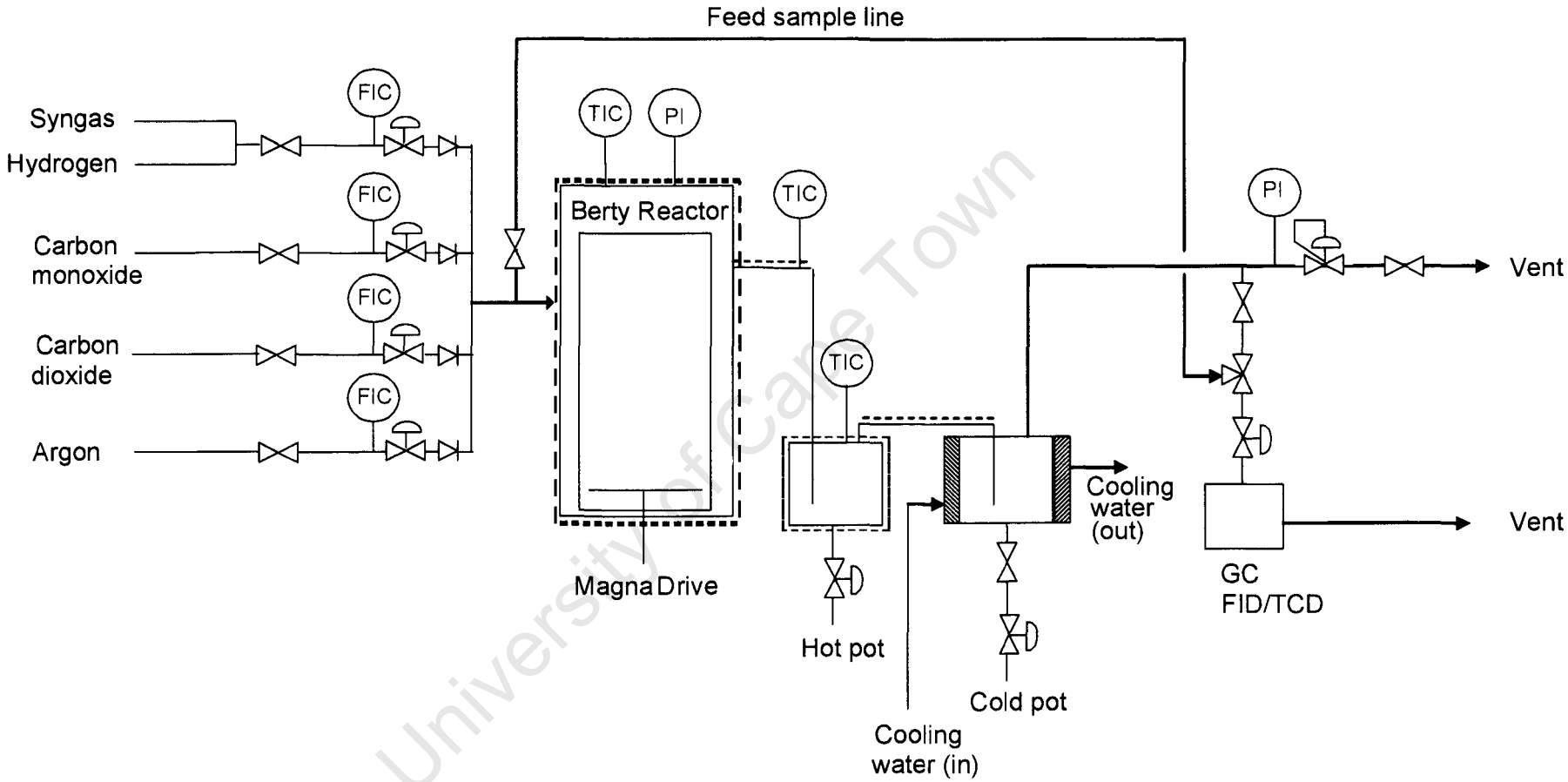

University of Cape Town

Figure 3.1.: Experimental Set-up for Fischer-Tropsch Synthesis

3.3.1. The Reactor

Fischer-Tropsch synthesis was performed in a differential internal-recycle Berty micro reactor (see Figure 3.2). The Berty reactor has a high internal recycle and is considered to approximate a continuous stirred tank reactor, CSTR. The reactor volume is approximately 300 cm^3 and it can be operated at high pressures (<100bar) and temperatures (<873K).

The catalyst was distributed across the insert and covered with a piece of glass wool to keep it in place. The insert, on which the catalyst is supported, is made up of a woven gauze that is stuck onto a metal mesh. The woven gauze has pores of approximately 12μm. The diameter of the insert on which the catalyst rests is 70mm and it has a surface area of 38.5cm^2.

The rotation of impeller vanes which are situated at the bottom of the reactor (see Figure 3.2) causes a slight reduction in the pressure underneath the gauze and this sucks reacting gases through the gauze. The gas flow in the reactor is then upwards from the impeller and then down through the catalyst bed.

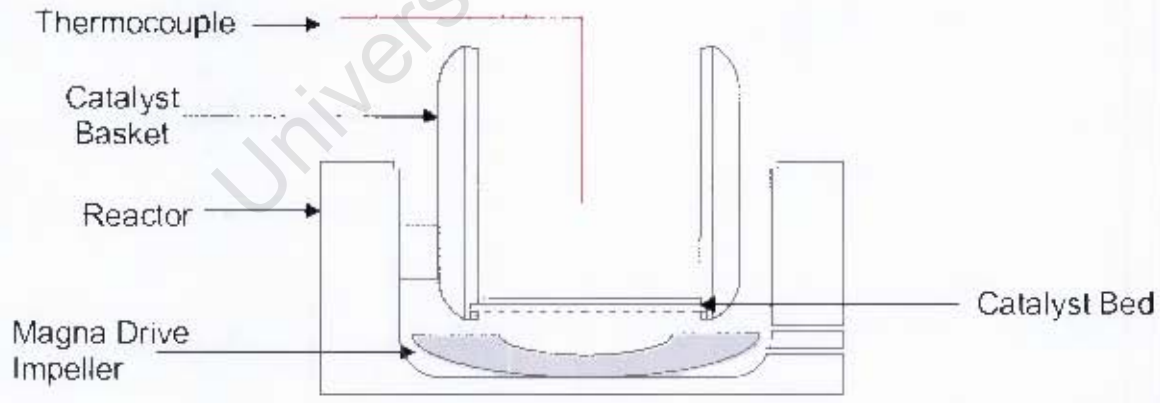

Figure 3.2: Schematic of a Berty microreactor set-up

University of Cape Town

The reactor is heated by a heating mantle. The temperature is measured by two thermocouples. The one thermocouple measures the temperature in the reaction medium and the other is inserted between the heating mantle and the reactor wall. The thermocouple inside the reactor is used by the master temperature controller, and the other is used by the slave controller.

The gas outlet and hot trap lines were heated by means of electrical heaters, each of which was controlled by separate temperature controllers. The pressure in the reactor was maintained at the set value by using a backpressure regulator.

3.3.2. Feed to the Reactor

The gases fed to the reactor were delivered from gas bottles through their respective lines. The gas flows were controlled with Brooks mass flow-controllers.

The gases fed to the reactor were: carbon monoxide; hydrogen, which collectively makes up what is known as synthesis gas (syngas); argon, which is fed as an internal standard; and carbon dioxide which was co-fed in an attempt to attain equilibrium of the water gas shift reaction.

3.3.3. Product sampling

The reactor set-up is configured so that the reactor effluent passes through cooling and knock-out stages. The hot knock-out pot (500ml) is kept at a temperature of 190°C and condenses waxy hydrocarbons. In the cold knock-out pot (500ml), the light oil and reaction water phases are condensed at 5°C. Negligible amounts of waxy hydrocarbons were produced under the current experimental conditions. The gas lines are connected to two on-line gas chromatographs after the cold knock-out pot.

University of Cape Town

3.3.4. Start-up of the reactor, activation of the catalyst, and synthesis conditions

The catalysts were ground and sieved to obtain a particle size distribution of between 38-150μm. The reactor was loaded with 5g of sieved catalyst placed onto the insert. The reactor was sealed off and heated to activation temperature under argon. During heating the pressure was increased to the set point with the back-pressure regulator. The reactor was then tested for leaks after which the catalyst was activated by passing pure hydrogen over it at the activation conditions (see Table 3.2).

Table 3.2: Activation conditions used prior to catalyst testing

Reducing gas	H_2
Unreduced catalyst mass	5.0 g
Temperature	693 K
Pressure	2.0 MPa
Reduction time	16 hrs

After activation the hydrogen flow is replaced by argon and the temperature is reduced to synthesis temperature. Once at synthesis conditions, the reactor is again checked for leaks. Table 3.3 summarizes the synthesis conditions.

After completion of the Fischer-Tropsch synthesis, all the gases to the reactor were shut off once synthesis was terminated with the exception of argon. The impeller was turned off, the temperature was reduced to room temperature and the pressure was gradually released. Once the reactor was cool the catalyst was unloaded.

University of Cape Town

Table 3.3: Reaction conditions for the Fischer-Tropsch synthesis after catalyst activation (see Table 3.2)

Unreduced catalyst mass	5.0 g
Temperature	603 K
Pressure	2.0 MPa
GHSV	13 $l_n/(g_{cat}.hr)$
Stirrer Speed/rpm	1700 rpm
Feed composition:	
y_{H2}	0.580
y_{CO}	0.145
y_{CO2}	0.130
y_{Ar}	0.145
$(H_2/CO)_{inlet}$	4

3.3.5. Analysis of Fischer-Tropsch Products

The feed and tail gas samples were analysed on two on-line gas chromatographs; the one equipped with two thermal conductivity detectors (Gow Mac TCD) and the other equipped with a flame ionization detector (HP FID). The TCD was used to analyse for the permanent gases H_2, CO, CO_2, Ar, CH_4 and N_2 and the FID was used to analyse the hydrocarbons in the gases, including CH_4. The liquid product knocked out in the cold-pot was drained and separated into an oil fraction and a water fraction. These products were analysed using an off-line GC equipped with a FID.

To enable the calculation of the hydrocarbon flow rates into and out of the system on the same basis as the flow rate of the permanent gases, a tie substance is required. Methane, which is detected by both the thermal conductivity and flame ionization detectors, is used as a tie component.

University of Cape Town

Table 3.4. Operating Conditions of the Gas Chromatographs

Species	GC	Column details	Temperature [°C]	Detector
H_2	Gow-Mac 600	Restek PPQ Molecular Sieve 5Å, Packed 1m x 45.7mm	25-120	TCD
CO, CO_2, CH_4, Ar, N_2	Gow-Mac 600	Restek Shin Carbon 80/100 µ, Packed 2m x 45.7mm	25-120	TCD
Hydrocarbons in tail gas	HP 6890	Varian CP Sil 5 CP, Capillary 25m x 150µm x 20µm	10-280	FID
Water fraction	HP 6890	Varian CP Sil Pona, Capillary 50m x 210µm x 0.50µm	35-120	FID
Oil Fraction	HP 6890	Varian CP Sil Pona, Capillary 50m x 210µm x 0.50µm	35-300	FID

For the analysis of H_2 on the Gow Mac TCD, argon was used as carrier gas. On the second TCD the CO, CO_2, CH_4, and Ar concentrations were determined with helium as the carrier gas. The TCDs were calibrated with gas mixtures, which contained known concentrations of Ar, N_2, CO, CH_4, H_2 and CO_2.

For the analysis of the gaseous organic products the on-line Perkin Elmer gas chromatograph was used with helium as the carrier gas. The separation of the gaseous hydrocarbons was achieved with a CPSil5 capillary column using a temperature program. The temperature program started off at 10°C, was held for 5 minutes, after which it was increased at 2°C per minute to 280°C. The other operatingl conditions are given in Table 3.4.

The light oil and water products from the cold knock-out pot were analysed on a HP gas chromatograph equipped with an FID and PONA capillary column. Hydrogen was used as carrier gas. For the analysis of the water fraction the temperature program started off at 35°C, was held for 5 minutes, after which it was increased at 4°C per minute to 120°C. For the analysis of the oil fraction the temperature program started off at 35°C, was held for 5 minutes, after which it was increased at 4°C per minute to 300°C where it was held for 14 minutes.

University of Cape Town

The acids in the water were determined by an acid base titration. The quantity of alkali needed to neutralize the acids was determined and the acidity was calculated and reported as mgKOH/g of water.

3.3.6. Data Analysis

3.3.6.1. Calculation of Flow Rates from Gas Chromatographic Analysis

The addition of Ar, as the internal standard at a known flow rate enables the calculation of the flow rates of the inorganic compounds and methane using the peak areas obtained in the GC analysis with a TCD.

$$\dot{n}_i = \frac{y_i^c}{y_{Ar}^c} \cdot \frac{A_{Ar}^{TCD,c}}{A_i^{TCD,c}} \times \frac{A_i^{TCD}}{A_{Ar}^{TCD}} \cdot \dot{n}_{Ar,in} \qquad (3.2)$$

$n_{Ar,in}$: molar flow of argon into the reactor (equals the molar flow rate out of the reactor assuming steady-state), mol/s

n_i: molar flow rate of compound i, mol/s

y_i^c: mole fraction of compound in the reference gas

y_{Ar}^c: mol fraction of Ar in the reference gas

A_{Ar}^{TCD}: peak area of argon from GC analysis in gas stream to be analysed

A_i^{TCD}: peak area of compound i in from GC analysis in gas stream to be analysed

$A_{Ar}^{TCD,c}$: peak area of argon from GC analysis in reference gas analysis

$A_i^{TCD,c}$: peak area of compound i in from GC analysis in reference gas analysis

Quantification of the hydrocarbons requires the use of another standard, since the FID is only able to detect hydrocarbon products and thus the results cannot be normalised to 100%. Methane is used as a tie substance as it is detected by both the TCD and FID. It is therefore accurately determined by the TCD by relating it to the flow rate of argon and this is then used to calculate the flows of the organic product compounds determined by the FID.

University of Cape Town

$$\dot{n}_i = \frac{A_i^{FID}}{A_{CH4}^{FID}} \cdot \frac{f_{CH_4}^{FID}}{f_i^{FID}} \cdot \dot{n}_{CH_4} \quad (3.3)$$

n_i: molar flow of hydrocarbon compound i, mol/s

n_{CH4}: molar flow of methane as determined using equation (3.2), mol/s

A_i^{FID}: peak area of compound fi in the FID chromatogram

A_{CH4}^{FID}: peak area of methane in the FID chromatogram

f_{CH4}^{FID}: FID correction factor for methane

f_i^{FID}: FID correction factor for compound i

The only compound, which is not measured, is water. The molar flow rate of water can be obtained from an oxygen balance. In a first estimate, the formation of organic oxygen containing compounds can be neglected.

$$\dot{n}_{H_2O,out} \approx \left(\dot{n}_{CO,in} - \dot{n}_{CO,out}\right) + 2 \cdot \left(\dot{n}_{CO_2,in} - \dot{n}_{CO_2,out}\right) \quad (3.4)$$

3.3.6.2. Calculation of Partial Pressures in the Reactor

The partial pressures of each component can be calculated by knowing the total molar composition of the gas and by assuming that the outlet gas composition is the same as the composition inside the reactor.

$$p_i = \frac{\dot{n}_i}{\sum_i \dot{n}_i} \cdot p_{reactor} \quad (3.5)$$

n_i: the molar flow rate of compound i

$p_{reactor}$: total reactor pressure

3.3.6.3. Conversion and Rate of Reaction Calculations

The overall CO conversion is calculated merely from the difference in flow of CO into the reactor and the flow of CO out of the reactor.

University of Cape Town

$$\%CO\ Conversion = X_{CO} = 100 \cdot \frac{(\dot{n}_{CO,in} - \dot{n}_{CO,out})}{\dot{n}_{CO,in}} \quad (3.6)$$

In the iron catalysed Fischer-Tropsch reaction, CO is consumed in the formation of organic products as well as the formation of CO_2 via the water-gas shift reaction. Calculation of the conversion to organic Fischer-Tropsch products alone requires the overall conversion to be reduced by the amount of CO going to the formation of CO_2.

%(CO+CO_2) Conversion

$$X_{CO+CO_2} = 100 \cdot \frac{(\dot{n}_{CO,in} - \dot{n}_{CO,out}) + (\dot{n}_{CO_2,in} - \dot{n}_{CO_2,out})}{\dot{n}_{CO,in} + \dot{n}_{CO_2,in}} \quad (3.7)$$

The rate of formation of organic Fischer-Tropsch products is calculated by eliminating the consumption of CO for the formation of CO_2.

$$r_{FT} = \frac{(\dot{n}_{CO,in} - \dot{n}_{CO,out}) + (\dot{n}_{CO_2,in} - \dot{n}_{CO_2,out})}{m_{catalyst}} \quad (3.8)$$

$m_{catalyst}$: mass of the unreduced catalyst

The rate of the water gas shift reaction is calculated from the amount of CO_2 formed.

$$r_{WGS} = \frac{\dot{n}_{CO_2,in} - \dot{n}_{CO_2,out}}{m_{catalyst}} \quad (3.9)$$

3.3.6.4. Selectivity Calculation

The selectivity towards the formation of a compound can be defined as the amount of the compound formed relative to the amount of CO consumed in the formation of organic products.

University of Cape Town

$$S_i = \frac{\left(\dot{n}_{i,out} - \dot{n}_{i,in}\right)}{\left(\dot{n}_{CO,in} - \dot{n}_{CO,out}\right) + \left(\dot{n}_{CO_2,in} - \dot{n}_{CO_2,out}\right)} \cdot C_N \cdot 100 \qquad (3.10)$$

S_i: Selectivity, calculated with regards to CO converted to all products, excluding CO_2, C-%

C_N : Carbon number of hydrocarbon species i

University of Cape Town

Chapter 4

EXPERIMENTAL RESULTS

4.1 Catalyst Characterisation

4.1.1 Elemental composition, pore volume and surface area

The elemental composition of the samples prior to calcination as well as after calcination at 625°C is shown in Table 4.1. The obtained hydrotalcites had a very low residual amount of alkali (~0.1Na/100Fe). It can thus be concluded that the removal of alkali during the washing step was sufficient. The catalysts that were prepared for testing in the Fischer-Tropsch synthesis had a Mg/Fe molar ratio of ca. 2/1. The promoter loadings are in the anticipated range.

The pore volume and BET-surface area measurements were carried out after calcination and prior to reduction of the catalysts. The surface areas and pore volumes of the two promoter impregnated catalysts were a little lower and this may be due to the surface and pore coverage by the promoter.

University of Cape Town

Table 4.1: Elemental analysis of the catalyst samples, surface area and pore volume of the calcined catalyst samples

Catalyst Name	Elemental Analysis					Pore Volume	Surface Area
	Fe/mass%		Mg/mass%		Promoter /100Fe		
HTlc 100 Mg/Fe 2/1	30.9*	37.2#	24.4*	32.4#	-	0.82	122
HTlc 101 Mg/Fe 2/1	31.2*	37.6#	25.4*	33.5#	-	-	-
HTlc 102 Mg/Fe 2/1	32.7*	39.4#	26.1*	33.9#	K_2O = 0.27	0.69	112
HTlc 103 Mg/Fe 3/1	21.7*	-	29.6*	-	-	-	-
HTlc 104 Mg/Fe 6/1	16.9*	-	44.6*	-	-	-	-
HTlc 105 Mg/Fe 2/1	29.7*	35.8#	24.3*	31.4#	Cu = 6.5	0.63	109

** Before Calcination*

 # After Calcination

University of Cape Town

4.1.2. X-ray Diffraction Analysis

X-ray diffraction is a useful technique for the characterisation of hydrotalcites. Despite the iso-structural nature of the material, the different hydrotalcites have unique XRD patterns because the positions and intensities of the peaks are dependant on the metals and their ionic radii.

Difficulties in analysing the X-ray pattern of hydrotalcites occur when the materials are poorly crystallised as this results in broad and asymmetric diffraction lines. XRD was done on all samples that were prepared prior to calcination to confirm the presence of the hydrotalcite.

Figure 4.1 shows the XRD pattern of HTlc 100 (Mg/Fe=2/1) before calcination. The XRD-pattern shows the diffraction lines attributable to the Mg-Fe hydrotalcite (Pyroaurite). The unit cell dimension (*a* and *c*) for the structure was determined from the XRD. It has a rhombohedral crystal structure with an *a* lattice spacing of 3.1Å and a *c* spacing of 23.4Å.

The first three peaks can be assigned to the layer-interlayer-layer structure of the hydrotalcite, with intensity ratio of 9:3:1. The first most intense peak at 2θ value 13,2° represents the (003) plane, the second at 26,5° the (006) plane and the third at 39,9° the (009) plane. This last peak however is very small and overlaps with the peak for (012) plane.

University of Cape Town

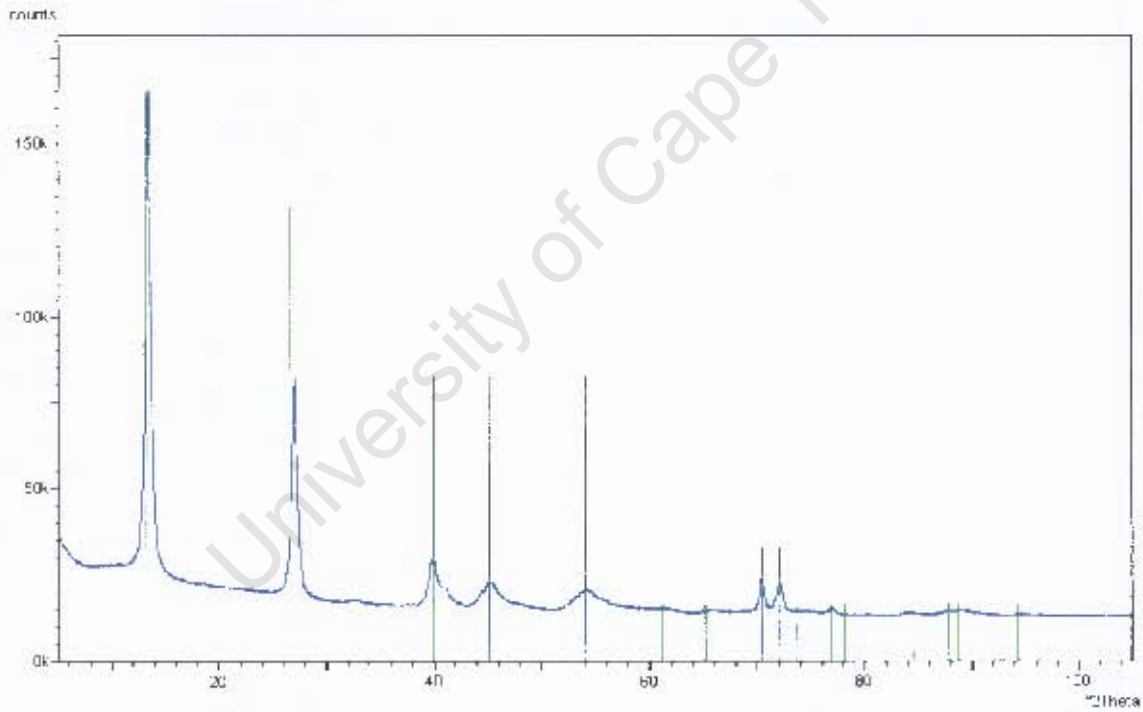

Figure 4.1: XRD pattern of a Mg-Fe-hydrotalcite with Mg/Fe=2/1 (HTlc 100) (Typical pattern of a Pyroaurite)

The two peaks at 70,2° and 71,8° ((110) and (113) respectively) with low intensity are determined by the distance between the cations (the *a* spacing). This first reflection at d=1,5Å has a (110) orientation to the hexagonal axes. This is thus independent of the kind of layer stacking and can therefore be used for the calculation of the parameter *a* as *a*=2d(110) .

The lattice parameter *a* depends on the nature of the cation (ionic radius) and on the ratio M^{2+}/M^{3+}. The *c* parameter is directly determined by the anion size and indirectly by the ratio M^{2+}/M^{3+}, which give the interlayer distance, and hence determines the first three sharp peaks [Cavani, 1991].

A Mg-Fe hydrotalcite with a molar ratio Mg/Fe ratio of 3:1 (HTlc 103) was also successfully prepared (refer to appendix 1 for diffractogram) however, it was not possible to prepare a pure hydrotalcite with a molar ratio of Mg/Fe of 6:1 (HTlc 104) as shown by figure 4.2. The XRD-pattern does show in addition to the pyroaurite the presence of $Mg_5(CO_3)_4(OH)_2 4\ H_2O$ and negligible amounts of goethite (FeO(OH)).

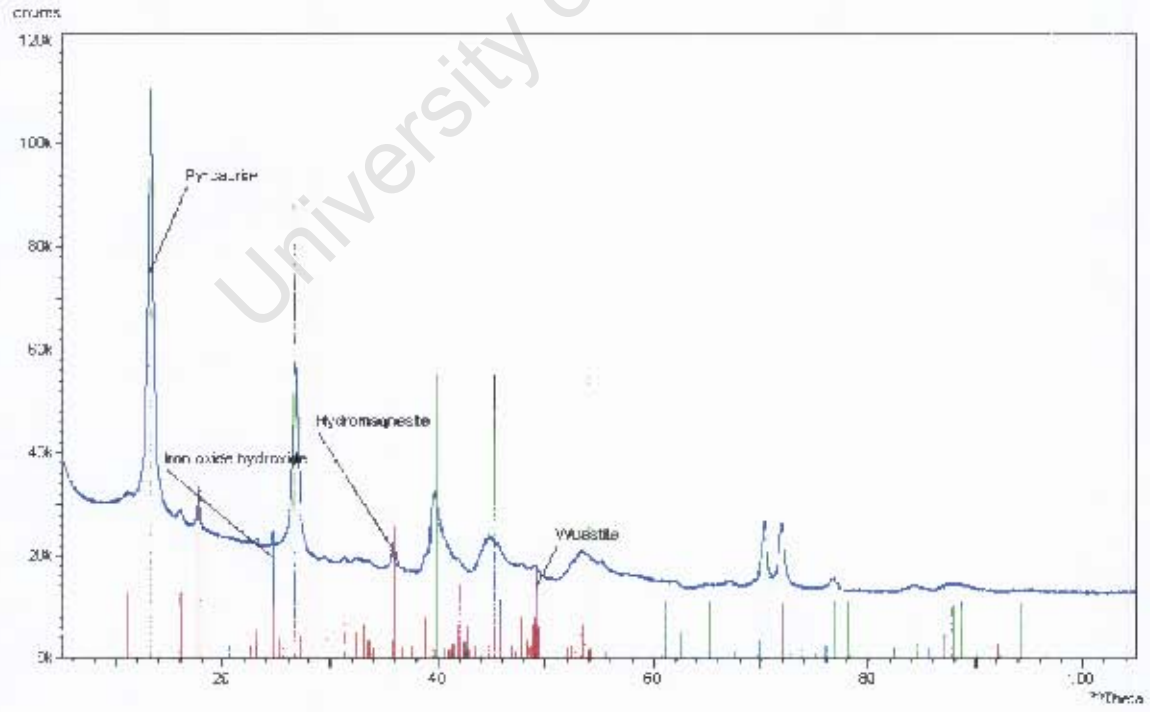

Figure 4.2: XRD-pattern of a Mg-Fe-hydrotalcite with Mg/Fe = 6/1 (HTlc 104)

University of Cape Town

XRD-analyses were also performed on the samples after calcination at 625°C (see Figure 4.3) The product of calcination of a $M^{2+}M^{3+}$ hydrotalcite is a spinel $M^{2+}M^{3+}{}_2O_4$, together with free $M^{2+}O$. [Cavani, 1991] Indeed, the phases that were found to be present in the calcined samples were periclase (MgO) and a magnesium iron spinel, magnesioferrite ($MgFe_2O_4$).

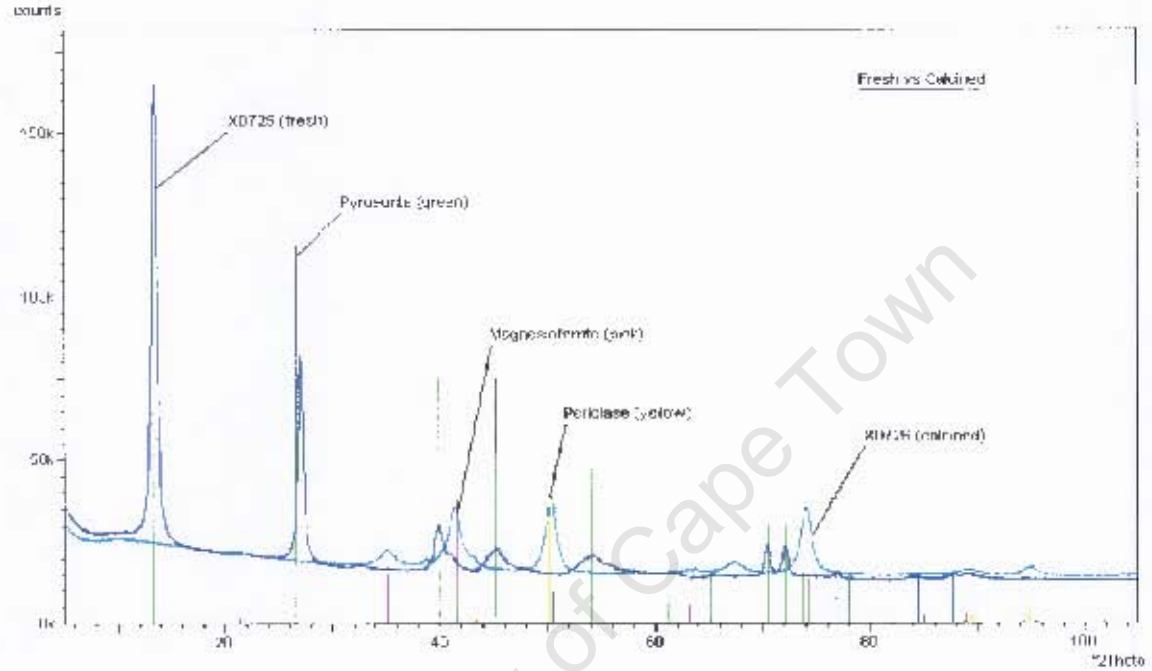

Figure 4.3: Comparison of a typical pyroaurite sample (HTlc 100) before and after calcination at 625°C

4.1.1.1 In-situ XRD calcination studies

The transformations taking place during heat treatment was studied further. A dried Mg-Fe hydrotalcite sample with a molar ratio of Mg to Fe of 2:1 was heated under nitrogen up to 800°C and the phase changes were monitored in-situ with XRD.

University of Cape Town

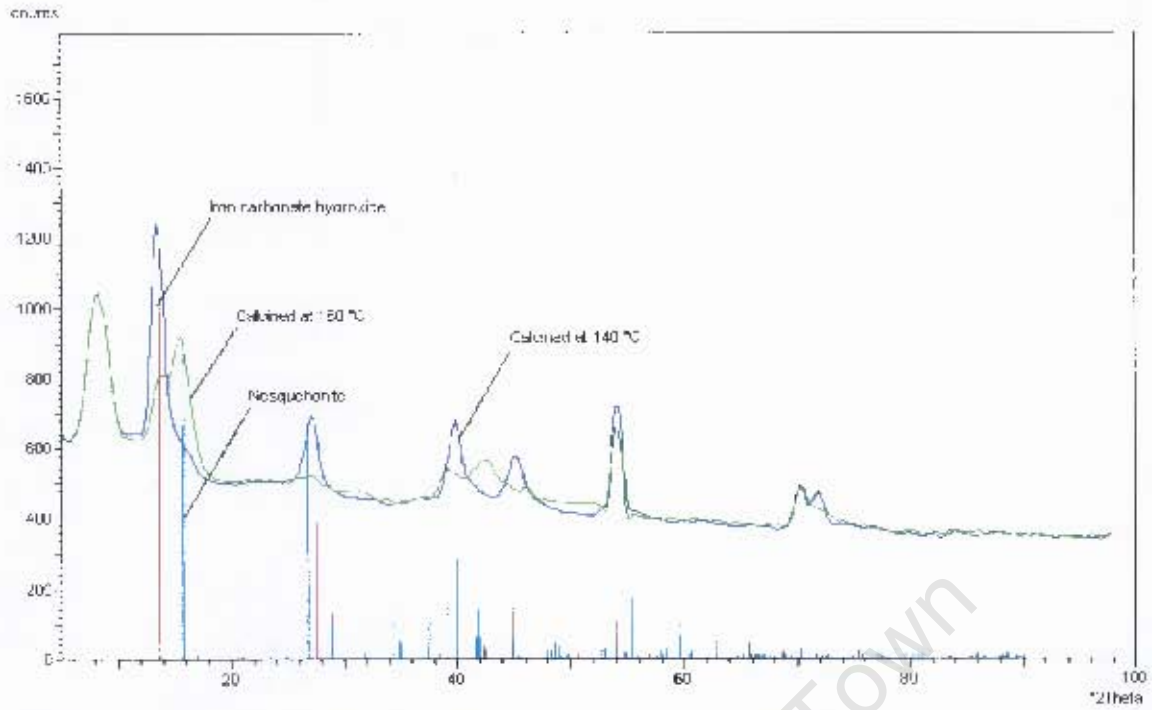

Figure 4.4: XRD-patterns of a Mg-Fe-hydrotalcite with Mg/Fe=2/1 (HTlc 101) after calcination at 140 and 160°C (calcination in nitrogen performed in-situ with a heating rate of 5°C/min)

It was found that at temperature larger than ca. 140°C the hydrotalcite structure appears to collapse (figure 4.4). This could be due to the loss of interlayer water and the decomposition of the carbonate anions. It is not certain as to what phases are present at this stage (the first peak appearing at 8 °2θ is a result of the polymer membrane Kapton used in the camera and the peak at ± 54 °2θ.is from the platinum sample holder/heating strip that is used). The possible phases that were assigned to the peaks were: the second peak at ± 14 °2θ is ascribed to iron carbonate hydroxide ($Fe(OH)_{12}CO_3$) and third peak at ± 16 °2θ to nesquehonite ($MgCO_3.(H_2O)_3$.

At temperatures of ca. 300°C the sample appears to become amorphous as illustrated in figure 4.5. Crystalline phases begin to re-appear at temperatures larger than 400°C. The peak that appears at 50° 2θ may be ascribed to the formation of magnesium oxide (MgO).

University of Cape Town

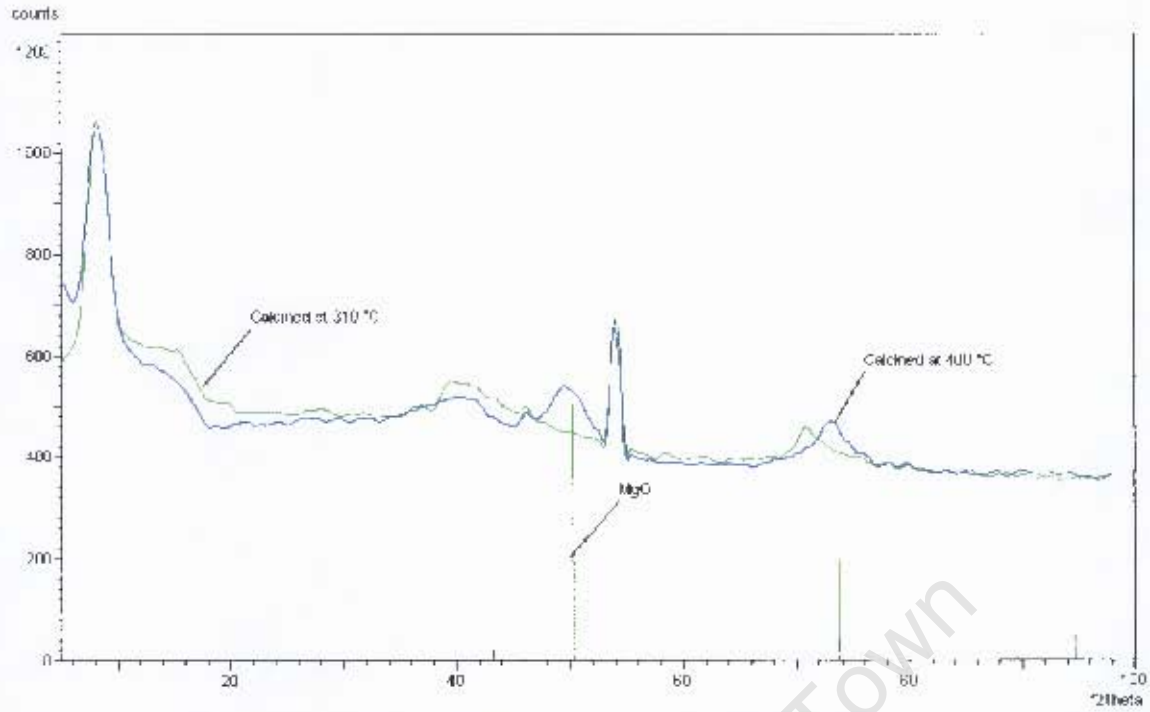

Figure 4.5: XRD-patterns of a Mg-Fe hydrotalcite with a molar ratio of Mg to Fe of 2:1 Mg/Fe=2/1 (HTlc 101) after calcination at 310 and 400°C (calcination in nitrogen performed in-situ with a heating rate of 5°C/min)

At temperatures around 625°C, a diffraction peak at approximately 41.5° 2θ starts to appear. This peak is assigned to a magnesioferrite spinel ($MgFe_3O_4$). No further phase changes appear to take place between 600°C and 800°C: however the phases present become more crystalline as the temperature increases

University of Cape Town

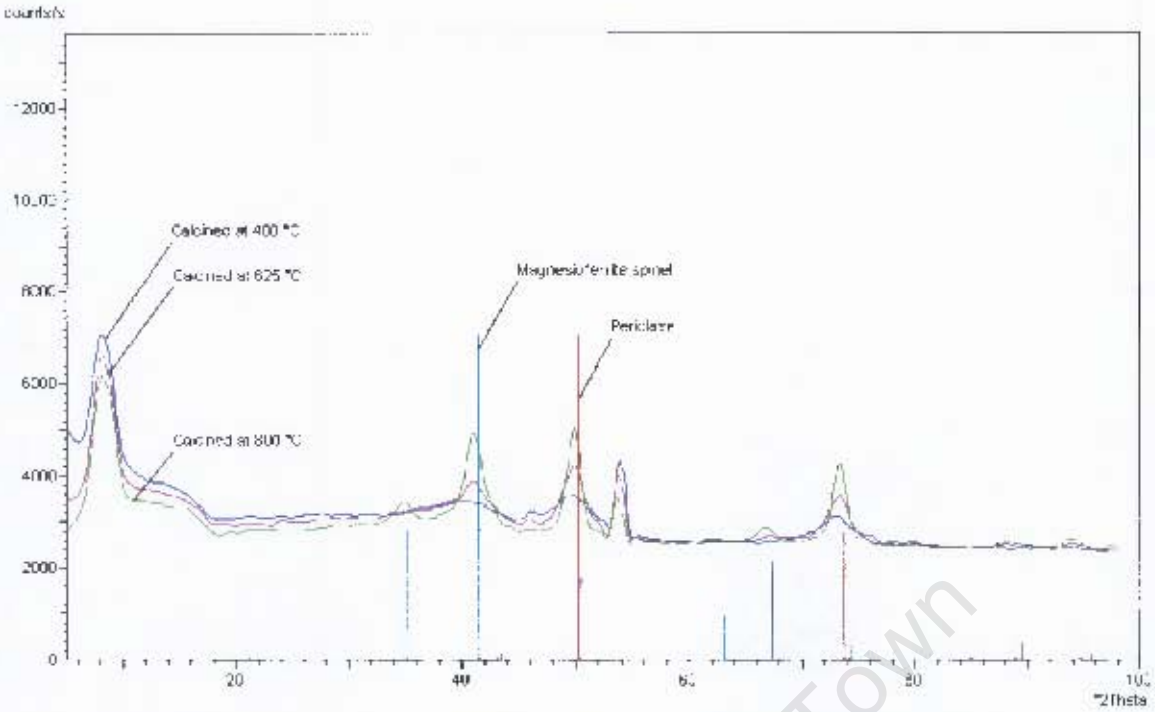

Figure 4.6: XRD-patterns of a Mg/Fe-hydrotalcite with a molar ratio of Mg to Fe of 2:1 (HTlc 101) after calcination at 400, 625 and 800°C (calcination in nitrogen performed in-situ with a heating rate of 5°C/min)

University of Cape Town

4.1.2.2 In-situ XRD reduction studies

After calcination at 625°C the pyroaurite ($Mg_6Fe_2CO_3(OH)_{16}.\ 4H_2O$) catalyst consists of a mixture of periclase (MgO) and a magnesium iron spinel, magnesioferrite ($MgFe_2O_4$). A calcined sample was heated under hydrogen and the phase changes taking place were observed with XRD to investigate the reduction behavior of the calcined hydrotalcite.

The composition of the sample was determined by Rietveld refinement quantitative phase analysis (QPA). The composition remains essentially unchanged upon heating up in hydrogen to 300°C as shown in figure 4.7. There is however small amounts of iron metal that start appearing from 250 °C. Between 300 and 350°C both MgO and $MgFe_2O_4$ are transformed into magnesium iron oxide ($Mg_xFe_{1-x}O$) and iron metal.

The value of x in the formula for magnesium iron oxide is estimated at 0.56 at 25°C, from experimental data obtained by application of Vegards rule. The true value of x at 350°C was not determined. The x value should increase with temperature as the iron metal content in the mixed oxide decreases. The change in the x value with temperature was however not determined as this variable was kept constant for the refinements. The amount of iron metal increases with increasing temperature however, the catalyst is not completely reduced at 560°C, where the experiment was terminated.

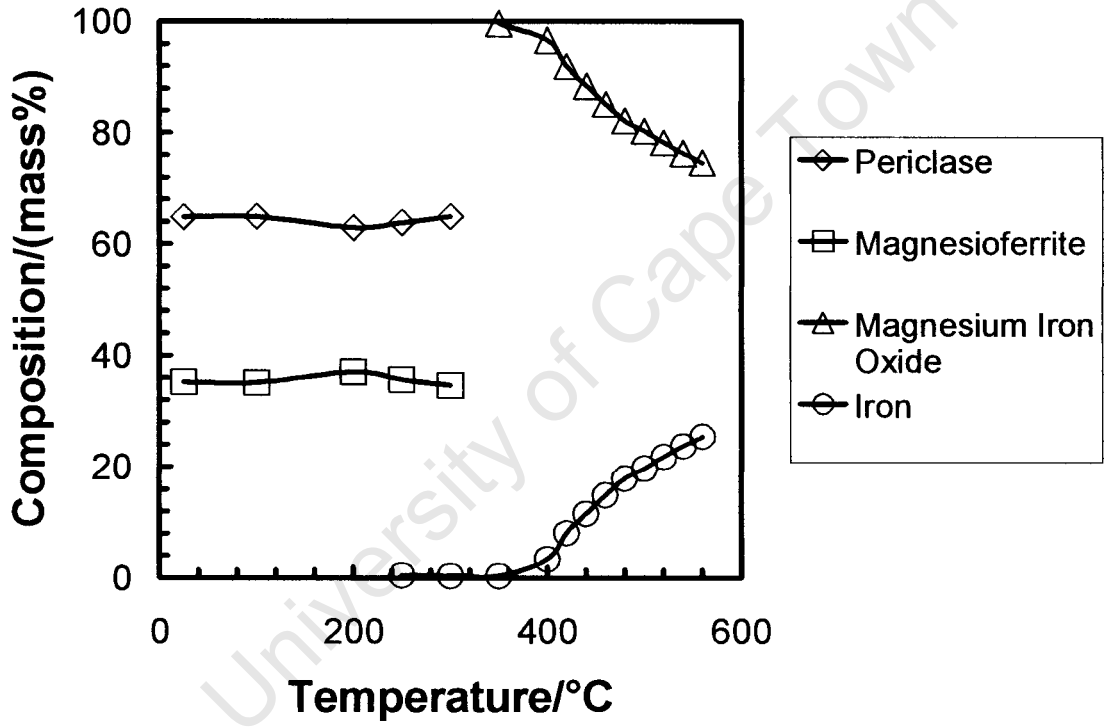

University of Cape Town

Figure 4.7: Composition of a calcined Mg-Fe-hydrotalcite ($T_{calcination}$ = 625°C) with a molar ratio of Mg to Fe of 2:1 as a function of the reduction temperature (reduction in hydrogen performed in-situ with a heating rate of 5°C/min)

The lattice constant of the iron metal increases as the temperature increases (see Figure 4.8). This is due to thermal expansion of the lattice. Extrapolation of the graph to room temperature (25°C) gives a lattice constant value of 2.847Å which is lower than the expected value of 2.866 Å. This has been attributed to the transformations taking place in the sample during reduction which would result in the change of the surface of the sample or level of the sample in the holder, thereby causing the diffraction peaks to shift. This influences the determination of the lattice constants and therefore the absolute values are not accurate. The trend that is observed, namely, the increase in the lattice constant value with increasing temperature is however correct.

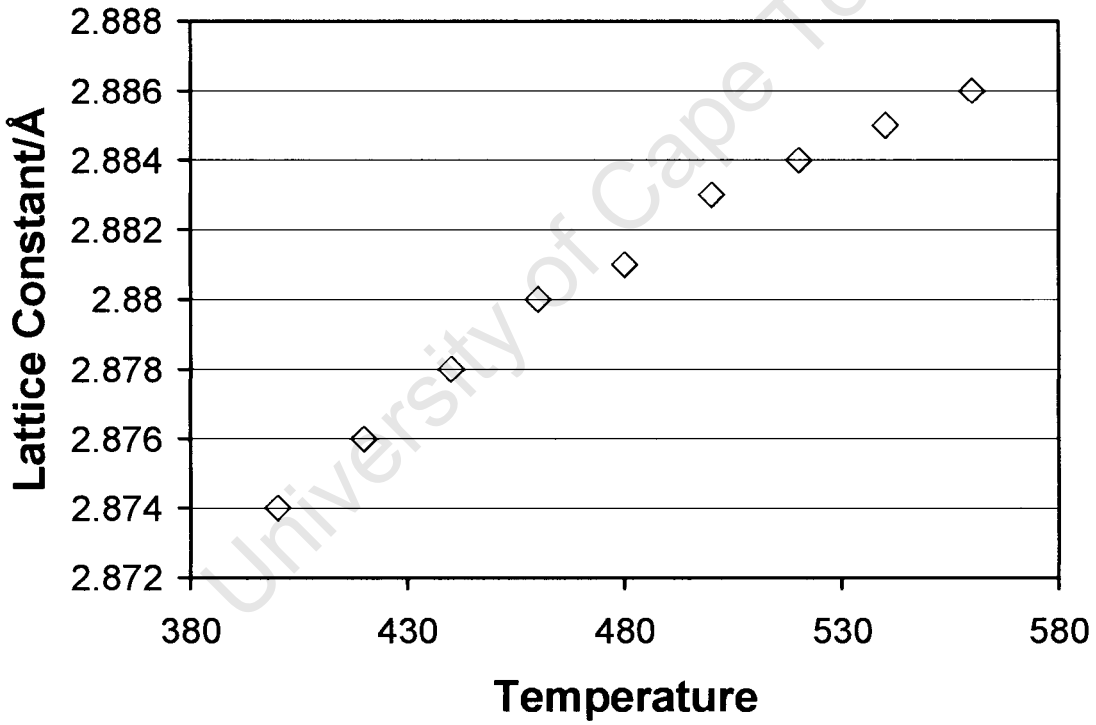

University of Cape Town

Figure 4.8: Change in the lattice constant of α-Fe formed in the reduction of calcined hydrotalcite with a molar ratio of Mg to Fe of 2:1 as determined using Rietveld refinement

The lattice constant of magnesium iron oxide $Mg_xFe_{1-x}O$ at 350°C, is 4.264 Å. Figure 4.9 shows that the lattice constant of magnesium iron oxide in the successive scans remains fairly constant despite the increase in temperature. It is thought that thermal expansion is not evident in this case because, as the reduction proceeds and more iron metal is formed, the magnesium iron oxide becomes enriched in magnesium. Since Mg^{+2} ion has a smaller crystal ionic radius (0.65 Å) than the Fe^{+2} ion (0.76 Å), the increase in the lattice constant of the oxide due to thermal expansion may be negated by the incorporation of more magnesium ions into the lattice.

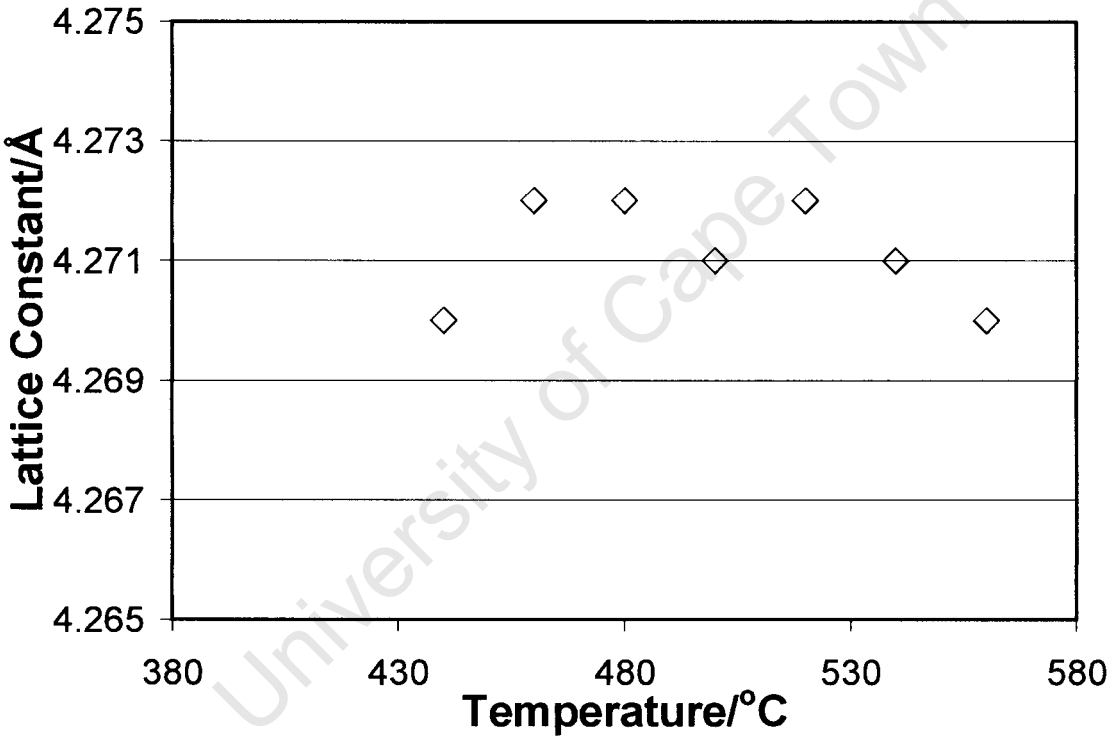

University of Cape Town

Figure 4.9: Change in the lattice constant of magnesium iron oxide $Mg_xFe_{1-x}O$ formed in the reduction of calcined hydrotalcite with a molar ratio of Mg to Fe of 2:1 as determined using Rietveld refinement

4.1.3 Differential scanning calorimetry (DSC) - thermal gravimetric analysis (TGA)

The thermal behaviour of hydrotalcites is generally characterised by two endothermic transitions, the one at low temperature is due to the loss of interlayer water and the other at a higher temperature is as a result of the loss of hydroxyl groups and anions. Both the first and second transitions that take place can occur in two stages. [Cavani, 1991]

Figure 4.10 shows the results of a thermal gravimetric analysis performed on an uncalcined Mg-Fe hydrotalcite with a molar ratio of Mg to Fe of 2:1. The TGA apparatus was coupled to a mass spectrometer and the products that were lost were thereby identified.

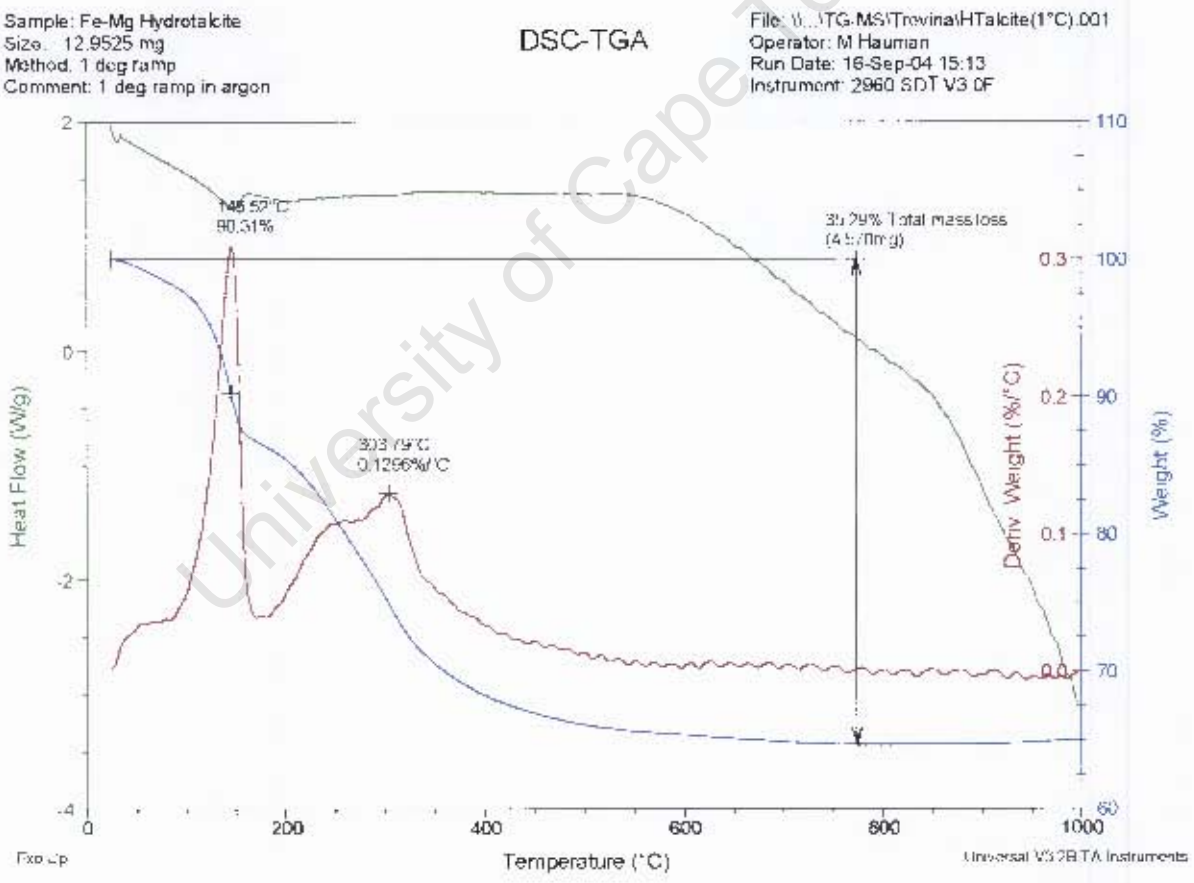

Figure 4.10: Thermal gravimetric analysis of a Mg-Fe hydrotalcite with a molar ratio of Mg to Fe of 2:1 in argon with a heating rate of 1°C/min

University of Cape Town

A sharp intense peak was observed at ca. 145°C, which corresponds to the loss of water (as confirmed using by MS – see Figure 4.11). The experiment was conducted at a low heating rate (1°C/min) to determine if the transition taking place at this temperature was occurring in two stages. This was however not evident.

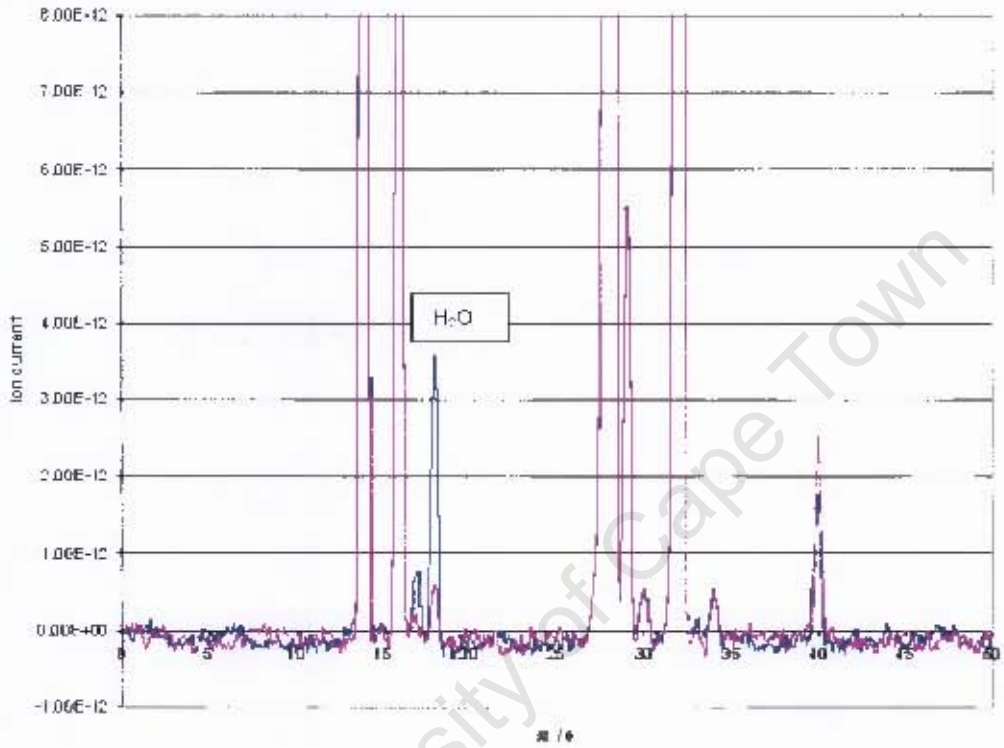

(red: background; blue: MS-spectrum of gas evolved)

Figure 4.11: Mass spectrum of products released during the thermal gravimetric analysis in argon at 145°C of a hydrotalcite with a molar ratio of Mg to Fe of 2:1 (heating rate of 1°C/min)

The second transition that occurs at ca. 300°C appears to take place in two stages. The shoulder on the peak at 300°C may correspond to a loss of hydroxyl groups bound to the iron. The peak at 300°C is as a result of the loss of hydroxyl groups connected with the magnesium as well as the decomposition of the carbonate anions [Cavani, 1991]. The MS (see Figure 4.12) confirmed the loss of water and carbon dioxide, which were the expected decomposition products from the sample during the second transition.

University of Cape Town

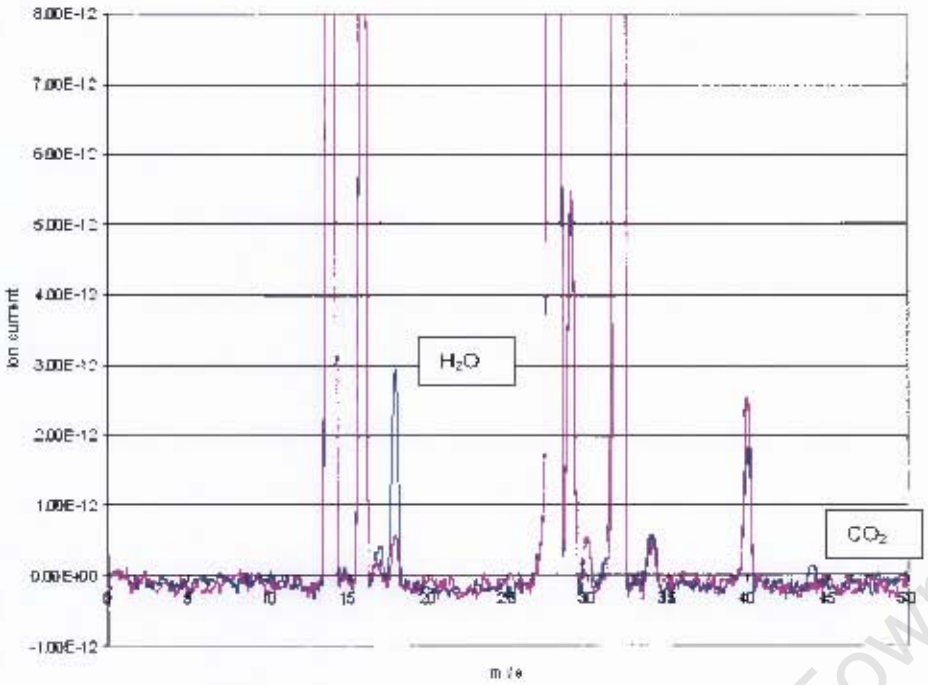

(red: background; blue: MS-spectrum of gas evolved)

Figure 4.12: Mass spectrum of products released during the thermal gravimetric analysis in argon at 300°C of a hydrotalcite with a molar ratio of Mg to Fe of 2:1 (heating rate of 1°C/min)

4.1.3 Temperature Programmed Reduction (TPR)

The reduction profile of the unpromoted calcined hydrotalcite was obtained with TPR and compared to that obtained from a fused iron catalyst. The calcined hydrotalcite profile shows two distinct peaks. The first peak is attributed to, the reduction of Fe^{3+} to Fe^{2+} and the second to, Fe^{2+} being reduced to Fe^{0}. [Shen, 1996]

The fused catalyst consists of magnetite which is a mixture of $Fe^{3+}$and Fe^{2+}. This is then reduced to Fe^{0} possibly via FeO (wustite). [Bukur, 1995] Wustite is thermodynamically unstable and the transition from FeO to metallic iron is believed to be very quick [Edstrom, 1953]. The shoulder on the peak for the fused catalyst at ca. 700°C may be as a result of this transient change. The fused catalyst starts to reduce at a much higher temperature compared to the calcined hydrotalcite.

University of Cape Town

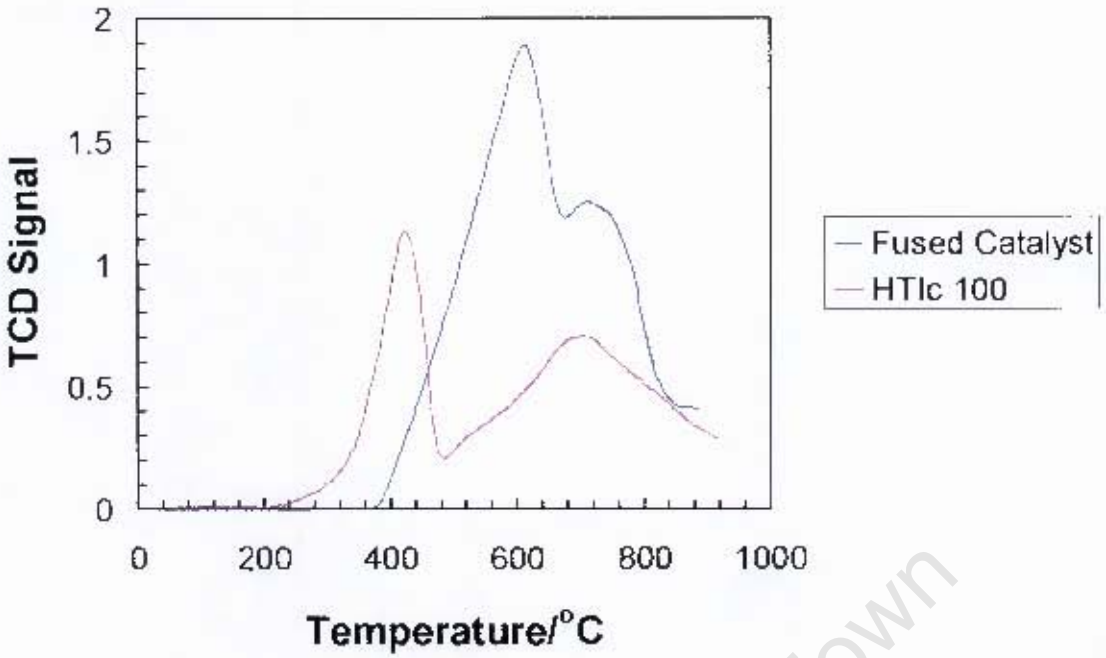

Figure 4.13: Temperature programmed reduction profile of a calcined hydrotalcite with a molar ratio of Mg to Fe of 2:1 heated at 10°C/min under H_2/Ar (10/90) with a flow rate of 0.05l/min.

University of Cape Town

4.2 Fischer-Tropsch synthesis

Hydrotalcite derived catalysts were prepared without any chemical promotion (HTIc 100), with potassium promotion (0.27 K_2O/100 Fe; HTIc 102) and with copper promotion (6.5 Cu/100 Fe; HTIc 105) and tested. The catalysts were tested in a CSTR reactor at high temperature Fischer-Tropsch synthesis conditions and compared to a fused catalyst that was tested at the same conditions.

4.2.1 CO and CO + CO_2 conversion

The overall CO conversion (see Figure 4.14) of the hydrotalcite derived catalysts (HDC) is comparable to a standard fused HTFT catalyst, despite the lower iron content in the HDC in comparison to the iron content in the fused iron catalyst. This might be due to the larger surface area of the iron phase in the HDC.

Furthermore, all catalysts are relatively stable over the reaction time studied and only the CO-conversion for the copper promoted HDC (sample HTlc 105) seem to decline slightly with time.

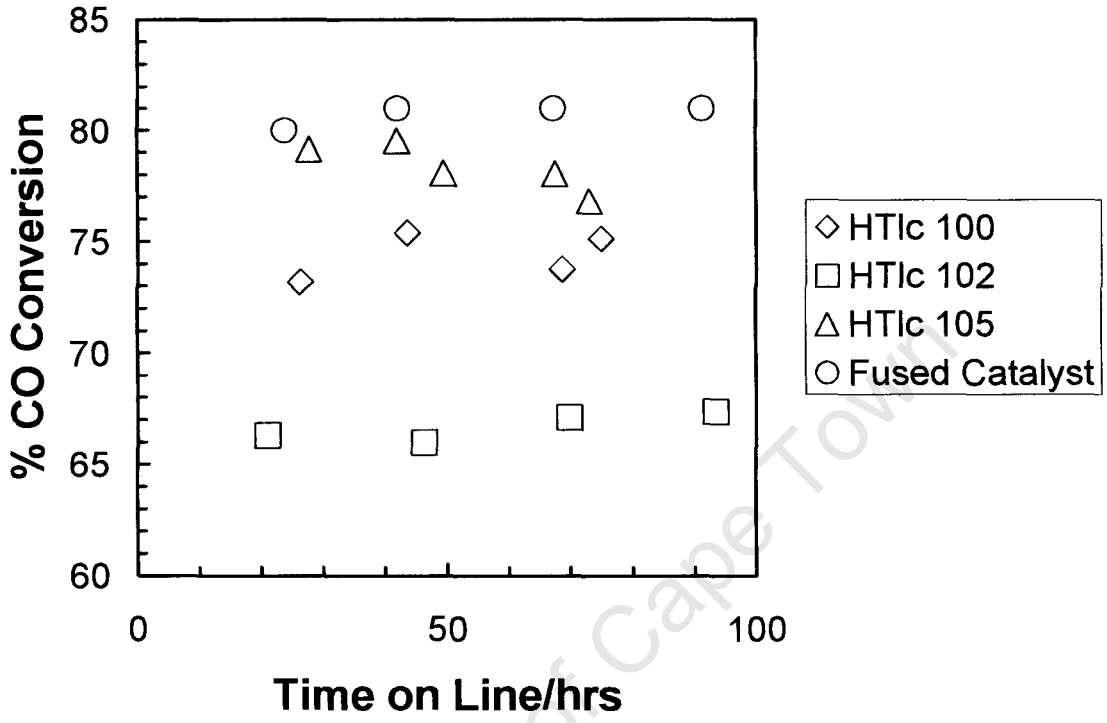

Figure 4.14: Conversion of carbon monoxide in the Fischer-Tropsch synthesis as a function of time-on-line of hydrotalcite derived catalysts compared with the standard fused iron catalyst

Potassium was added to the hydrotalcite in an attempt to increase the basicity of the catalyst without adversely affecting the reducibility of the iron by the addition of more magnesium (HTlc 102). The CO conversion of this catalyst is much lower than the unpromoted catalyst. This is not in line with what was expected.

The addition of copper to the catalyst (HTlc 105) has resulted in an increase in the conversion of the catalyst compared to the other HDCs and the conversion is similar to that of the fused catalyst. In previous studies copper has been shown to improve the reducibility of the iron. [Bukur, 1990a]

University of Cape Town

The HDCs do not undergo complete reduction under the conditions used and the copper was added in an attempt to increase the amount of active metallic iron present and to thereby improve the catalytic activity.

Figure 4.15 shows the $CO+CO_2$ conversion as a function of time on line as an indication of the Fischer-Tropsch activity, i.e. the formation of hydrocarbons. The trends in the CO-conversion are also observed in the Fischer-Tropsch activity.

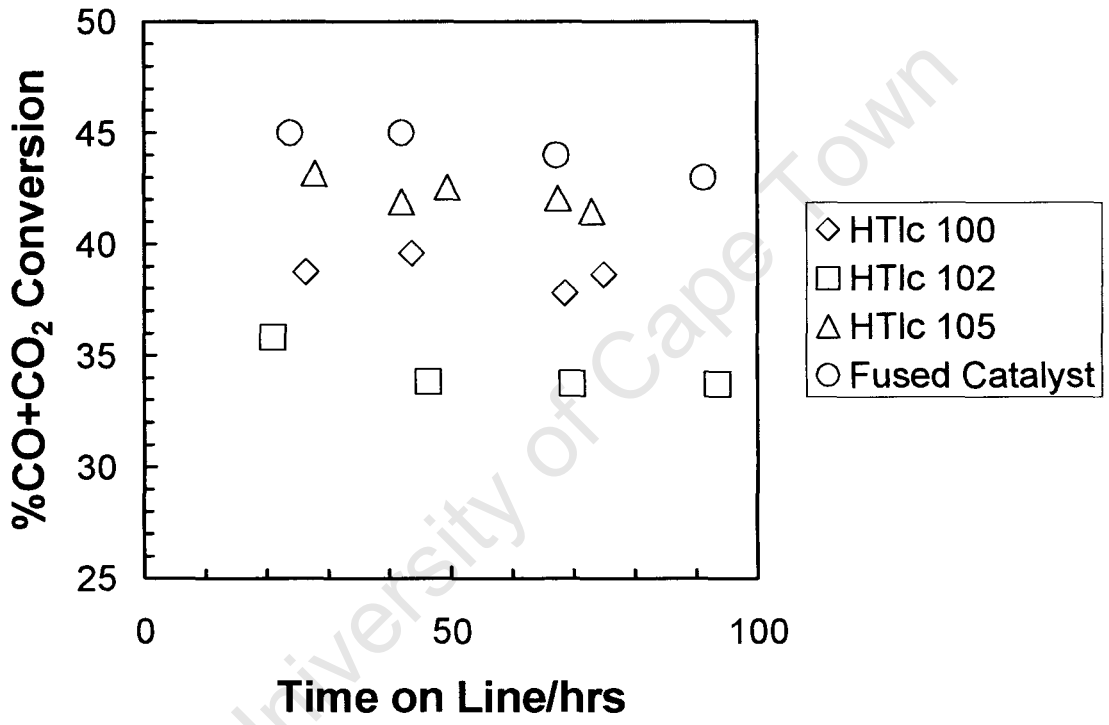

University of Cape Town

Figure 4.15: Conversion of $CO+CO_2$ in the Fischer-Tropsch synthesis indicating the Fischer-Tropsch activity as a function of time-on-line of hydrotalcite derived catalysts compared with the standard fused iron catalyst

4.2.2 CO_2-Selectivity

Carbon monoxide is in the Fischer-Tropsch synthesis either converted to hydrocarbons (the actual Fischer-Tropsch reaction) or to CO_2 via the water gas shift (WGS) reaction, which is described by the following equation:

$$CO + H_2O \longleftrightarrow CO_2 + H_2$$

The amount of CO converted to CO_2 is an indication of the extent to which the forward water gas shift (fWGS) reaction is taking place. This is an undesirable reaction because: it produces CO_2 that needs to be removed downstream from the process and it uses up the CO. In the high temperature Fischer-Tropsch synthesis it is possible to maintain the WGS reaction at or close to equilibrium by co-feeding CO_2 into the reactor.

Figure 4.16 shows the carbon dioxide selectivity based on the inlet molar flow rate of carbon monoxide as a function of time on line. The hydrotalcite derived catalysts have a higher CO_2 selectivity compared to the fused catalyst. These catalysts also show a lower conversion of carbon monoxide. Therefore, the selectivity for carbon dioxide is actually much higher with the HDCs than with the fused iron catalyst. In the HDCs iron oxide may be present as they are not completely reduced under the conditions used. Iron oxide has been shown to catalyse the WGS reaction [Wang, 2003].

The potassium promoted hydrotalcite derived catalyst seems to have initially the lowest CO_2 selectivity compared to the other hydrotalcite derived catalysts, but the yield increases through out the run. The potassium promoted catalyst does however have a lower conversion compared to the other catalysts, both overall CO conversion and $CO+CO_2$ conversion. The latter is the source of the water that is a reactant in the fWGS reaction. This may account for the lower initial point. Potassium has been found to be a promoter for the WGS reaction over iron oxide catalysts [Rao, 1992]. This could be the reason why the potassium promoted catalyst eventually has the highest CO_2 yield.

University of Cape Town

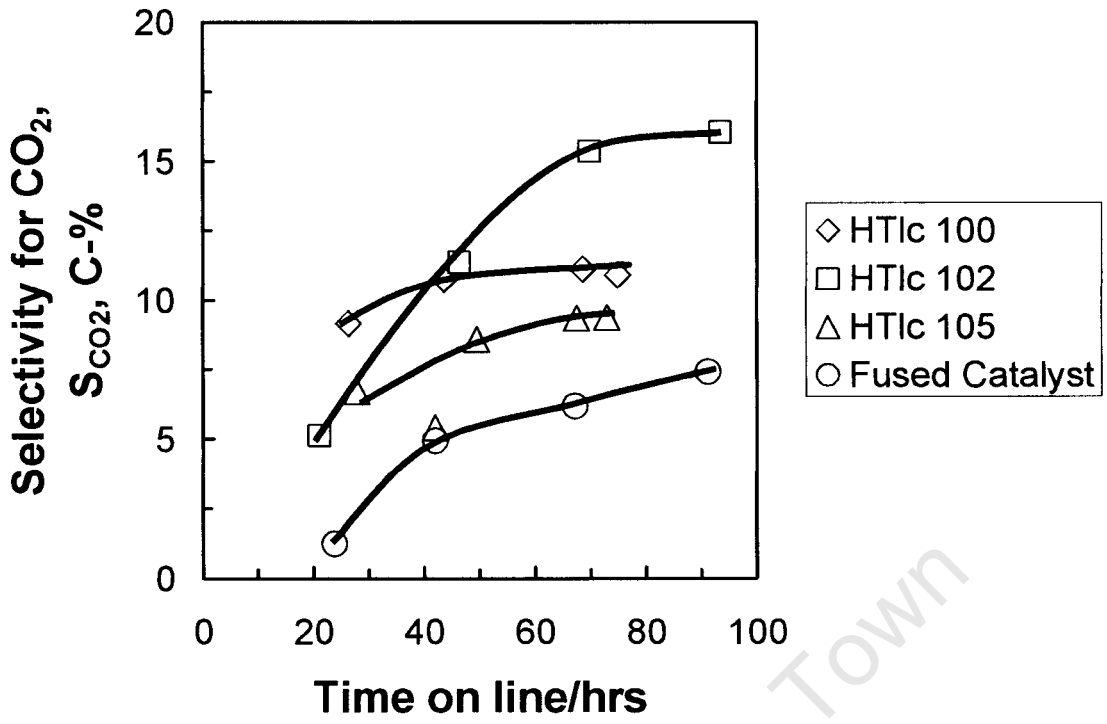

Figure 4.16: CO_2 selectivity in the Fischer-Tropsch synthesis as a function of time-on-line of hydrotalcite derived catalysts compared with the standard fused iron catalyst

The copper containing catalyst has a lower CO_2 selectivity compared to the unpromoted hydrotalcite derived catalyst. This could be as a result of the improved reducibility of the catalyst and thus a decrease in the amount of iron oxide present. This catalyst also has a slightly higher overall conversion than the unpromoted catalyst and this needs to be taken into account when comparing the results. In addition CO + CO2 conversion, which results in the formation of water that is consumed in the fWGS reaction, was also higher and, the fWGS reaction, could thereby be increased.

University of Cape Town

4.2.3 Water partial pressure in the reactor

Figure 4.17 shows the water partial pressure in the reactor (assuming perfect CSTR-behaviour) as a function of time on line. The water partial pressure was the highest with the fused catalyst. This may be as a result of the increased $CO+CO_2$ conversion as well as a decrease in the WGS reaction compared to the other catalysts.

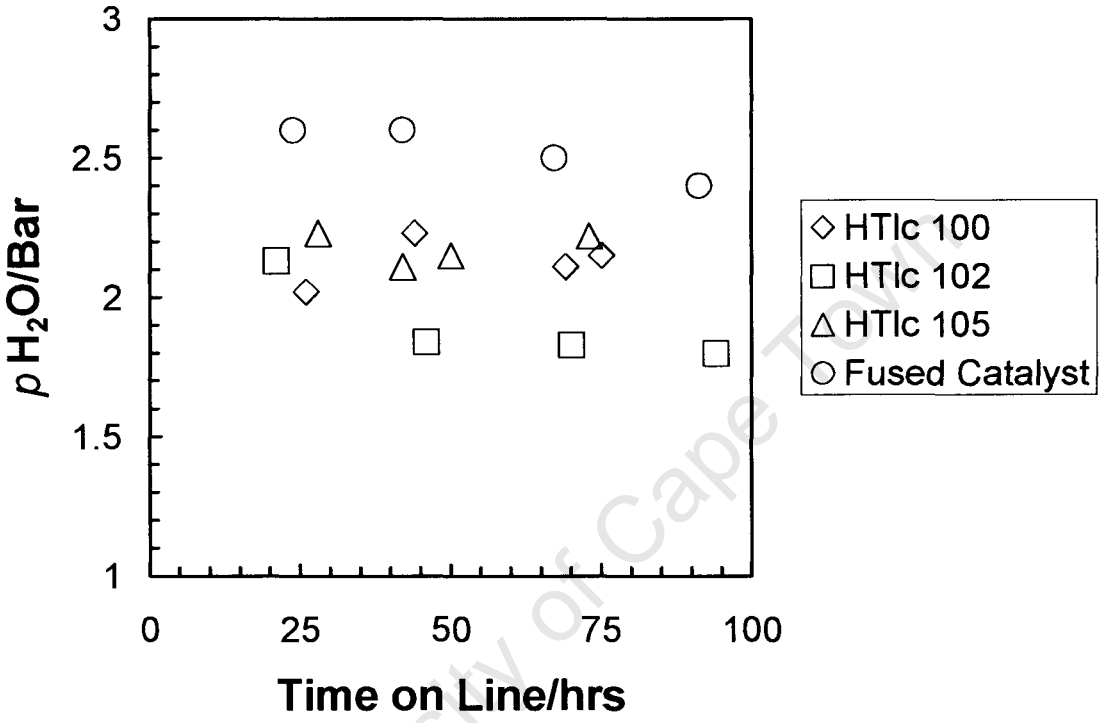

Figure 4.17: Water partial pressure in the reactor during the Fischer-Tropsch synthesis as a function of time-on-line of hydrotalcite derived catalysts compared with the standard fused iron catalyst

The hydrotalcite derived catalysts all are being exposed to a similar initial water partial pressure. The higher overall CO and $CO+CO_2$ conversion of the copper containing catalyst and the lower CO and $CO+CO_2$ conversion of the potassium containing catalysts needs to always be considered when comparing the results. The water partial pressures decline with time on stream, due to the increase in the CO_2-yield with time on line.

University of Cape Town

4.2.4 H_2 Conversion

The H_2-conversion as a function of time-on-line is shown in Figure 4.18. The conversion is calculated based on the amount of H_2 fed to the reactor and the amount of H_2 leaving the reactor. This is therefore also dependent on the amount of H_2 that is produced in the reactor via the forward WGS reaction. The hydrogen conversion over the fused catalyst is higher than all the other catalysts. It has been shown above that the fused catalyst under these conditions appears to have the lowest rate of the fWGS reaction and it would therefore also have the lowest H_2 make. This and the overall higher CO + CO_2 conversion, which consumes the hydrogen fed to the reactor, may be the reason for the higher H_2-conversion.

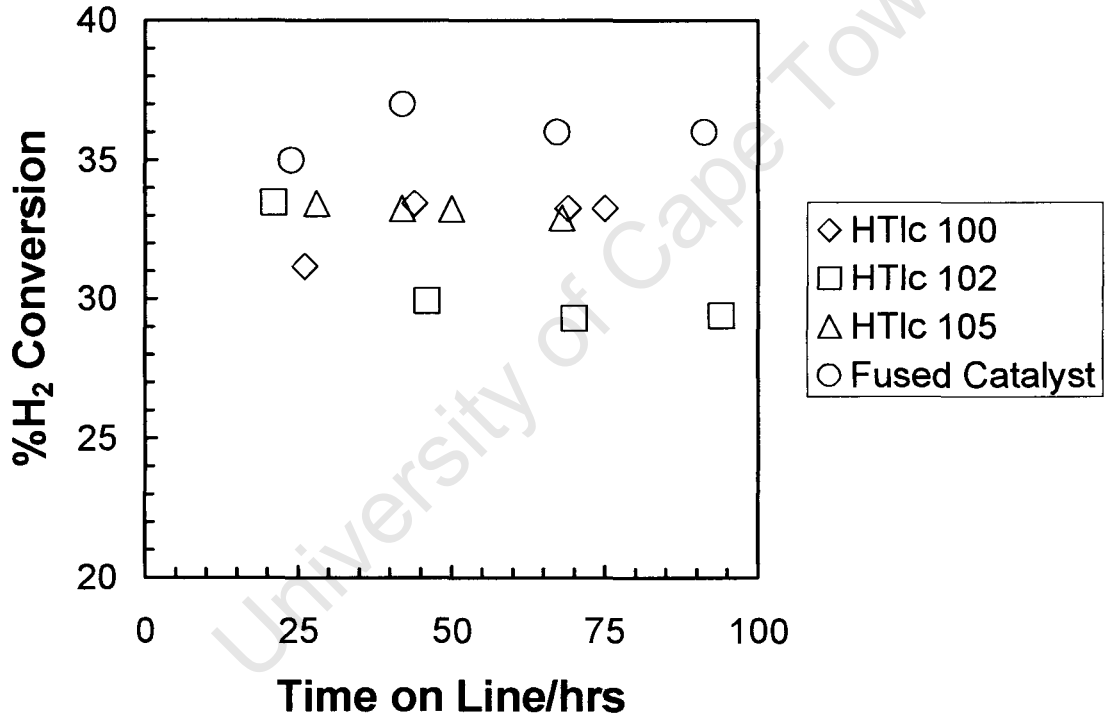

University of Cape Town

Figure 4.18: Hydrogen conversion during the Fischer-Tropsch synthesis as a function of time-on-line of hydrotalcite derived catalysts compared with the standard fused iron catalyst

The H_2 conversion of the potassium promoted hydrotalicte derived catalyst (HTlc 102) decreases with time on line. This may be a result of the increase in the fWGS reaction with this catalyst. However, this catalyst produced higher amounts of hydrogenated products compared to the other catalysts (see 4.21 and 4.22).

Similar hydrogen conversions are obtained with the unpromoted hydrotalcite derived catalyst (HTlc 100) and with the copper promoted hydrotalcite derived catalyst (HTlc 105), as in the case of the water partial pressure in the reactor. The copper promoted catalyst has a higher $CO+CO_2$ conversion compared to the unpromoted catalyst. The latter has a higher WGS activity and produces more hydrogenated products compared to the copper containing catalyst.

4.2.5 H_2/CO ratio in the reactor

At a constant reactor partial pressure, the H_2/CO reactor ratio is of importance for selectivity considerations. Figure 4.19 shows the hydrogen to carbon monoxide ratio in the reactor as a function of time on line over the various catalysts. The fused catalyst has the highest ratio (between 12 and 15). The unpromoted hydrotalcite derived catalyst (HTlc 100) and the copper promoted hydrotalcite derived catalyst (HTlc 105) have a similar H2/CO- ratio in the reactor (ca. 10), which does not change much with time on line. This may again be attributed to the $CO+CO_2$ conversion and the WGS activity of the catalysts. The H_2/CO-ratio in the reactor is the lowest (ca. 8) with potassium promoted hydrotalcite derived catalyst (HTlc 102).

University of Cape Town

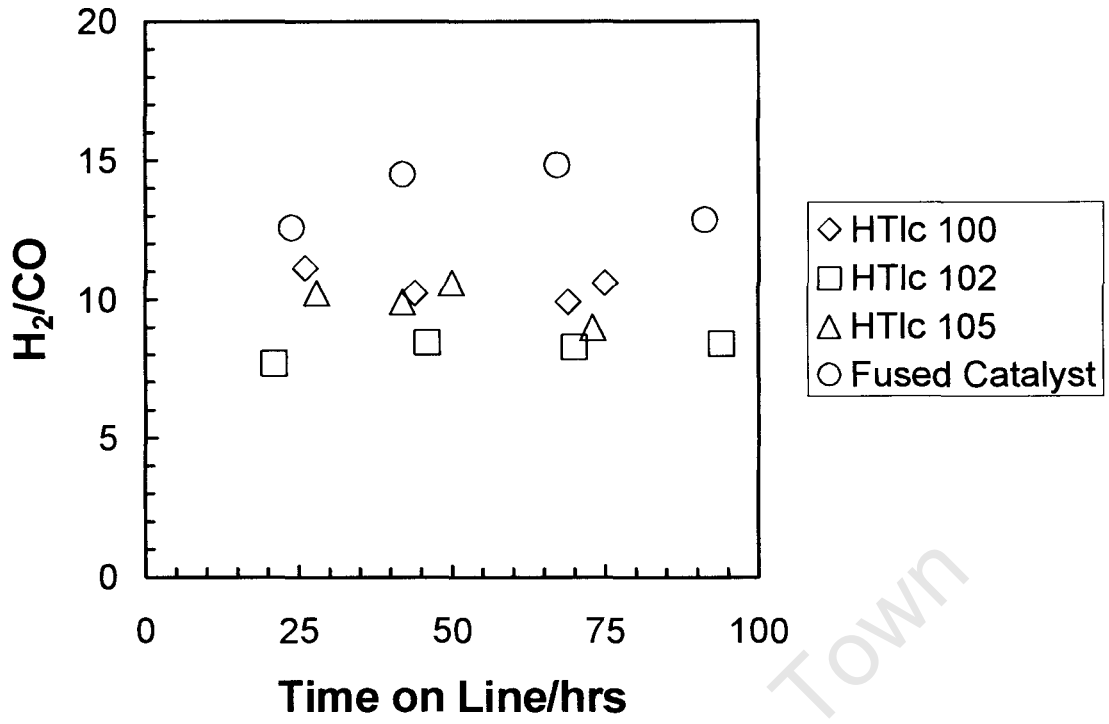

Figure 4.19: H_2/CO ratio in the reactor during the Fischer-Tropsch synthesis as a function of time-on-line of hydrotalcite derived catalysts compared with the standard fused iron catalyst

University of Cape Town

4.2.6 Selectivity in the Fischer-Tropsch synthesis

The products obtained from the different runs were analysed as described in chapter 3 and the results are presented below.

The hydrotalcite derived catalysts appear to produce a lighter product spectrum compared to the fused catalyst as illustrated by figure 4.20. The products up to C_4 appear to be higher than the fused catalyst and thereafter the fused catalyst produces similar or higher quantities of the longer chain products.

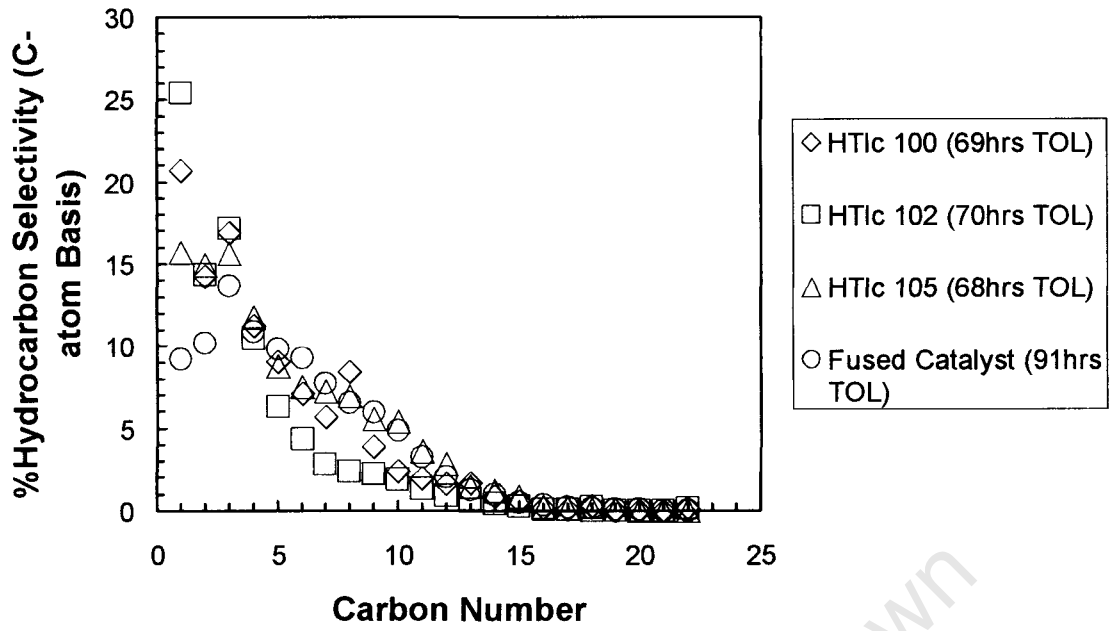

Figure 4.20: %Hydrocarbon Selectivity as a function of carbon number of hydrotalcite derived catalysts compared with the standard fused iron catalyst

Figure 4.21 provides a closer look at the methane selectivity of the different catalysts with time on line. The fused catalyst has the lowest methane production. The high methane make of the hydrotalcite derived catalysts may be a result of the incomplete reduction of the iron. These catalysts would thus have a larger amount of iron oxide present and as mentioned above, this phase of iron has been shown to promote the WGS activity [Wang, 2003]. An increase in the forward WGS activity of the catalyst would result in the production of hydrogen. This would lead to a more hydrogen-rich environment in the reactor and consequently the production of methane may be enhanced.

HTIc 102 produces the highest amount of methane compared to all the other catalysts. This is again in contradiction of what is expected from an iron catalyst doped with alkali. The methane produced by HTIc 105 is much lower than that produced by the HTIc 100.

University of Cape Town

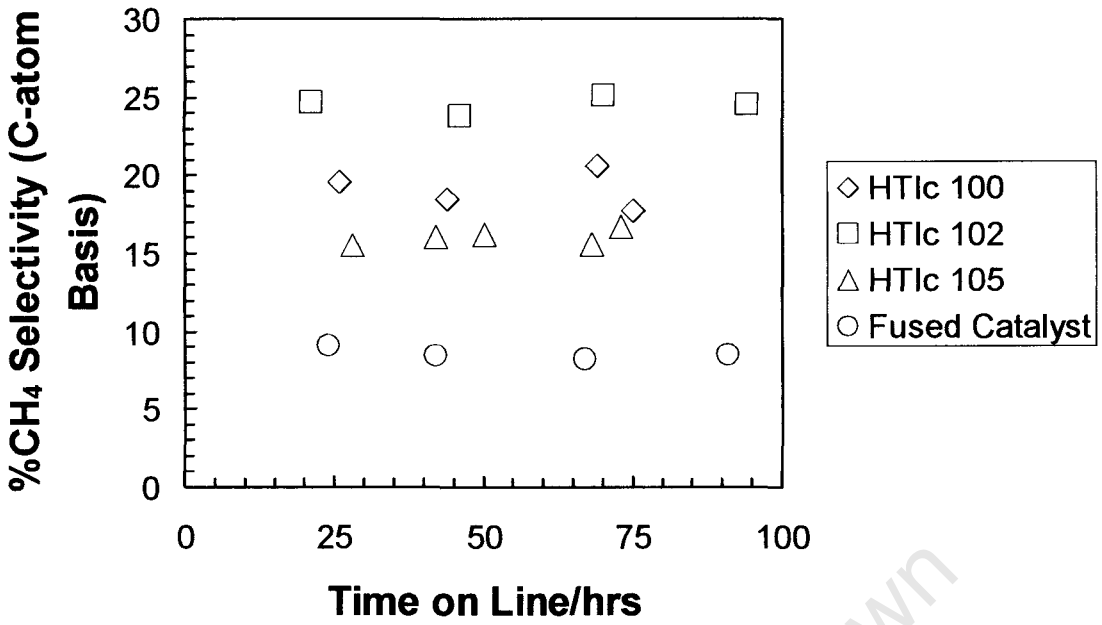

Figure 4.21: Methane selectivity during the Fischer-Tropsch synthesis as a function of time-on-line of hydrotalcite derived catalysts compared with the standard fused iron catalyst

In accordance with that discussed above, it is also observed that the hydrotalcite derived catalysts produce more hydrogenated products compared to the fused catalyst as shown in figure 4.21 and 4.22. The product spectrum of the hydrotalcite derived catalyst is also more paraffinic, with the exception of the selectivity towards propene (figure 4.23).

University of Cape Town

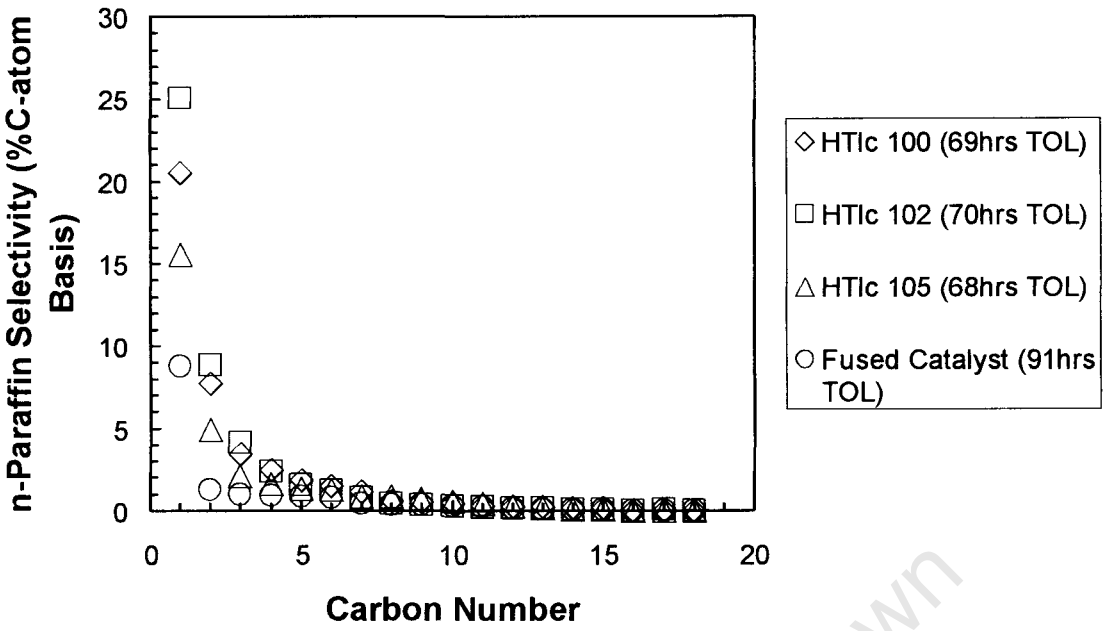

Figure 4.22: n-Paraffin selectivity during the Fischer-Tropsch synthesis as a function of time-on-line of hydrotalcite derived catalysts compared with the standard fused iron catalyst

University of Cape Town

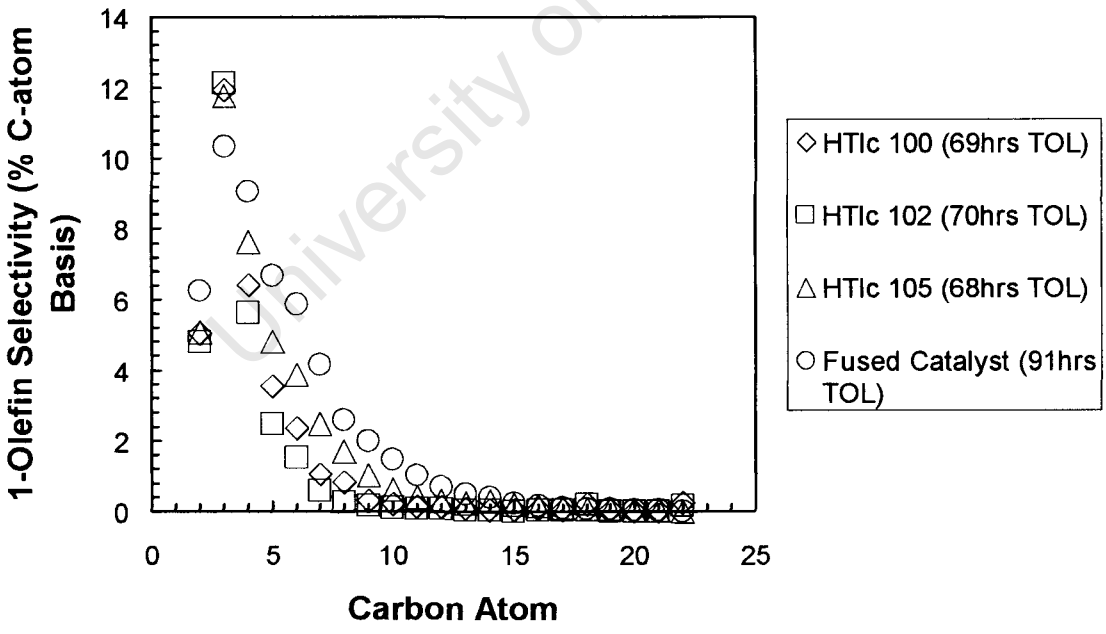

Figure 4.23: 1-Olefin selectivity during the Fischer-Tropsch synthesis as a function of time-on-line of hydrotalcite derived catalysts compared with the standard fused iron catalyst

The alcohol selectivity of the fused catalyst is higher compared to the hydrotalcite derived catalyst with the exception of the copper promoted catalyst, HTlc 105 which produces a much higher quantity of ethanol and similar amounts of the other alcohols compared to the fused catalyst (see figure 4.22).

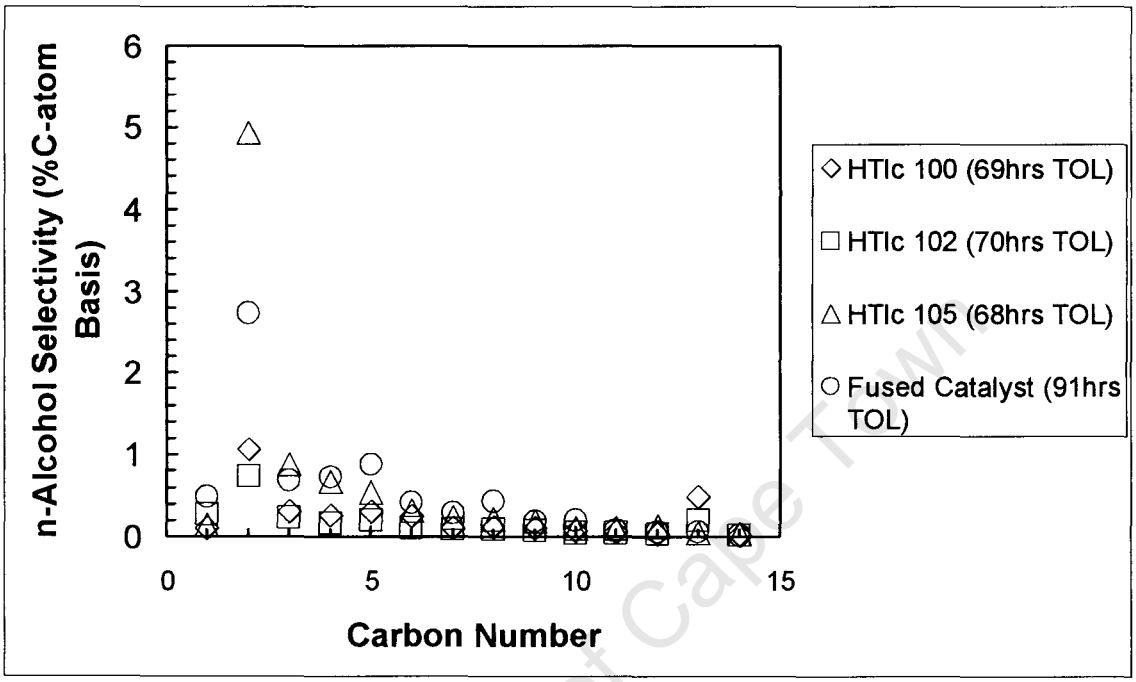

Figure 4.22: n-Alcohol selectivity during the Fischer-Tropsch synthesis as a function of time-on-line of hydrotalcite derived catalysts compared with the standard fused iron catalyst

University of Cape Town

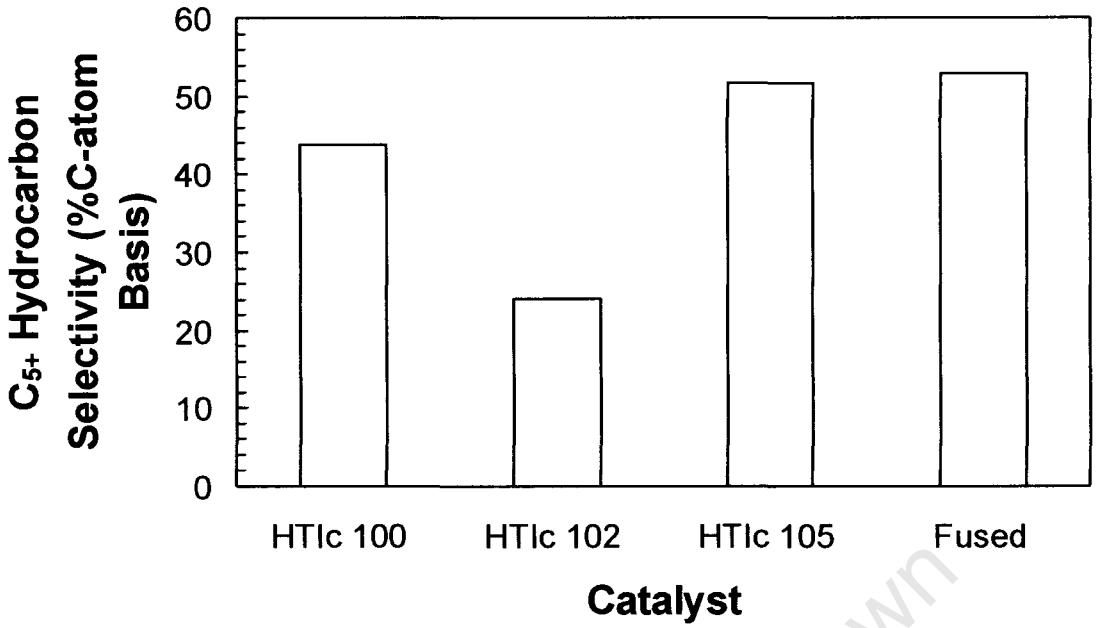

Figure 4.25: C_{5+} selectivity of hydrotalcite derived catalysts compared with the standard fused iron catalyst

The fused catalyst and HTIc 105 have similar C_{5+} selectivities as illustrated by figure 4.25, which is higher than the other HDCs. It is surprising as the copper promoted HDC appears to have produced higher quantities of the shorter chain products compared to the fused catalyst and it would therefore be expected to have a lower C^{5+} selectivity. There could be error in the analysis due to the combination of the cold tail analysis and the oil analysis to obtain the selectivity as well an error in the methods that are used. The error may be amplified in the higher carbon number products as lower quantities of these products are formed.

Again the potassium promoted catalyst results are in contradiction to what is expected of an iron catalyst doped with alkali, as it appears to have the lightest product spectrum.

University of Cape Town

The hydrocarbon selectivity data was used to derive Anderson-Schulz-Flory (ASF) plots for the catalysts as shown by figure 4.26. In addition to the expected deviation for the methane and the C_2 products, there is significant deviation from C_6 to the higher carbon numbers. This is due to the combination of the analysis of the tail gas with that of the oil phase.

ASF plots from C_9-C_{15} (see figure 4.27) give straight lines with acceptable R^2 values as shown in table 4.2 together with the alpha values that have been calculated.

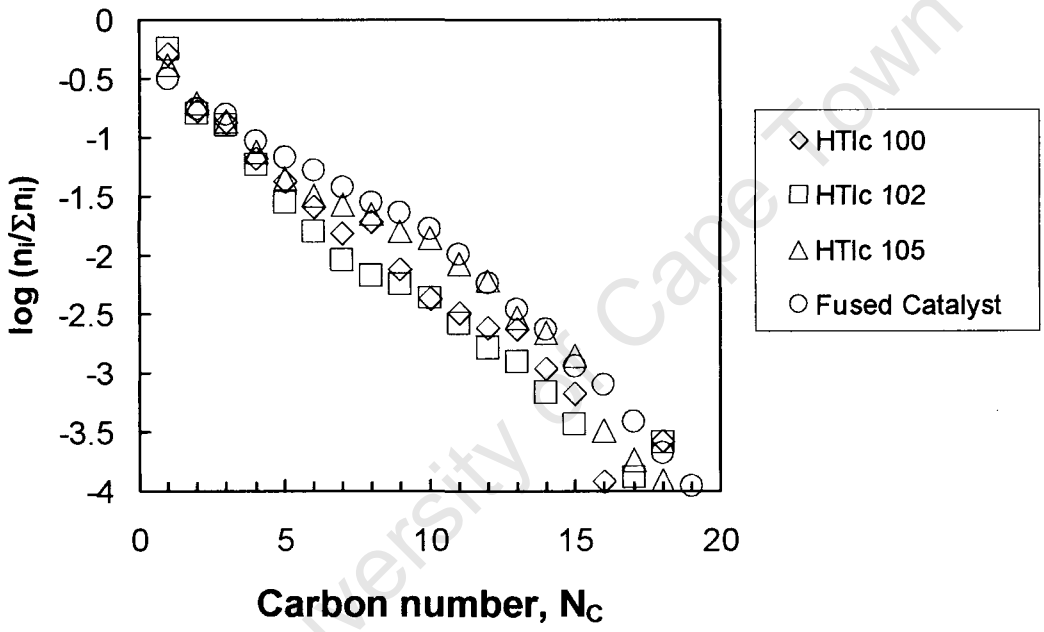

Figure 4.26: Anderson-Schulz-Flory distribution of C_1-C_{20} products calculated from the combination of the tail gas and the oil phase analysis for hydrotalcite derived catalysts compared with the standard fused iron catalyst

University of Cape Town

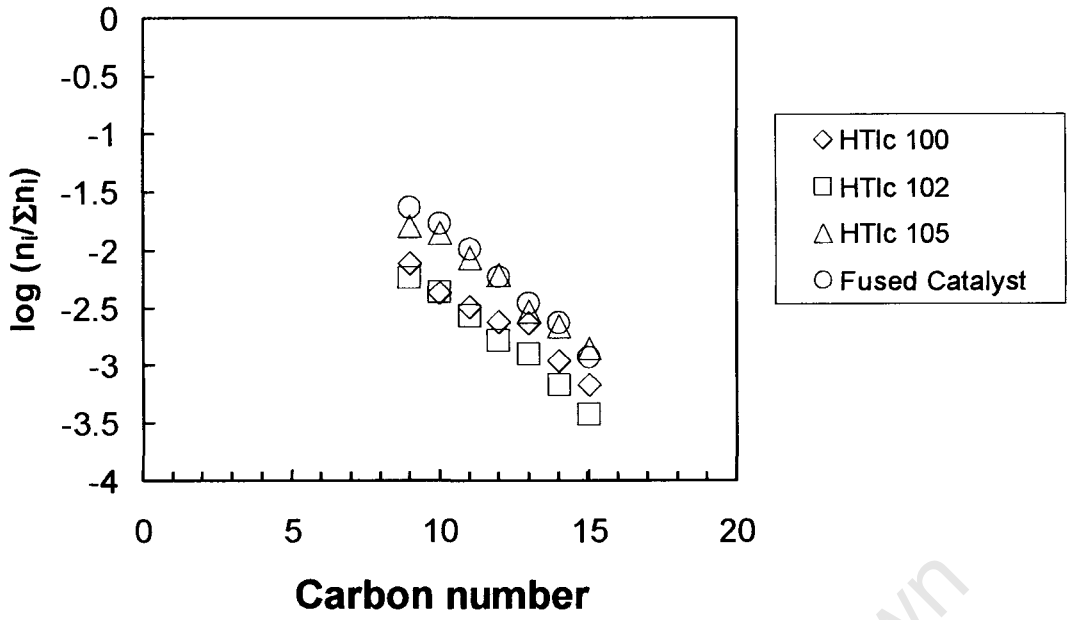

Figure 4.27: Anderson-Schulz-Flory distribution of C_9-C_{15} products calculated from the combination of the tail gas and the oil phase analysis for hydrotalcite derived catalysts compared with the standard fused iron catalyst

Table 4.2: Alpha values calculated from Anderson-Schulz-Flory plots in the range (C_9-C_{15}) for hydrotalcite derived catalysts and a standard fused catalyst

Catalyst	Alpha Value	R^2
HTlc 100	0.69	0.9542
HTlc 102	0.64	0.9876
HTlc 105	0.65	0.9821
Fused Catalyst	0.61	0.9936

The alpha values of the hydrotalcite derived catalyst are higher than that of the fused catalyst. This implies that the hydrotalcite derived catalyst produce longer chain hydrocarbons compared to the fused catalyst. This is not in line with the results that have been obtained where the methane selectivity of the HDCs as well as the amounts of short chain products was found to be much higher than the fused catalyst.

University of Cape Town

This could be due to errors in the analysis of the higher carbon number products as the quantities of these products are much lower and the error may thus be amplified. In addition there may be errors arising from the combination of data from the tail gas and the oil phase analysis which would overlap in this region.

Table 4.3: Relative Acid Make of the Catalysts

Catalyst	Relative Acidity
HTlc 100	0.19
HTlc 102	0.11
HTlc 105	0.24
Fused catalyst	1

The acidity of the reaction water was determined by an in house method described in the chapter 3 to yield what is termed an acid number. The acid number of the fused catalyst was the highest compared to the hydrotalcite derived catalyst. The acid numbers of the hydrotalcite derived catalysts were calculated relative to the value of the fused catalyst. This gives an indication of the amount of acidic products produced by the different catalyst.

The potassium promoted catalyst has the lowest acid make. This is again is not in line with what was expected from this catalyst.

The copper containing catalyst has a slightly lower acid make compared to the unpromoted catalyst. This may be either a direct or an indirect effect brought about by the addition of copper to the catalyst.

University of Cape Town

Chapter 5

DISCUSSION

5.1. Catalyst Preparation

Three methods of precipitation are commonly used to prepare hydrotalcites, namely: titration with NaOH and/or $NaHCO_3$ (increasing pH method), precipitation at constant pH and high supersaturation conditions and precipitation at constant pH and low supersaturation conditions. The latter method is the one that has been employed in this study. Low supersaturation conditions usually give rise to precipitates which are more crystalline in comparison to those obtained at high supersaturation conditions. At high supersaturation a large number of particles is obtained, which are usually small in size as the rate of nucleation is much higher than the rate of crystal growth. [Cavani, 1991].

University of Cape Town

Another factor influencing the crystallite size is the temperature at which the precipitation is done. In this study, the precipitation was carried out at room temperature. If the temperature is increased, this would result in an increase in the rate of nucleation and a decrease in the rate of crystal growth thereby producing smaller crystals.

To obtain a pure hydrotalcite, it was essential to maintain the pH between approximately 8 and 10 during preparation. When the pH exceeded 10 during the preparation, the hydrotalcite precipitate appeared to partially redissolve and

it was believed that $Mg(OH)_2$ started to precipitate out. This was deduced from the change in colour of the solution and the decrease in the viscosity of the slurry. Below pH 8, $Fe(OH)_3$ may precipitate out.

Hydrotalcites with a Mg/Fe ratio of 2/1 and 3/1 were successfully prepared. It was however not possible to prepare a hydrotalcite with a Mg/Fe ratio of 6/1. Shen *et al.* (1996) successfully synthesized Mg-Al hydrotalcites with Mg/Al ratio of 6:1. The synthesis of Mg-Al-hydrotalcites with a Mg/Al-ratio between 5:1 and 10:1 can be accomplished by carefully controlling the co-precipitation conditions such as mixing, pH and temperature (Schaper *et al.*, 1989). The hydrotalcites prepared by Shaper *et al.* were however described as being synthesized without the formation of *considerable* amounts of separate magnesium compounds. Therefore, *pure* hydrotalcites, without the formation of *any* separate compounds, within the above mentioned range (5:1 and 10:1) were not obtained. by Shaper *et al.*

It has been found that it is only possible to obtain *pure* hydrotalcites for $0.2 \leq x \leq 0.33$ (where $x = M^{3+}/(M^{2+} + M^{3+})$) which correspond to a ratio of magnesium to iron of 4 to 2 [Cavani, 1991]. Work on Mg-Al hydrotalcites has shown that for x values greater than 0.33, the increased likelihood for neighboring Al octahedra leads to the formation of $Al(OH)_3$ and similarly, low values of x leads to a high density of Mg octahedra in the sheets which act as a nuclei for the formation of $Mg(OH)_2$ [Cavani, 1991].

Following this reasoning, the presence of $Mg(OH)_2$ was expected in a Mg-Fe hydrotalcite with a ratio of magnesium to iron of 6 (x=0.14). However, the phases that were identified in the sample with a ratio of Mg to Fe of 6:1 were in addition to the hydrotalcite, hydromagnesite ($Mg_5(CO_3)_4(OH)_2.4H_2O$), and Goethite (FeO(OH)). The sample may have changed during the aging or these phases may have formed initially.

University of Cape Town

5.2. Catalyst Characterisation

5.2.1. Transformation of Mg-Fe Hydrotalcite during Heat Treatment

The thermal decomposition behavior of an unpromoted Mg-Fe hydrotalcite with a ratio of magnesium to iron of 2 was investigated by DSC-TGA (coupled with MS) and in-situ XRD. Two endothermic transitions were shown to take place with the TGA.

The first at low temperature (~145°C) corresponds to the loss of interlayer water. The second transition, at higher temperature (~300°C) is due to the loss of hydroxyl groups from the brucite-like layer, as well as of the anions. This was as described in literature [Cavani, 1991].

Work done on Al-containing hydrotalcites has shown that the temperature of the first transition that takes place ranges from 97-297°C and the second from 347-447°C. However, these two transitions were found to depend, both quantitatively and qualitatively, on factors like M^{2+}/M^{3+} ratio, type of anion and on the drying/heat treatment conditions used [Cavani, 1991].

From the in-situ XRD results, it was found that, at approximately 140°C, the hydrotalcite structure appears to have collapsed or transformed into other phases that could not be identified with certainty. This corresponds to the temperature at which the first transition takes place as shown by the TGA and would be due to the loss of interlayer water. This is however in contradiction to what is expected from literature [Cavani, 1991] as the first transition that takes place has been reported to be reversible and to occur without the collapse of the structure.

At temperatures above 300°C the XRD scans show that the sample appears to become amorphous. This change corresponds with the temperature at which the second transition takes place as shown by the TGA, where some the hydroxyl groups bound to the metals are lost as H_2O and the interlayer carbonate anions come off as CO_2.

University of Cape Town

No further mass loss is observed with the TGA after the second transition. However, a number of phase changes are shown by the XRD scans to have taken place on continued heating. At 400°C, some degree of crystallinity starts to re-appear with the formation of MgO. Above 600°C the formation of a magnesioferrite spinel ($MgFe_3O_4$) is observed. The sample becomes more crystalline on further heating up to 800°C however; no further phase changes take place.

5.2.2. Transformations of Mg-Fe Hydrotalcite during Activation in H_2

The activation procedure used for iron-based Fischer-Tropsch synthesis catalysts has a great influence on the activity and selectivity of the catalyst. [O'Brien, 1996] The HTFT fused catalyst is activated by passing H_2 over the catalyst at temperatures in the region of 350-450°C. Fused iron oxides are non-porous and hence their areas are extremely low (~1m^2/g). Activation/reduction is therefore essential to develop the area required for acceptable FT activity [Steynberg, 2004].

In addition, it is believed that, for optimal performance of the catalyst during synthesis, it needs to be reduced to metallic iron. Therefore the objective of the activation is to generate a high surface area metallic catalyst. The reduction route that is followed by the fused iron catalyst is illustrated by equations 5.1 and 5.2.

$$Fe_3O_4 + H_2 \Leftrightarrow FeO + H_2O \qquad (5.1)$$

$$FeO + H_2 \Leftrightarrow Fe_{metal} + H_2O \qquad (5.2)$$

The fused catalyst starts out as Fe_3O_4 (magnetite) which consists of a mixture of Fe^{3+} and Fe^{2+} species. This is then reduced to α-Fe (metallic iron) possibly via FeO (wustite) [Bukur, 1995]. Wustite is a thermodynamically metastable

University of Cape Town

phase with respect to magnetite and iron at temperatures below 570°C [Edstrom, 1953].

Since the fused catalyst has such a low initial surface area, the uptake of hydrogen only takes place from ca. 400°C as shown by the TPR results. Many factors can influence the rate of reduction and the final product of the reduction process, such as, the H_2/H_2O ratio, flow rate of reducing gas, crystallite size and the surface area of the catalyst. Under the same TPR conditions, the profile of the calcined hydrotalcite is very different compared to the fused catalyst.

The calcined hydrotalcite consists of MgO and a magnesium iron spinel $MgFe_2O_4$ (magnesioferrite). In the TPR there are two distinct peaks present. The first peak is attributed to the reduction of Fe^{3+} to Fe^{2+} [Shen, 1996]. The hydrogen uptake starts at around 250°C. In-situ XRD under hydrogen showed the segregation of small quantities of metallic iron starting at ca. 250°C. This is accompanied by a transformation of the initial phases (MgO and $MgFe_2O_4$) into a magnesium iron oxide ($Mg_xFe_{1-x}O$). It is believed that the mixed oxide consists of both Fe^{3+} and Fe^{2+} species, thus resulting in hydrogen consumption.

The second peak is attributed to the reduction of Fe^{2+} to Fe^0 [Shen, 1996]. This peak appears at a much higher temperature. This could be because the Fe^{3+} to Fe^{2+} transition takes place with greater ease compared to the Fe^{2+} to Fe^o transition. It could also be a result of the increase in concentration of irreducible oxides surrounding the unreduced iron as the mixed oxide becomes enriched in magnesium when the iron metal segregates out upon reduction.

The calcined hydrotalcite starts to reduce at around 250°C as opposed to the fused catalyst which only starts to take up hydrogen at around 400°C. This might be attributed to the high surface area (~110m^2/g) of the calcined hydrotalcite compared to the pre-reduced fused catalyst (~1m^2/g). A more fair comparison would however be based on the metal surface areas of the catalysts.

University of Cape Town

The uptake of hydrogen starts at around 250°C from the TPR results however it is only at around 400°C that *significant* amounts of iron is detected using the in-situ XRD. This could be due to the sensitivity of the instruments. In the TPR, the thermal conductivity detector would easily pick up the change in hydrogen concentration however; the XRD would only be able to detect the iron phase once there is a discernable amount of iron present to form a packed structure.

From the in-situ reduction experiment, it is shown that the amount of iron metal increases with increasing temperature however, the catalyst is not completely reduced at 560 °C. This could be due to the formation of irreducible iron species. It could also be due to the conditions within the instrument. The XRD has a large dead volume surrounding the sample where back mixing of the reactant and product gases can take place. Thus, if there is residual H_2O from the reduction, it could result in retardation of further reduction process or even re-oxidation of the catalyst.

University of Cape Town

5.3. Fischer-Tropsch Data

5.3.1. CO and CO+CO_2 Conversion

The fused iron HTFT-catalyst showed a higher total CO conversion and the conversion of CO solely to FT products. However, the pre-reduced fused iron catalyst contains approximately 70% iron, whereas hydrotalcite derived catalyst prior to reduction only contains approximately 40% iron. If the iron content of the catalysts is taken to account, the efficiency of the hydrotalcite derived catalysts are clear (see Figure 5.1. and 5.2.). In addition it must be noted that the hydrotalcite derived catalysts may not be completely reduced and thus the amount of active metal available for FT may be even lower.

The metal surface area is where the reaction takes place and the activity is thus related to the surface area of the iron crystallites. Hence, the metal surface area per unit mass of iron must be higher for the hydrotalcite catalysts. This should be confirmed by chemisorption measurements.

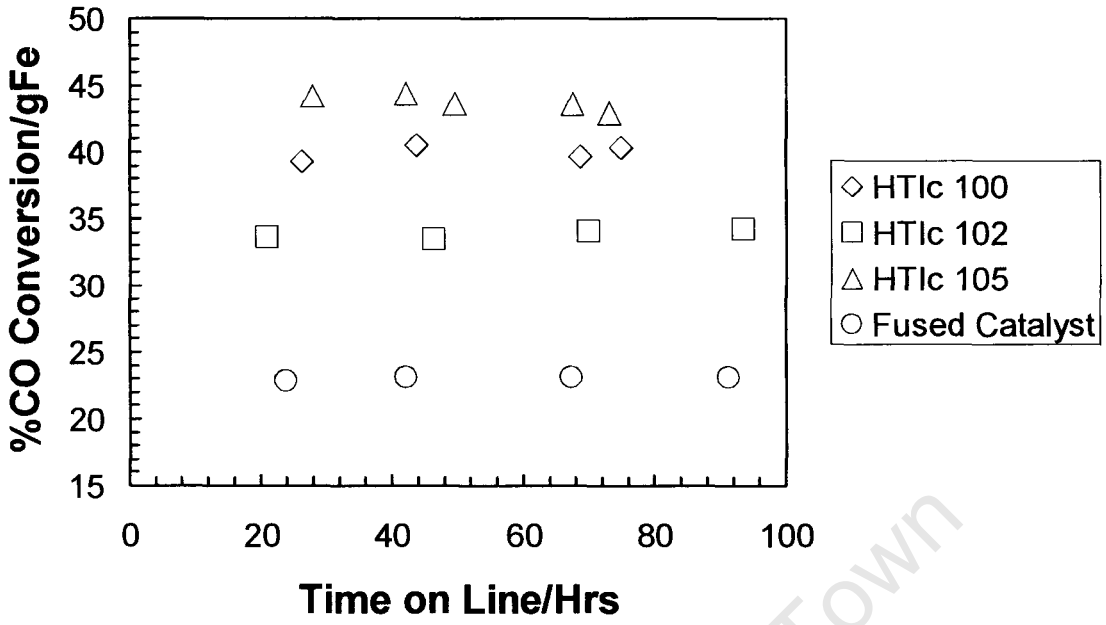

Figure 5.1.: %CO Conversion during the Fischer-Tropsch synthesis calculated per gram of iron as a function of time-on-line of hydrotalcite derived catalysts compared with the standard fused iron catalyst

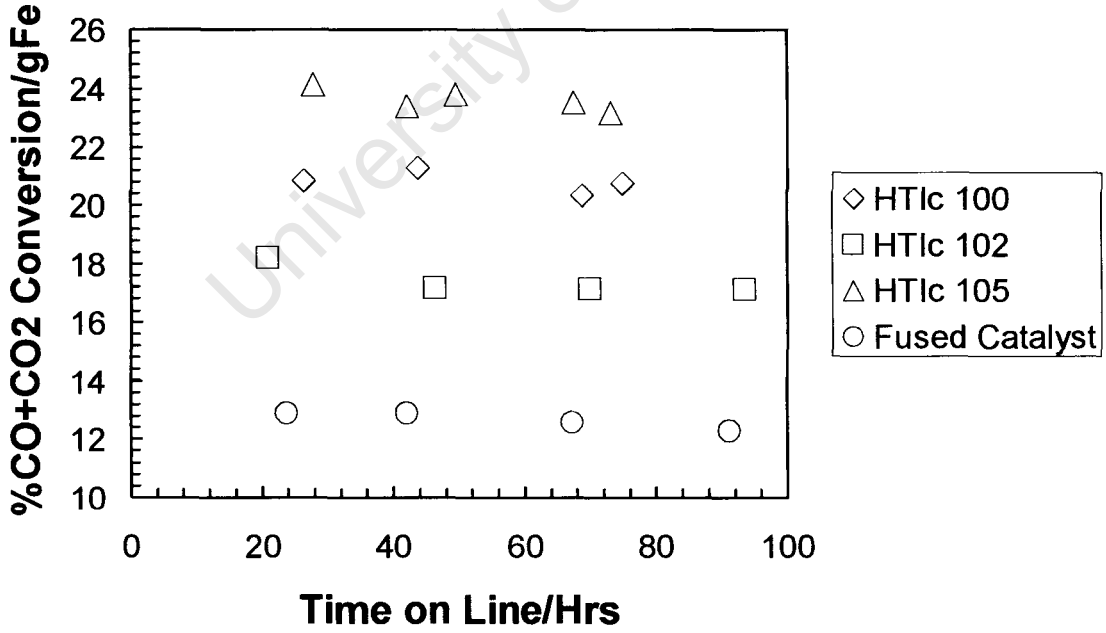

Figure 5.2: %CO+CO_2 Conversion during the Fischer-Tropsch synthesis calculated per gram of iron as a function of time-on-line of

University of Cape Town

hydrotalcite derived catalysts compared with the standard fused iron catalyst

The CO and the CO+CO_2 conversion per gram of iron of the HDC is almost twice that of the fused catalyst. Thus the performance of the HDCs is similar to the fused catalyst and the efficiency of the HDCs is higher than the fused catalyst, despite the lower iron content.

5.3.2. FT selectivity

Under the HTFT reaction conditions, the water-gas shift reaction might be considered to be a consecutive reaction following the consumption of carbon monoxide for the formation of hydrocarbons:

$$2H_2 + CO \rightarrow (CH)_2 + H_2O \qquad r_{FT} \qquad (5.3)$$

$$CO + H_2O \Leftrightarrow H_2 + CO_2 \qquad r_{WGS} \qquad (5.4)$$

The rates of the two reactions, and hence the FT selectivity is dependent on a number of factors such as, the catalyst (including the promoters), the operating conditions, the compositions of the feed gas as well as the partial pressures of the gases inside the reactor. The latter factor may influence the FT selectivity both directly and indirectly.

An increase in the rate of the FT reaction will result in a decrease in the partial pressure of H_2 and CO and an increase in the partial pressure of H_2O. A higher concentration of H_2O in the reactor results in a higher probability of deactivation of the catalyst via re-oxidation. A change in the catalyst phase results in a change in the FT selectivity. Oxides have been shown to promote the water-gas shift reaction. [Wang, 2003]. An increase in the partial pressure of water will shift the water-gas shift reaction towards the production of hydrogen and CO_2 resulting in an increase in the partial pressure of H_2 and CO_2 in the reactor and a decrease in the partial pressure of CO.

The hydrotalcite derived catalysts contain unreduced/irreducible iron oxides which enhance the water-gas shift (WGS) reaction. An enhancement in the

University of Cape Town

forward water-gas shift reaction results in a decrease in the partial pressure of CO and an increase in the partial pressure of H_2 inside the reactor. Thus, the hydrogen to carbon monoxide ratio within the reactor will increase due to the water-gas shift reaction, which may favour the formation of short chain hydrocarbons [Roper, 1983]. This was indeed observed with the catalysts tested and is shown in Figure 5.3, which shows a correlation between the observed methane selectivity (in C-%) as a function of the water partial pressure in the reactor. With an increase in the water partial pressure, a reduction in the methane selectivity is observed. The fused catalyst had the highest water partial pressure and the lowest methane selectivity compared to the hydrotalcite derived catalysts. The potassium promoted hydrotalcite derived catalyst has the highest methane and the lowest partial pressure of water. As mentioned in the results section, this is in contradiction to what was expected of a catalyst doped with alkali.

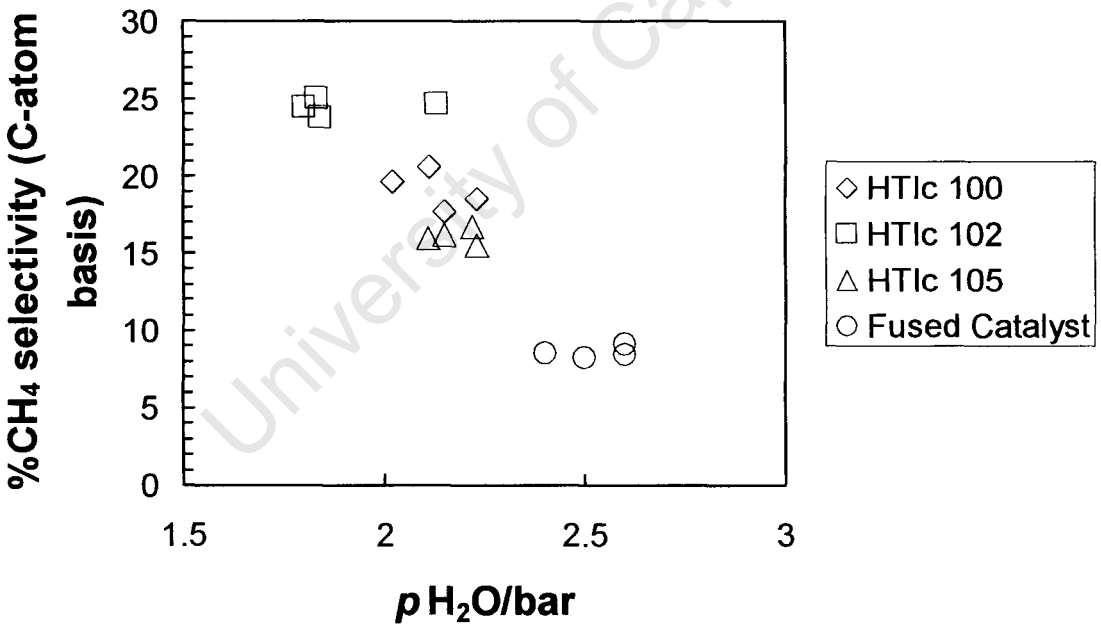

Figure 5.3: Methane selectivity (C-%) in the Fischer-Tropsch synthesis as a function of the water partial pressure inside the reactor for hydrotalcite derived catalysts compared with the standard fused iron catalyst

University of Cape Town

The amount of short chain products (C_2 and C_3) are higher with the hydrotalcite derived catalysts compared to the fused catalyst. Figure 5.4 shows the product distribution within the C_2-fraction for the various catalysts. The fused iron catalyst shows the highest ethene content, despite the high H_2/CO ratio to which this catalyst was exposed (see Figure 4.19). The ethene content in the C2-fraction is approximately constant for the hydrotalcite derived catalysts.

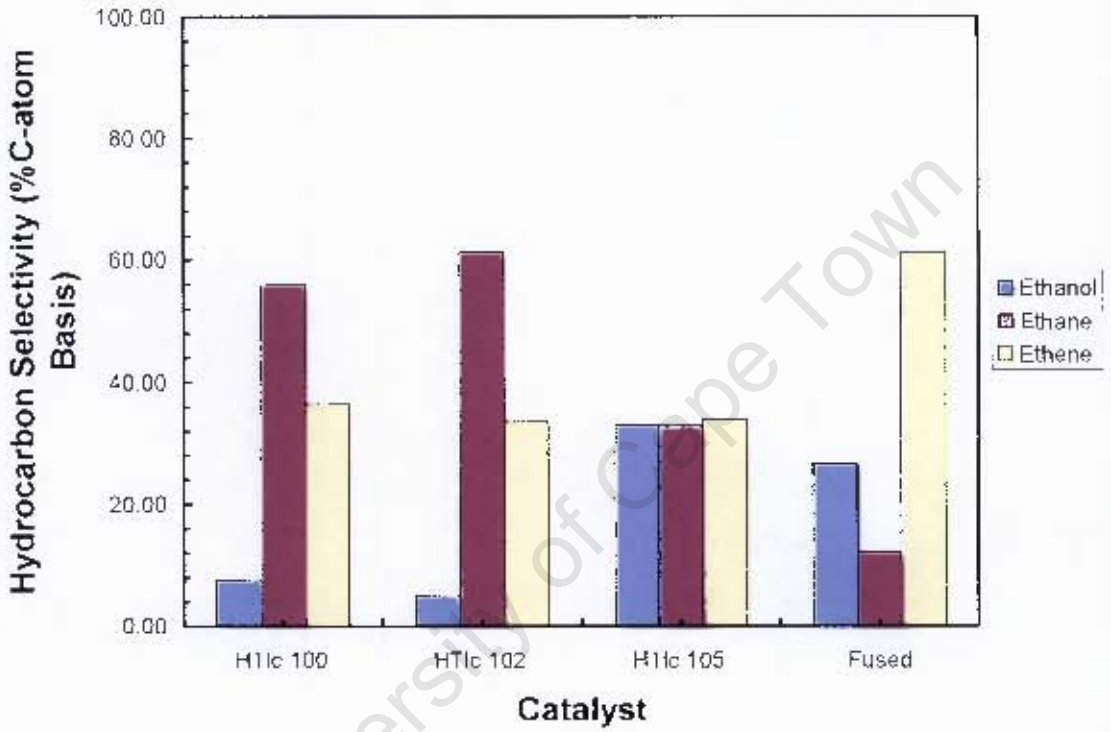

Figure 5.4: Normalised C_2 hydrocarbon selectivity for hydrotalcite derived catalysts compared with the standard fused iron catalyst

The ethanol content in the copper promoted hydrotalcite derived catalyst (HTlc105) is significantly higher than with the other hydrotalcite derived catalysts. This might be attributed to copper, a known compound in catalysts for alcohol synthesis. Copper promotion of iron catalysts has been shown to enhance the formation of alcohols [Cavani, 1991]. Cu-Zn-Cr and Cu-Zn-Al hydrotalcites have been tested for methanol synthesis and have shown above 90% selectivity towards the formation of methanol.

University of Cape Town

The synthesis of higher alcohols has been achieved by doping the hydrotalcite derived catalyst with alkali. [Cavani,1991]. The potassium promoted hydrotalcite derived catalyst did not produce the expected results. Potassium has been shown to act as a poison when added in high amounts. It has been observed that the activity of an iron catalyst promoted with potassium passes through a maximum as the potassium content is increased and thereafter it may result in a decrease in the activity of the catalyst [Dry, 1981]. The amount of potassium added to the catalyst is however fairly low and has shown beneficial results for iron catalysts in the high temperature Fischer-Tropsch synthesis [Steynberg, 2004]. The conflicting results should therefore be investigated further as the possibilities of a hydrotalcite derived catalyst would be much greater if the positive effects of alkali promotion can be attained.

From the C_3 cut, the paraffin content of the hydrotalcite derived catalysts is again higher compared to the fused catalyst (see Figure 5.5). The dominant product in this cut is the olefin. All the hydrotalcite derived catalysts have similar propene selectivity which is slightly lower than that produced by the fused catalyst. For the hydrotalcite derived catalysts it is again interesting to note that the paraffin and the alcohol content vary and that the olefin content in the C_3-fraction remains fairly unchanged. The HTIc 105 catalyst shows the highest alcohol content in the C_3-fraction (similar to the observation on the product distribution in the C_2-fraction). However this is only marginally higher compared to the fused catalyst.

University of Cape Town

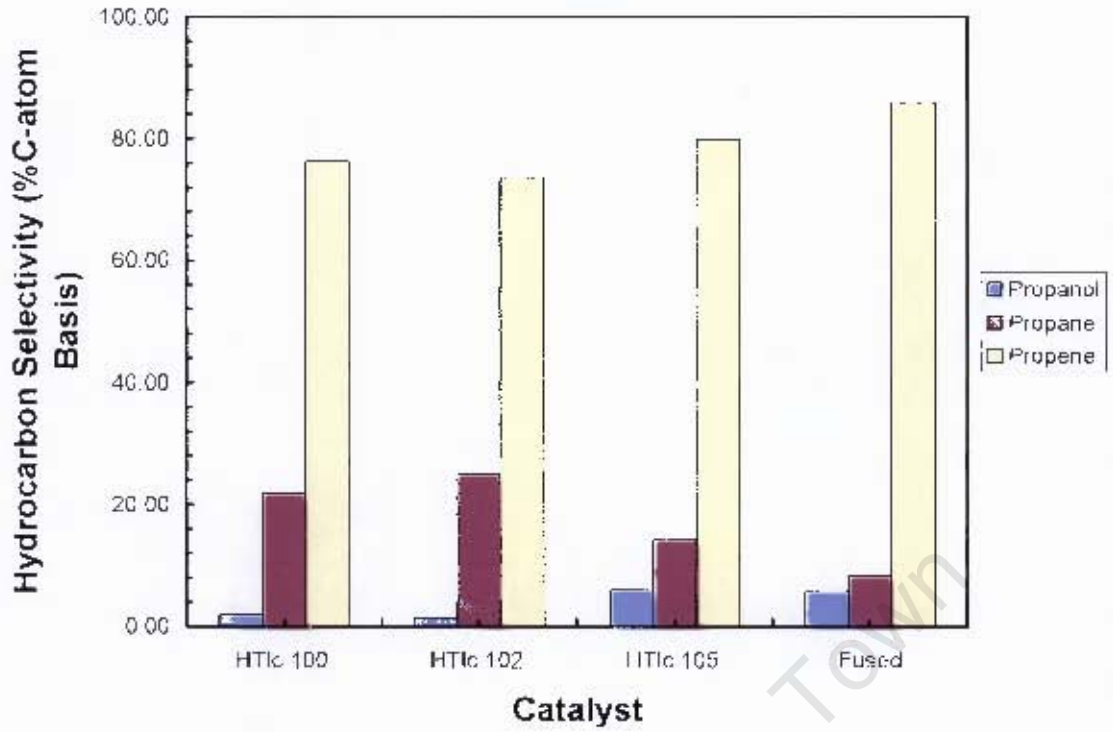

Figure 5.5: Normalised C_3 hydrocarbon selectivity for hydrotalcite derived catalysts compared with the standard fused iron catalyst

The olefin content as a fraction of the linear hydrocarbon products (n-olefins and n-paraffins) is shown in Figure 5.6. The olefin content is almost independent of carbon number for the fused catalyst. The hydrotalcite derived catalysts show a strong carbon number dependency on the olefin content in the fraction of linear hydrocarbons, which is characteristic for secondary olefin hydrogenation [Claeys, 1999]. The olefin content shows a maximum at C_3, since this olefin is less reactive than ethene and has the lowest concentration in the catalyst pores. The extent of secondary olefin hydrogenation is more pronounced with the hydrotalcite derived catalysts, either unpromoted or promoted with potassium. The copper promoted hydrotalcite derived catalyst appears to be less sensitive for secondary olefin hydrogenation.

University of Cape Town

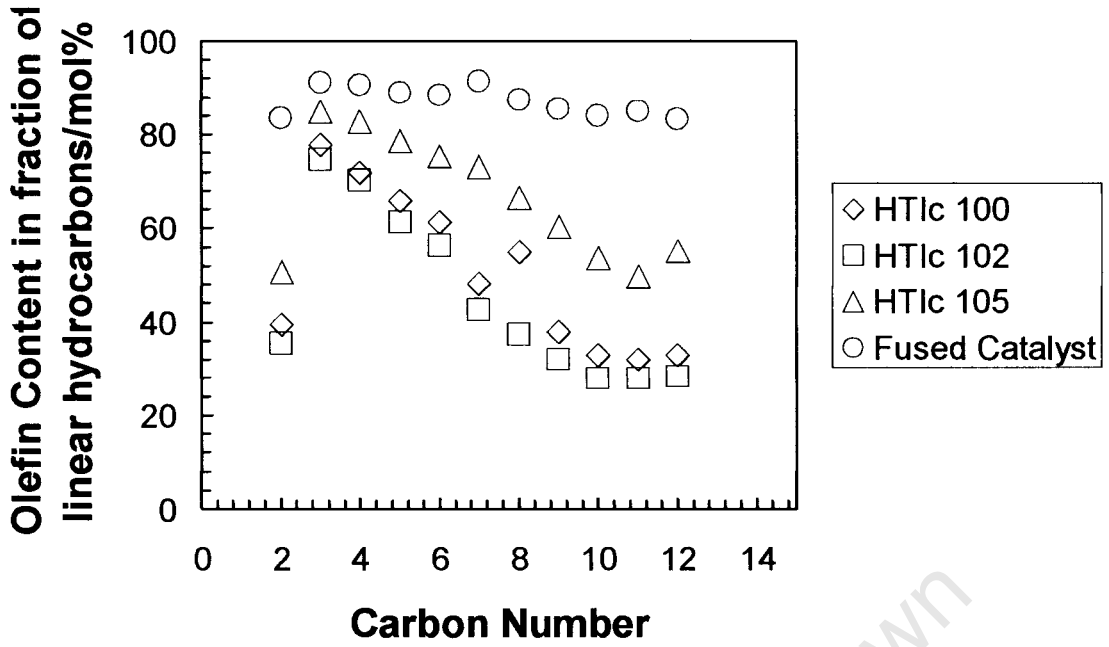

Figure 5.6: Olefin content in fraction of linear hydrocarbons as a function of carbon number for hydrotalcite derived catalysts compared with the standard fused iron catalyst (approximately 70 hours on line)

Figure 5.7 shows the alcohol content in the linear products as a function of carbon number after approximately 70 hours on line. The alcohol content as a function of carbon number shows the characteristic dependency as observed previously [van Steen, 1993]. The alcohol content in the C_1-fraction is relatively low and typically shows an absolute maximum at C_2. The alcohol content typically shows a minimum at C_3-C_5 and passes a maximum at higher carbon numbers. The origin of this peculiar trend is up to now unclear. The alcohol content is the highest with the copper promoted hydrotalcite derived catalyst, as was already seen in the evaluation of the C_2 and the C_3-fraction. However, the methanol content in the C_1-fraction is with this catalyst in line with what is observed for the other hydrotalcite derived catalysts and lower than for the fused iron catalysts.

University of Cape Town

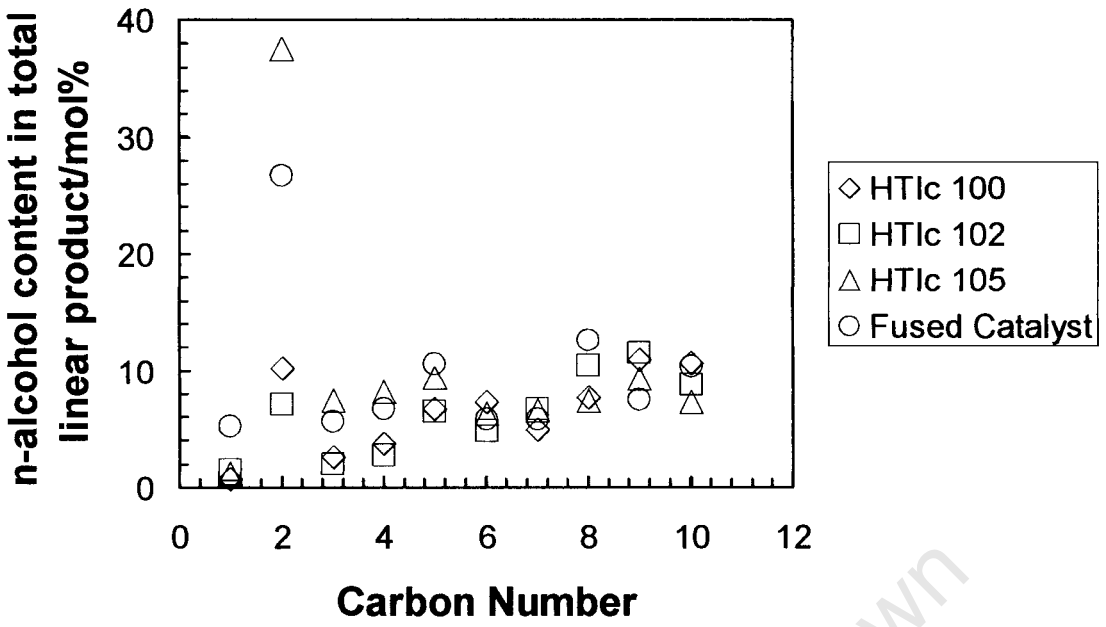

Figure 5.7: n-Alcohol content in fraction of linear organic product compounds as a function of carbon number for hydrotalcite derived catalysts compared with the standard fused iron catalyst (approximately 70 hours time on line)

University of Cape Town

However, despite the increase in reactor partial pressure of hydrogen for the hydrotalcite derived catalysts, the selectivity towards the shorter chain alpha olefins is similar for the C_2 fraction and higher in the case of propene compared to the fused catalyst. A more hydrogenating environment is generally conducive to a decrease in the formation of acidic products. This is in line with the results obtained for the HDCs. Therefore the hydrotalcite derived catalyst has produced higher quantities of valuable short chain olefins with a lower acid make.

The hydrotalcite derived catalyst thus has the advantages of a supported catalyst, in that only a small amount of iron is needed to achieve similar conversions as a bulk iron catalyst. In addition, the magnesium appears to have a satisfactory basicity with respect to its selectivity compared to the fused catalyst with the added benefit of a lower acid make.

Chapter 6

CONCLUSIONS AND RECOMMENDATIONS

The hypothesis that, a Mg-Fe hydrotalcite derived catalysts would provide a high surface area basic catalyst suitable for use in the Fischer-Tropsch synthesis was tested. The Mg-Fe hydrotalcites were produced by precipitation at constant pH and low supersaturation conditions. Under the conditions used, it was only possible to produce hydrotalcites with Mg/Fe ratios of up to 3/1. There are a number of preparation variables such as, the precipitation pH and temperature, the reagent concentrations, the flow rates of the reagents and the ageing times and temperatures, that can be changed and optimised in the catalyst preparation and these should be investigated as they also affect the physical properties of the final catalyst.

The hydrotalcites were thereafter calcined and activated prior to synthesis under high temperature Fischer Tropsch (HTFT) conditions. At the calcinations temperature employed (625°C), the Mg-Fe hydrotalcite was transformed into MgO and $MgFe_3O_4$ (magnesioferrite spinel). No further phase changes took place up to 800°C however surface enrichment of the iron may have may have occurred. Further work should be done to determine if this does take place and its possible effect on the reducibility and basicity of the catalyst. The pre-reduced hydrotalcite derived catalyst had a much higher surface area compared to the fused catalyst.

University of Cape Town

The suitability of their performance was determined by comparing them to a "standard" fused catalyst used in the HTFT process. A Mg-Fe hydrotalcite with a Mg/Fe ratio of 2/1 was tested and it showed an overall CO conversion of ca. 75% and conversion to FT products of ca. 40%. The performance was comparable to that of the fused catalyst. The selectivity results of the hydrotalcite derived catalyst compared well with the fused catalyst but differed in that the former produced a lighter, more paraffinic hydrocarbon spectrum.

Thus the hydrotalcite derived catalyst had the advantages of a supported catalyst, as only a small amount of iron was required to achieve similar conversions as a bulk catalyst. In addition, the magnesium appears to have a satisfactory basicity with respect to its selectivity compared to the fused catalyst with the added benefit of a lower acid make. Hence, the hypothesis has in most part been proven.

A further aim of the work was to assess the responsiveness of the catalyst to chemical promotion. Two important aspects that needed to be considered in the development of this catalyst for FT synthesis were its reducibility and basicity as this affected both the activity and selectivity of the catalyst. Both aspects are dependent on the Mg/Fe ratio of the catalyst. An increase in the ratio would result in an increase in the basicity and a decrease in the reducibility of the catalyst.

Potassium was added to the calcined hydrotalcite in an attempt to increase the basicity without adversely affecting the reducibility of the iron. The results from this catalyst however were in contradiction to what was expected from a potassium promoted catalyst. This should be investigated further as the possibilities of a hydrotalcite derived catalyst would be far greater if the positive effects of alkali promotion can be attained.

University of Cape Town

The hydrotalcite derived catalysts did not undergo complete reduction under the conditions used and copper was added in an attempt to increase the amount of active metallic iron present and to thereby improve the catalytic activity. This was successful as the copper promoted catalyst had improved conversions and showed a marked decrease in the amount of methane formed. The catalyst also produced a much higher quantity of ethanol and similar amounts of the other alcohols compared to the fused catalyst. The levels of copper added to the catalyst should be optimised. Further studies can also be done to determine the effect of incorporating the promoters into the hydrotalcite structure. The closer interaction of the metals may lead to synergistic effects.

The calcinations temperature will also affect the activity and selectivity of the catalyst. This relationship is however more complex. Changes in the Mg/Fe ratio or calcination temperature do not *only* affect the reducibility and basicity of the catalyst. These changes can also affect the surface area (and therewith active/accessible sites) of the catalyst and the crystallite size of the iron.

The reduction/activation conditions as well as the synthesis conditions also need to be optimised for this catalyst. The work is directly related to the investigations that need to be carried out to further characterise the catalyst, bulk and surface phases and the determination of the possible changes in these phases under synthesis conditions. This will provide insight into the limitations or flexibility of the catalyst systems.

University of Cape Town

References

Anderson, R.B.,
'The Fischer-Tropsch Synthesis, Academic Press, Orlando, (1984)

Augustine, R.L.,
'Heterogeneous Catalysis for the Synthetic Chemist', Marcel Dekker, New York, (1996)

Bukur, D.B., Mukesh, D., Patel, S.A.,
'Promoter Effects on Precipitated Iron Catalysts for Fischer-Tropsch Synthesis', *Industrial Engineering Chemistry Research*, 29, (1990a), 194

Bukur, D.B., K. Okabe, M.P. Rosynek, C., Wang, D., Rao, K.R.P.M and G.P. Huffman,
Journal of Catalysis, 155 (1995) 353-365

Cavani, F., Trifiro, F. & Vaccari, A.,
'Hydrotalcite-Type Anionic Clays: Preparation, Properties and Applications', *Catalysis Today*, (1991), vol 11(2), pp173-221.

Claeys, M. van Steen, E.
'Fischer-Tropsch synthesis: fundamentals', *Studies in Surface Science and Catalysis* 152 (2004), 601-680.

Di Cosimo, J.I., Diez, V.K., Iglesia, E. & Apesteguia, C.R.,
1998, 'Structure and Surface and Catalytic Properties of Mg-Al Basic Oxides', *Journal of Catalysis*, (1998), vol.178, pp. 499-510.

Dictor, R.A., Bell, A.T.,
Fischer-Tropsch Synthesis over reduced and unreduced iron oxide catalysts, *Journal of Catalysis*, 97, (1986), 121

University of Cape Town

Dry, M.E.
Fischer-Tropsch synthesis – industrial, *Encyclopaedia of Catalysis,* Vol. 3, p. 347-403 (Hotvath, I.T., Ed.), John Wiley and Sons, New York (2003).

Dry, M.E.
Fischer-Tropsch reactions and the environment, *Applied Catalysis A: General* 189 (1999), 185-190.

Dry, M.E.
The Fischer-Tropsch process: 1950-2000, *Catalysis Today* 71(3-4) (2002), 227-241.

Dry, M.E.,
The Fischer-Tropsch synthesis in "*Catalysis Science and Technology*", Vol. 15-255, p. 1 (Anderson, R.B and Boudart, M., Eds.), Springer-Verlag, Berlin (1981).

Dry, M.E.,
Studies Surface Science and Catalysis 152 (2004), 533-600

Edström, J.O.,
Journal of the Iron and Steel Institiute, November 1953, 289-304

O'Brien, R.J, Xu, L,Spicer, R.L and. Davis, B.H.,
Energy & Fuels, 10 (1996) 921-926

Geertsema, A.,
Presentation at the University of Karlsruhe, (1995)

Gibson, P.,
Process Technology Course Presentation, 1999

University of Cape Town

Rao, V.U.S., Stiegel, G.J., Cinquegrane, G.J., and Srivastava, R.D.,
'Iron Based Catalyst for Slurry-phase FT Process', *Fuels Processing Technology*, 30 (1992), 83-107.

Roper, M,
Fischer-Tropsch Synthesis in "Catalysis in C1 Chemistry (W.Keim, Ed.), pp. 41, D., Reidel Dordrecht, The Netherlands (1983).

Schaper, H., Berg-Slot, J.J., & Stork, W.H.J.,
'Stabilized Magnesia: a Novel Catalyst (Support) Material', *Applied Catalysis*, (1989), vol 54, pp 79-90.

Schulz, H, Claeys, M.,
Applied Catalysis A: General 186 (1999b), 91

Schulz, H, Claeys, M.,
Applied Catalysis A: General 186 (1999a), 71

Schulz, H, Zh. Nie, Ousmanov, F.,
Catalysis Today 71 (2002), 351

Shen, J., Guang, B., Tu, M., & Chen, Y.,
'Preparation and Characterisation of Fe/MgO Catalysts Obtained from Hydrotalcite-Like Compounds', *Journal of Catalysis*, (1996), vol 30, pp 77-82.

Shen, J., Tu, M., Hu, C.,
'Structural and Surface Acid/Base Properties of Hydrotalcite-Derived MgAlO Oxides Calcined at Varying Temperature', *Journal of Solid State Chemistry* (1998), vol 137, pp 295-301.

Spamer, A.,
Sasol Technology, Internal Report, Hydrotalcites: Synthesis, properties and uses, (2000).

University of Cape Town

Steynberg, A.P., Dry, M.E.,
'Fischer-Tropsch Technology', *Studies in Surface Science and Catalysis*, Elsevier, Amsterdam, (2004).

Vaccari, A.,
'Clays and Catalysis: a promising future', Applied Clay Science, (1999) vol 14, pp 161-198.

Van Steen, E.,
PhD Thesis, University of Karlsruhe (1993)

Van Steen, E., Schulz, H.
Polymerisation kinetics of the Fischer-Tropsch CO hydrogenation using iron and cobalt based catalysts
Applied Cataysis A: General 186 (1999), 309-320.

Wang, X.,
'The Effect of Fe and other Promoters on the Activity of Pd/ceria for the Water-Gas Shift Reaction', *Applied Cataysis*, 247 (2003), 157-162

Xu, L., Bao, S., O'Brian R.J., Raje, A., Davis, B.H.
'Don't rule out iron catalysts for Fischer-Tropsch synthesis'
CHEMTECH 28(1) (1998), 47

University of Cape Town

Websites:

NIRE Annual Report, 1995
http://www.aist.go.jp/NIRE/r_office/mater/silica/si/talcite/topic.htm

http://www.synetix.com/technical/catalysts-testing.htm

Bibliography

Beres, A., Palinko, I., Fudala, A., Kiricsi, I., Kiyozumi, Y., Mizukami, F. & Nagy, J.B.,
'Behaviour of Hydrotalcite and its $Fe(CN)_6^{4-}$ Pillared Derivative on Heat Treatment', Journal of Thermal Analysis and Calorimetry, 1999, vol 5-6, pp 311-316.

Kellar, C.P., Schutz, A., & Marcelin, G.,
'Acid-Base Properties of Catalysts Derived from Anionic Hydroxides', American Chemical Society, 1988, pp 324-333.

Miyata, S.,
'Physico-chemical Properties of Synthetic Hydrotalcites in Relation to Composition', Clays and Clay Minerals, 1980, vol 28, no. 1, pp 50-56.

Reichle, W.T.,
'Catalytic Reactions by Thermally Activated, Synthetic Anionic Clay Minerals', *Journal of Catalysis*, 1985 vol. 94, pp. 547-557.

Reichle, W.T., Kang, S.Y. & Everhardt, D.S.,
'The Nature of the Thermal Decomposition of a Catalytically Active Anionic Clay Mineral', *Journal of Catalysis*, 1986, vol. 101, pp. 352-359.

Sato, T., Fujita, H., Endo, T., Shimada, M.,
'Synthesis of Hydrotalcite-like compounds and their physio-chemical', *Reactivity of Solids*, 1998, vol 5, pp 219-228.

Shen, J., Kobe, J.M., Chen, Y. & Dumesic, J.A.,
'Synthesis and Surface Acid/Base Properties of Magnesium-Aluminium Mixed Oxides Obtained from Hydrotalcites', Langmuir, 1994, vol 10, pp 3902-3908.

University of Cape Town

Appendix A

XRD Results Prior to Calcination of Catalysts that were Used in the FT Synthesis

HTlc 100

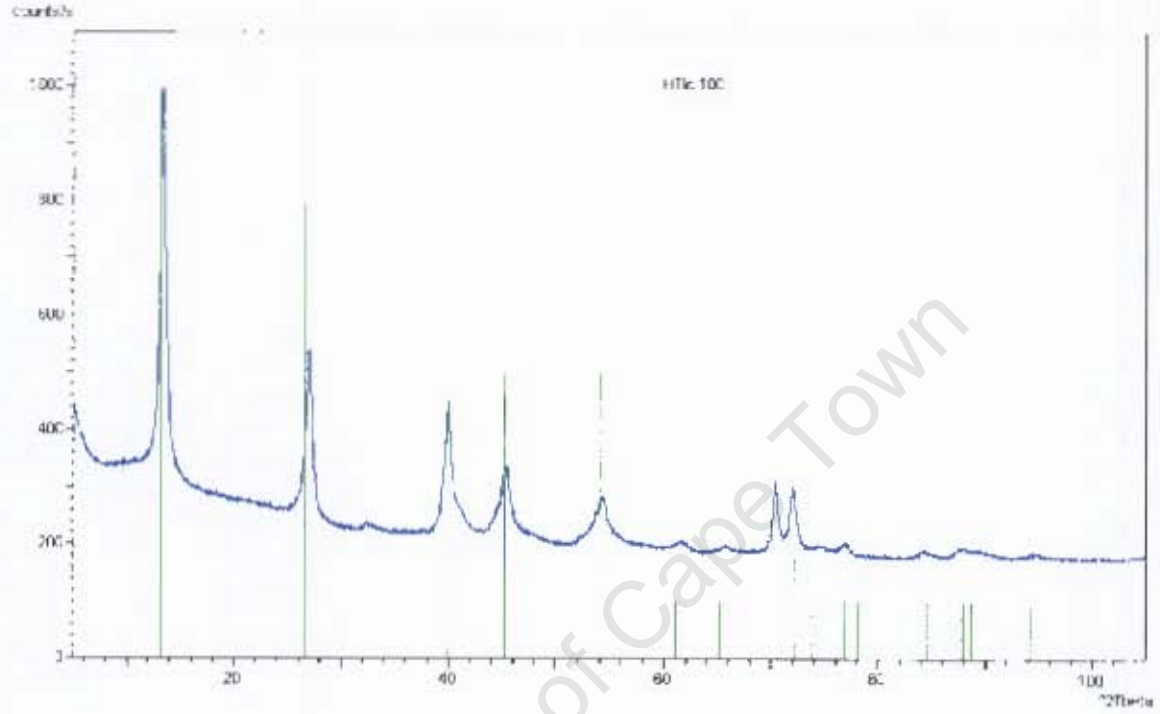

HTlc 102

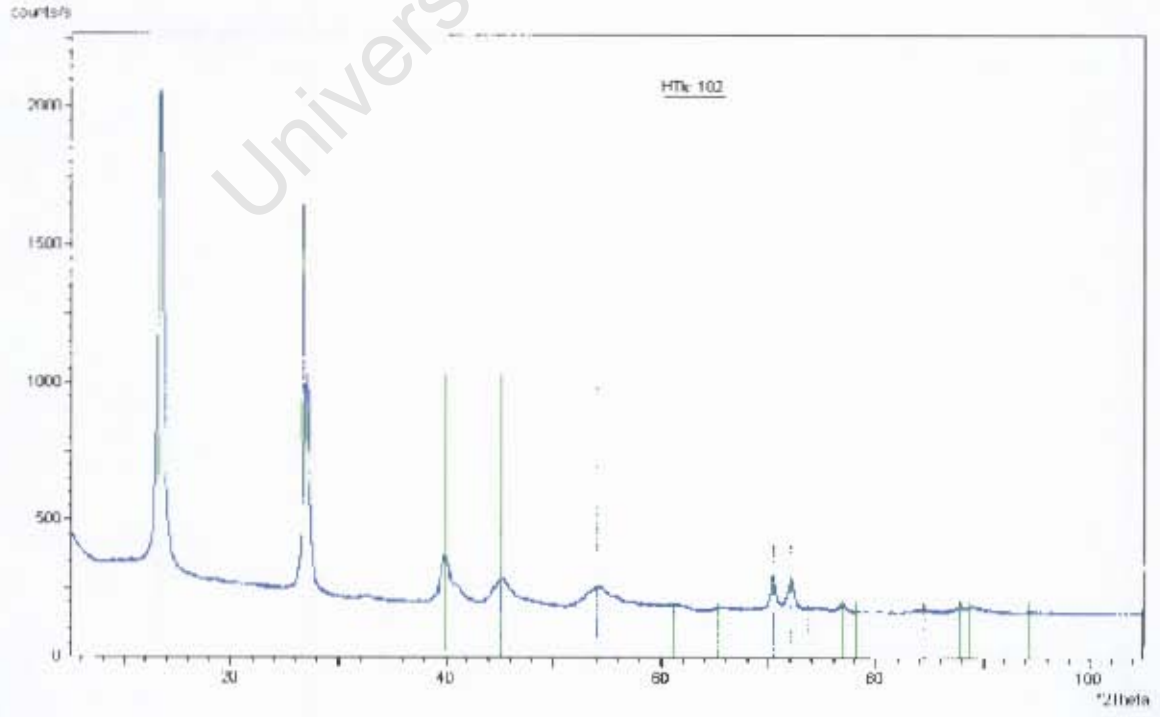

University of Cape Town

HTlc103 (Mg/Fe = 3/1)

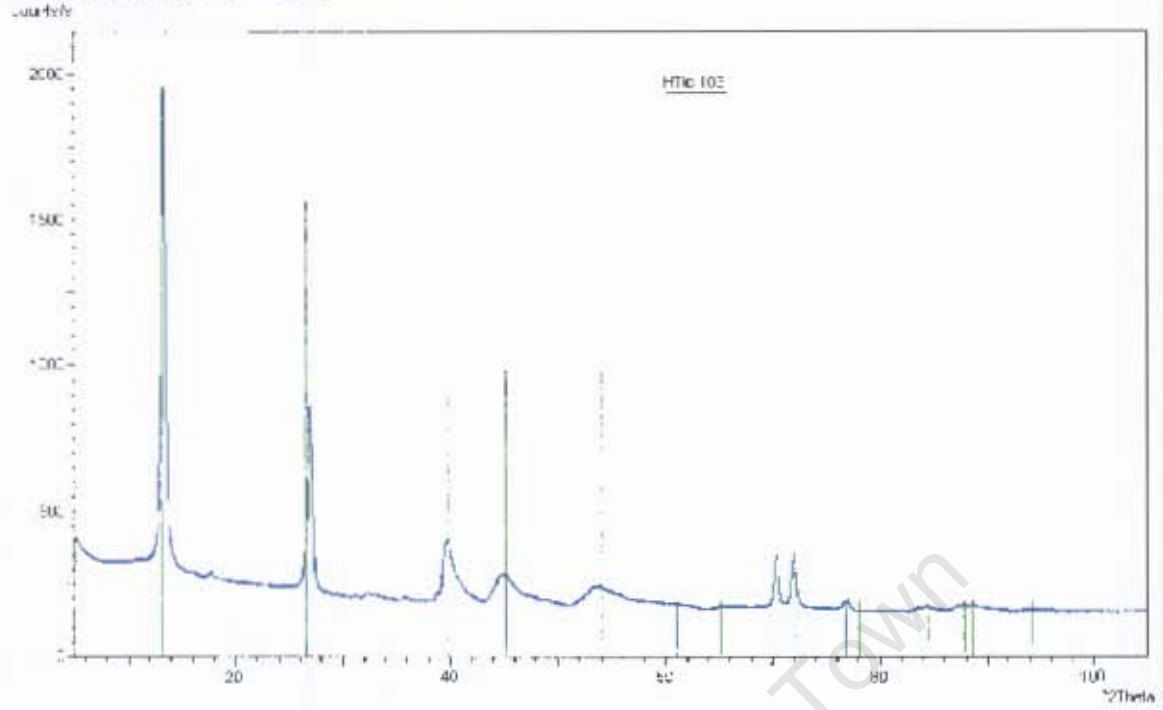

HTlc105

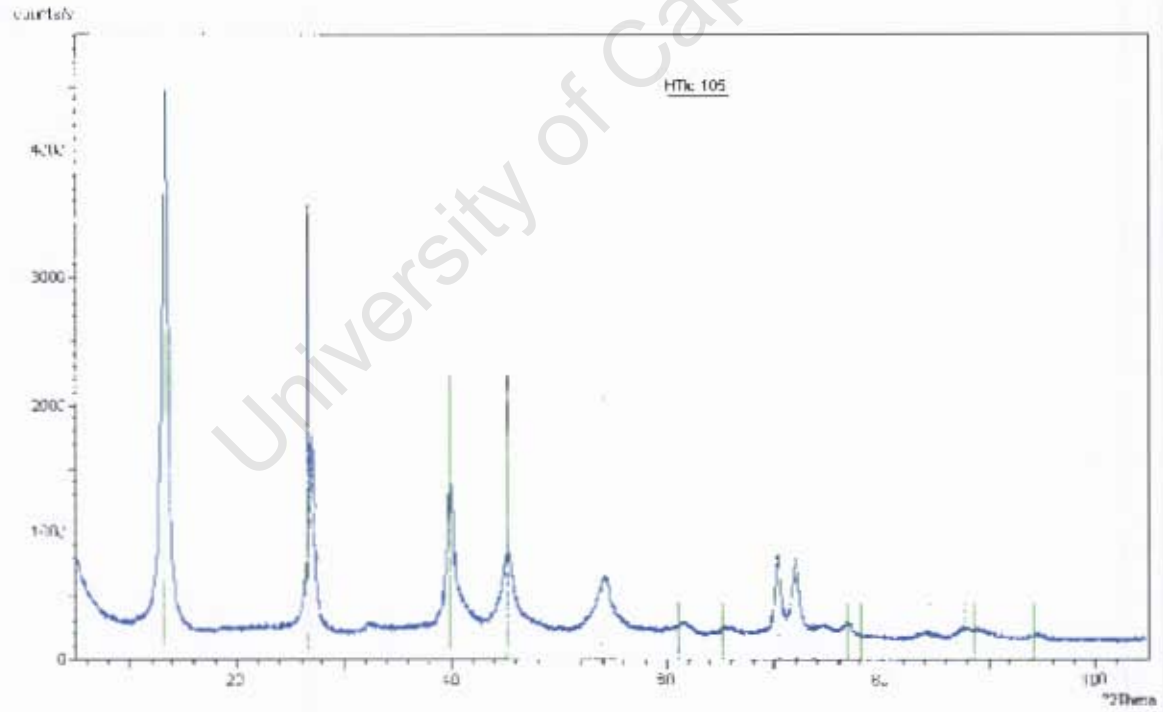

University of Cape Town

XRD Results from an Unsuccessful Preparation

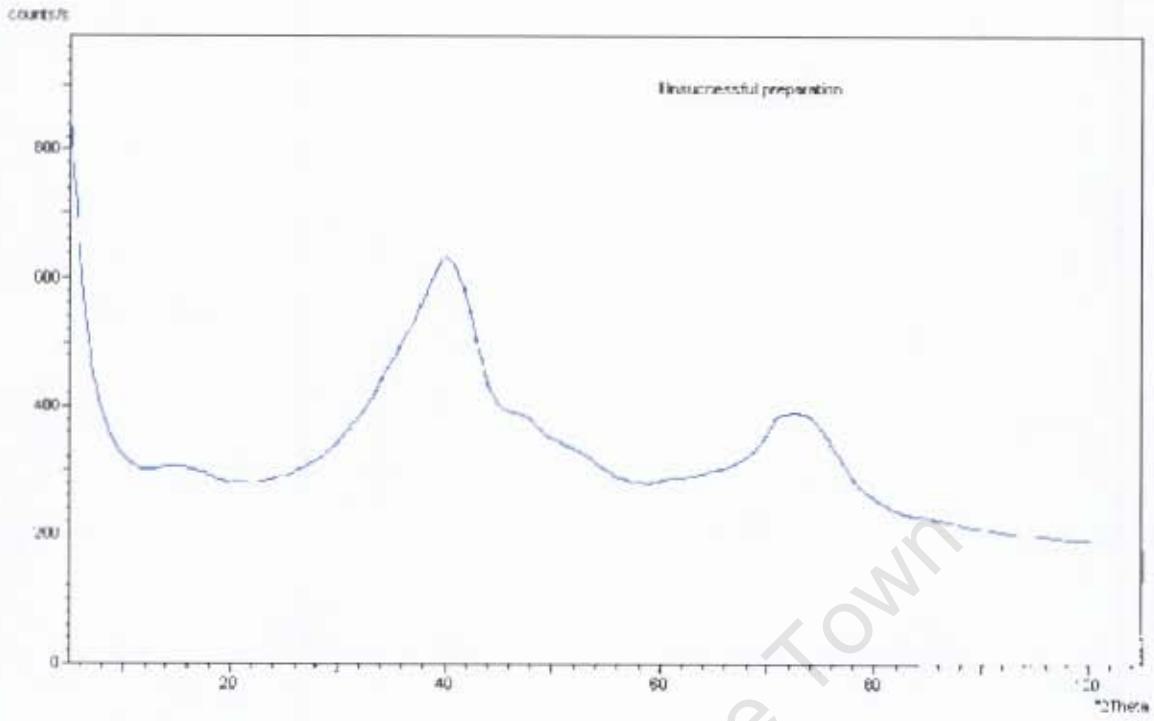

University of Cape Town

Appendix B

Experimental Data

Catalytic Performance and Selectivity

University of Cape Town

HTIc 100								
Time on Line	% CO converted to CO2	pH2O/Bar	H2/CO Reactor Ratio	Usage Ratio	Ribblet Ratio	% H2 Conversion	pCO2/Bar	pH2/Bar
26	6.7	2.02	11.13	1.85	1.01	31.17	2.59	9.52
44	8.1	2.23	10.23	1.68	0.89	33.43	2.87	8.91
69	8.2	2.11	9.92	1.76	0.89	33.24	2.92	8.92
75	8.2	2.15	10.6	1.75	0.91	33.25	2.9	9.01
HTIc 102								
Time on Line	% CO converted to CO2	pH2O/Bar	H2/CO Reactor Ratio	Usage Ratio	Ribblet Ratio	% H2 Conversion	pCO2/Bar	pH2/Bar
21	3.4	2.13	7.69	1.97	0.89	33.47	2.8	8.93
46	7.5	1.84	8.46	1.86	0.93	29.93	2.8	9.43
70	10.3	1.83	8.3	1.74	0.9	29.3	2.92	9.36
94	10.8	1.8	8.4	1.73	0.9	29.39	2.92	9.36
HTIc 105								
Time on Line	% CO converted to CO2	pH2O/Bar	H2/CO Reactor Ratio	Usage Ratio	Ribblet Ratio	% H2 Conversion	pCO2/Bar	pH2/Bar
28	5.3	2.23	10.23	1.68	0.89	33.43	2.43	9.92
42		2.11	9.92	1.76	0.89	33.24	2.54	10.03
50	6.7	2.15	10.6	1.75	0.91	33.25	2.47	9.94
68	7.3			1.95	0.9	32.91	2.49	9.81
73	7.2	2.22	9	1.13	0.97		2.5	9.93
Fused Catalyst								
Time on Line	% CO converted to CO2	pH2O/Bar	H2/CO Reactor Ratio	Usage Ratio	Ribblet Ratio	% H2 Conversion	pCO2/Bar	pH2/Bar
23.8	1	2.6	12.57	1.8	0.93	35	2.6	8.8
42	4	2.6	14.50	1.8	0.93	37	2.7	8.7
67.2	5	2.5	14.83	1.8	0.96	36	2.7	8.9
91.2	6	2.4	12.86	1.8	0.96	36	2.7	9

University of Cape Town

Carbon Number	HTlc 100 (69hrs TOL)	HTlc 102 (70hrs TOL)	HTlc 105 (68hrs TOL)	Fused Catalyst (91hrs TOL)
	% Hydrocarbon Selectivity			
1	20.70	25.36	15.71	9.21
2	14.20	14.38	14.95	10.19
3	16.89	17.19	15.66	13.70
4	11.20	10.45	11.79	10.84
5	9.08	6.29	8.78	9.82
6	7.07	4.32	7.47	9.27
7	5.66	2.81	7.23	7.70
8	8.40	2.39	6.97	6.50
9	3.83	2.26	5.54	5.99
10	2.37	1.92	5.39	4.84
11	1.96	1.30	3.58	3.24
12	1.60	0.88	2.80	2.03
13	1.69	0.73	1.46	1.29
14	0.85	0.42	1.17	0.95
15	0.56	0.25	0.81	0.50
16	0.11	0.04	0.20	0.37
17	0.06	0.10	0.12	0.19
18	0.27	0.21	0.08	0.11
19	0.03	0.01	0.05	0.06
20	0.02	0.01	0.03	0.04
21	0.01	0.01	0.02	0.02
22	0.16	0.16	0.02	0.01

University of Cape Town

Carbon Number	HTlc 100 (69hrs TOL)	HTlc 102 (70hrs TOL)	HTlc 105 (68hrs TOL)	Fused Catalyst (91hrs TOL)
	1-Olefin Selectivity			
2	5.02	4.82	5.07	6.24
3	11.93	12.15	11.77	10.33
4	6.40	5.64	7.61	9.06
5	3.53	2.47	4.81	6.66
6	2.35	1.53	3.86	5.85
7	1.06	0.59	2.49	4.14
8	0.81	0.25	1.69	2.60
9	0.29	0.16	1.01	2.01
10	0.19	0.11	0.63	1.46
11	0.12	0.07	0.40	1.02
12	0.10	0.05	0.30	0.70
13	0.06	0.04	0.22	0.50
14	0.04	0.02	0.29	0.38
15	0.02	0.01	0.19	0.24
16	0.07	0.04	0.16	0.16
17	0.04	0.03	0.11	0.11
18	0.20	0.21	0.08	0.08
19	0.02	0.01	0.05	0.05
20	0.00	0.01	0.03	0.03
21	0.01	0.01	0.02	0.02
22	0.23	0.16	0.02	0.01

University of Cape Town

Carbon Number	HTIc 100 (69hrs TOL)	HTIc 102 (70hrs TOL)	HTIc 105 (68hrs TOL)	Fused Catalyst (91hrs TOL)
	n-Paraffin Selectivity			
1	20.56	25.09	15.56	8.73
2	7.73	8.81	4.91	1.23
3	3.41	4.12	2.08	1.01
4	2.48	2.38	1.59	0.93
5	1.83	1.56	1.31	0.83
6	1.48	1.18	1.25	0.77
7	1.13	0.79	0.87	0.39
8	0.59	0.42	0.83	0.37
9	0.47	0.34	0.67	0.34
10	0.39	0.28	0.55	0.28
11	0.26	0.19	0.40	0.18
12	0.20	0.14	0.26	0.14
13	0.19	0.13	0.12	0.10
14	0.15	0.10	0.07	0.06
15	0.11	0.06	0.06	0.05
16	0.01	0.00	0.03	0.03
17	0.00	0.07	0.01	0.03
18	0.00	0.00	0.01	0.01

University of Cape Town

Carbon Number	HTlc 100 (69hrs TOL)	HTlc 102 (70hrs TOL)	HTlc 105 (68hrs TOL)	Fused Catalyst (91hrs TOL)
	n-Alcohols Selectivity			
1	0.10	0.27	0.15	0.48
2	1.06	0.73	4.92	2.72
3	0.30	0.23	0.88	0.68
4	0.26	0.16	0.66	0.72
5	0.29	0.20	0.53	0.88
6	0.24	0.10	0.31	0.41
7	0.10	0.08	0.23	0.28
8	0.11	0.08	0.21	0.43
9	0.09	0.07	0.18	0.19
10	0.07	0.04	0.10	0.20
11	0.06	0.04	0.10	0.07
12	0.03	0.02	0.13	0.06
13	0.49	0.20	0.05	0.05
14	0.01	0.01	0.04	0.02

University of Cape Town